STRUCTURE–ACTIVITY RELATIONSHIPS IN OLEFIN

POLYMERIZATION CATALYSTS

A Dissertation

by

CRAIG JUSTIN PRICE

Submitted to the Office of Graduate Studies of
Texas A&M University
in partial fulfillment of the requirements for the degree of

DOCTOR OF PHILOSOPHY

August 2007

Major Subject: Chemistry

STRUCTURE–ACTIVITY RELATIONSHIPS IN OLEFIN

POLYMERIZATION CATALYSTS

A Dissertation

by

CRAIG JUSTIN PRICE

Submitted to the Office of Graduate Studies of
Texas A&M University
in partial fulfillment of the requirements for the degree of

DOCTOR OF PHILOSOPHY

Approved by:

Chair of Committee,	Stephen Miller
Committee Members,	Donald Darensbourg
	François Gabbaï
	Jaime Grunlan
Head of Department,	David Russell

August 2007

Major Subject: Chemistry

ABSTRACT

Structure–Activity Relationships in Olefin Polymerization Catalysts. (August 2007)

Craig Justin Price, B.S., North Carolina State University

Chair of Advisory Committee: Dr. Stephen A. Miller

The thermodynamic parameters associated with the copolymerization of ethylene and carbon dioxide were calculated using bond dissociation energies, the Benson additivity method and density functional theory calculations (DFT). In all cases, the formation of an alternation copolymer was found to be endergonic at any reasonable polymerization temperatures (the ceiling temperature is calculated to be -159 °C). However, the polymerization was calculated to be exergonic at room temperature, as long as the incorporation of CO_2 is less than 29.7 mol%. Experiments failed to provide evidence of any CO_2 incorporation, despite previously published reports claiming up to 30 mol%.

Octamethyloctahydrodibenzofluorenyl (Oct) has profound steric consequences when incorporated into metallocene olefin polymerization catalysts – including increased catalytic activity and stereoselectivity. However, the electronic effect of the ligand's four electron-donating tertiary alkyl groups is less understood. NMR and DFT calculations were used to study the electronic nature of the Oct moiety – both as a part of *ansa*-metallocene pre-catalysts and as an independent molecule. The results show that Oct is more electron rich than other cyclopentadienyl analogues and that the electronics of the ligand are readily conveyed to the metal center.

Upon activation, the steric bulk of the Oct moiety dominates the immediate environment around the metal center. Evidence is presented that supports previous theories about Oct's ability to influence the counteranion distance, thereby increasing the catalytic activity. In addition, excess trimethyl aluminum (TMA) is known to be detrimental to catalytic activity and results uphold this belief – although the magnitude of the effect varies depending on the metallocene being studied. However, UV-Vis data do not support the theory that TMA binds to the catalytically-active metal center, thereby decreasing the catalytic activity; but does not offer an alternate mechanism.

For Joanna, Mom and Dad.

ACKNOWLEDGMENTS

As difficult as graduate school can be sometimes, properly thanking the many many people who helped you during your graduate career can be just as challenging.

First, I would like to thank all the members of the Miller Crew who have shared time with me here at A&M. Levi Irwin, Joe Grill, and Jesse Reich came before me and helped me get settled in the lab. I especially thank Brittany Beckstead – who joined the Miller Crew at the same time as I – for being an awesome friend and labmate. Eric Schwerdtfeger and Paul Zeits have been great labmates, teammates and awesome friends. I am grateful to both of you for your help – both in and out of the lab. I was very fortunate to be able to work with a stellar undergrad research assistant – Marie Launer. Her work on the UV-Vis project was invaluable.

I especially thank those members of the Miller Crew who coauthored publications with me: Jesse Reich worked with me on the ethylene/CO_2 project; Paul Zeits synthesized the manganese tricarbonyls for the electronic nature of Oct project; and finally, Marie Launer for her work on the UV-Vis project. I couldn't have done it without you guys. I was also lucky enough to be able to work with several other members of the Miller Crew on projects not presented in this dissertation. I thank Andrea Ilg for picking up the trioxane copolymerization project; and Nathan Rife and Paul Zeits for a few month's worth of hard work on the cyanide project.

I would also like to thank my advisor, Professor Stephen Miller, who has supported me throughout my graduate career. I am also indebted to the rest of my

TABLE OF CONTENTS

LIST OF FIGURES

LIST OF TABLES

CHAPTER I

INTRODUCTION

In 1898, Hans von Pechmann stumbled upon polyethylene when he accidentally heated diazomethane, forming a white waxy solid.[1] Upon characterization, he realized that the substance consisted of numerous $-CH_2-$ units and called the material *polymethylene.* The first industrially-viable production of polyethylene from gaseous ethylene was discovered, also accidentally, in 1933 by Eric Fawcett and Reginald Gibson at Imperial Chemical Industries.[2,3] While studying the effects of high pressures on chemical reactions, the pair subjected a mixture of ethylene and benzaldehyde to ~1400 atmospheres at 175 °C. They also produced a white waxy solid, and were able to recover the unreacted benzaldehyde; however these results were difficult to reproduce. In 1935, Michael Perrin, another chemist at Imperial, realized that the reaction observed by Fawcett and Gibson had been initiated by trace amounts of oxygen in the system – which explained the reproducibility problems.[4,5] Further experiments led to the first reliable industrial process for the polymerization of ethylene.

In the 1950s, Karl Ziegler discovered that linear polyethylene could be produced at much lower temperatures and pressures with the addition of certain transition metals and organometallic species.[6] Shortly after this publication, Giulio Natta reported that the catalyst system was capable of polymerizing α-olefins stereoselectivly.[7] With the

This dissertation follows the style and format of the *Journal of the American Chemical Society*.

discovery of these systems (Figure 1.1), higher molecular weights and more linear polymer chains than were possible, compared with radical polymerization processes that were previously used.[8] In 1963, Ziegler and Natta shared the Nobel Prize in Chemistry for these contributions to olefin polymerization. This discovery caused an explosion in the research on transition metal mediated olefin polymerization.[9-13] The research showed that two components are necessary for the catalysts systems to be highly active: a transition metal – usually from groups 4-8 – and an organometallic Lewis acid to activate the transition metal complex.

$$n \quad /\!\!/ \quad \xrightarrow{\text{TiCl}_3 \text{ / AlEt}_3} \quad \left(\!\!\!\diagdown\!\!\diagup\!\!\!\right)_n$$
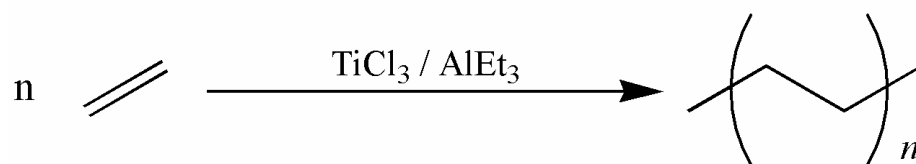
Figure 1.1: A typical Ziegler-type heterogeneous system for the polymerization of ethylene.

Later work showed that the most efficent activator was methylaluminoxane (MAO) – a partially hydrolyzed trimethyl aluminum compound.[14] MAO activates a transition metal pre-catalyst by alkylating the metal, and then creates an open coordination site by abstracting a halide or an alkyl group. Figure 1.2 shows an olefin binding to the metal at this open coordination site, where it is added to the growing polymer chain via a migratory insertion mechanism.[15,16] Repetition of this process produces high polymer.
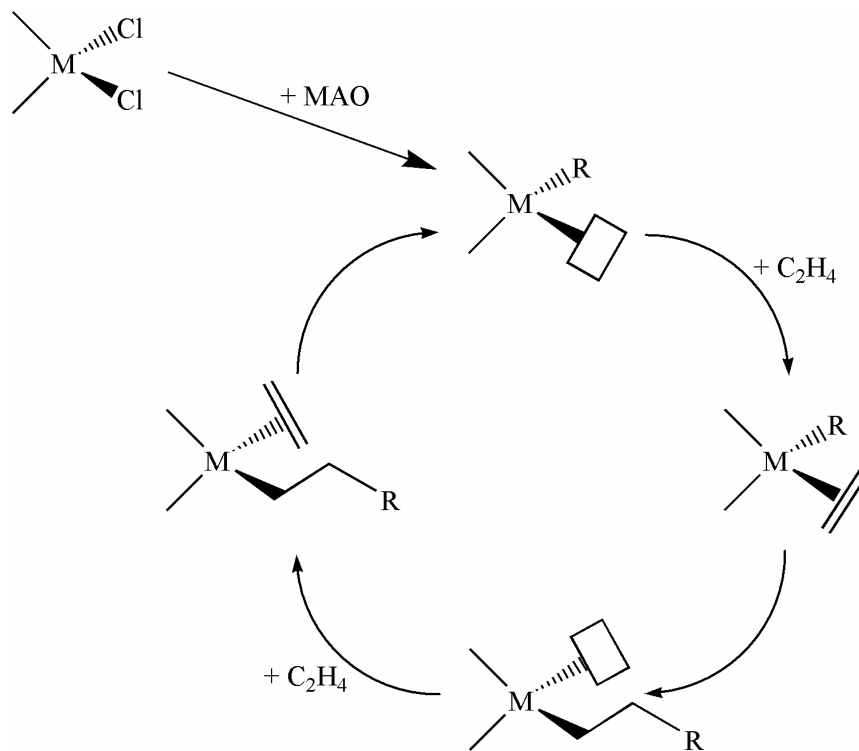
Figure 1.2: The use of MAO to generate a coordinativly unsaturated metal center, and the subsequent catalytic cycle for the polymerization of ethylene (R = alkyl or growing polymer chain).

However, heterogeneous systems such as this have several disadvantages. One of the most important weaknesses of heterogeneous systems is the broad molecular weight distributions. The most common explanation for this observation is the presence of several different active sites on the surface of the insoluble support – each with different relative rates of insertion and termination. In addition, although heterogeneous systems can produce tactic polymers, generally they are not highly stereoselective, and it is often difficult to predict if a given system will produce atactic, isotactic, or

syndiotactic polymer.[9,17]   Heterogeneous systems are also generally incapable of producing highly syndiotactic polymers.[18]

The properties of polymers depend greatly on the type, and the density of regular stereocenters along the polymer backbone. There is a great need for highly tactic polymers, as well as the need to produce polymers with specific properties (engineering plastics). These needs fueled the explosion of research efforts directed towards discrete homogeneous catalysts for olefin polymerization based on α-diimine complexes of late transition metals[19] and early transition metal metallocene complexes.[20,21]

These homogeneous catalysts have several advantages. The homogenous nature of the catalyst provides for nearly every metal center to be catalytically active and explains their high activity compared to the heterogeneous systems mentioned above. The ability of homogeneous α-diimine catalysts to produce high molecular weigh polyethylene with a branched structure gives rise to unique properties.[22-26] In addition, homogeneous metallocene and *ansa*-metallocene complexes, such as $Me_2C(\eta^5\text{-}C_5H_4)(\eta^5\text{-}C_{13}H_8)ZrCl_2$ discovered by Ewen,[27] are capable of producing tactic polymers by discriminating between the two enantiofaces of α-olefins.[28] Homogeneous olefin polymerization catalysts such as these are the focus of this dissertation.

Chapter II focuses on α-diimine and pyridine-diimine complexes of late transition metals for the attempted copolymerization of ethylene and CO_2. There is considerable interest in producing polymers that are derived partly, or in whole, from renewable resources since the vast majority of all synthetic polymers are derived from petroleum feedstocks. This chapter focuses on the thermodynamic and kinetic aspects of

the copolymerization and provides a critical assessment of previous reports claiming up to 30 mol% CO_2 incorporation in light of the fact that they are not reproducible in our hands.

Chapters III and IV focus on a series of sterically-expanded ligands for *ansa*-metallocene olefin polymerization catalysts, especially those containing the octamethyloctahydrodibenzofluorenyl (Oct) moiety (Figure 1.3). Oct has profound steric consequences when incorporated into olefin polymerization catalysts, but its electronic contributions are less understood. The electronic nature of this ligand has been studied using NMR, IR, and UV-Visible spectroscopies as well as density functional theory (DFT) calculations. In addition, the time-dependent activation of *ansa*-metallocenes has been followed with UV-Visible spectroscopy and correlated to catalytic activity. The detrimental effect of excess trimethyl aluminum (TMA) on the catalyst systems has been studied and it has been determined that the magnitude of this effect varies depending on the catalyst employed. In addition, evidence is presented that refutes the previous theory that excess TMA decreases catalytic activity by binding to the active metal center.
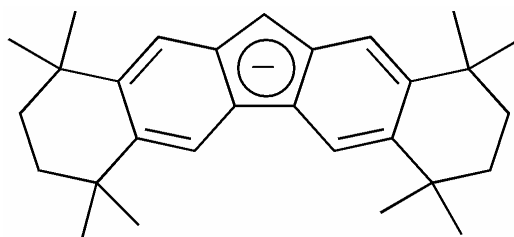
Figure 1.3: The octamethyloctahydrodibenzofluorenyl moiety.

CHAPTER II

KINETIC AND THERMODYNAMIC CONSIDERATIONS IN THE COPOLYMERIZATION OF ETHYLENE AND CARBON DIOXIDE[*]

SYNOPSIS

The thermodynamics of ethylene and carbon dioxide copolymerization were evaluated using average bond dissociation energies (BDE), the Benson additivity method, and density functional theory (DFT) calculations (B3LYP/6-31G[†]). According to the DFT calculations, the formation of an alternating copolymer is exothermic ($\Delta H = -4.31$ kcal/mol per repeat unit), but endergonic at most temperatures (> -159°C, the ceiling temperature), and is therefore practically inaccessible because of entropic factors. However, these thermodynamic calculations show that at room temperature (25°C) the polymerization is favorable (exergonic) when the molar ratio of ethylene/carbon dioxide exceeds 2.37 (29.7 mol% CO_2 or less). Catalytic amounts of late transition metal complexes (Fe, Co, Ni, Cu), in combination with MAO (methylaluminoxane), produced polymers or oligomers which contain only ethylene under various copolymerization conditions. The lack of ester functionality in the resulting products was confirmed by mass spectrometry and ^{13}C NMR; and indicates the suspicious nature of previous reports claiming up to 30 mol% incorporation of carbon dioxide.

INTRODUCTION

The vast majority of synthetic polymers are derived from petroleum feedstocks. Given that these feedstocks are non-renewable, there is considerable interest in developing routes to synthetic polymers that are based, partly or completely, on renewable resources. Carbon dioxide, which is present at 370 ppm in the Earth's atmosphere,[29] has received considerable attention in this regard. Incorporating CO_2 into useful polymers serves two important functions: it takes advantage of a renewable, relatively inexpensive, and extremely abundant C_1 building block; and it serves to remove a greenhouse gas from the atmosphere. Since Inoue's discovery of catalysts for the copolymerization of CO_2 and epoxides in 1969[30], considerable research effort has been directed toward developing other catalytic systems that are capable of incorporating CO_2 into polymer chains. There have been multiple reports of copolymerizing CO_2 with high-energy comonomers such as epoxides[31] and aziridines[32,33] to form polycarbonates and polyurethanes, respectively. In addition, the copolymerization of CO_2 with dienes and with vinyl ethers has been reported.[34] Research in this group has focused on ethylene and propylene polymerizations, so we were intrigued when, in 2002, Zou and coworkers reported the copolymerization of ethylene and CO_2 to form high molecular weight polyesters with a significant degree of CO_2 incorporation (up to 30 mol%)[35].

RESULTS AND DISCUSSION

Bond dissociation energy thermodynamics. The copolymerization enthalpy for ethylene and CO_2 can be calculated using several methods. One approach employs average bond dissociation energies (BDE), such as those found in common organic chemistry textbooks.[36] Scheme 2.1 shows a simplified copolymer chain that is used for these calculations. This model avoids adjacent carbon dioxide monomers, an arrangement that is very thermodynamically unfavorable.[37-39] The BDE calculations, as
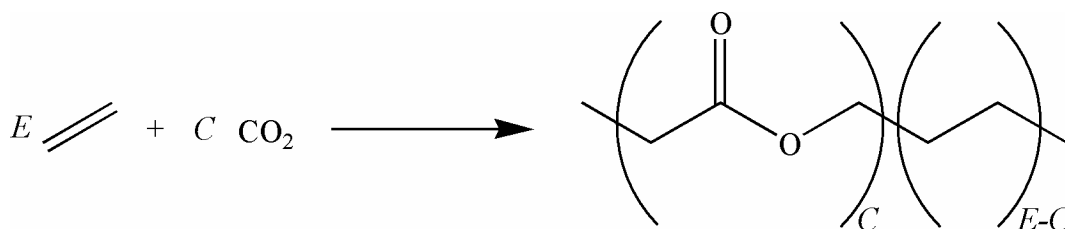
Figure 2.1: The copolymerization of ethylene and carbon dioxide to form a random copolyester. This model avoids the thermodynamically unfavorable possibility of adjacent carbon dioxide monomer units.

shown in Table 2.1, yields ΔH_{poly} values of -14 kcal/mol for ethylene incorporation and -10 kcal/mol for the incorporation of an isolated carbon dioxide unit. Using these values, we arrive at Equation 2.1, in which E is defined as the number of ethylene units and C is defined as the number of carbon dioxide units, according to Figure 2.1. Therefore, Equation 2.1 gives the polymerization enthalpy per monomer as a function of the
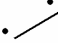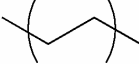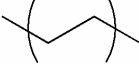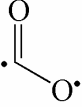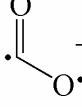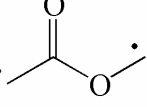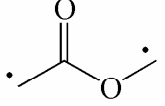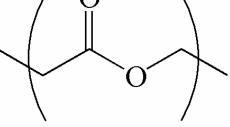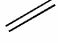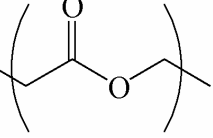
ethylene/carbon dioxide quotient (*E/C*). Equation 2.3 gives the value of ΔG_{poly} (per monomer), which can be determined by substituting Equation 2.1 into the Gibbs free energy equation (Equation 2.2) and assuming that ΔS = -0.030 kcal/molK per monomer incorporated.[40] This method predicts that the copolymerization will be exergonic for *E/C* $\geq$ 2.56. This also suggests that the perfectly alternating copolymer is thermodynamically inaccessible. According to Equation 2.3, its ceiling temperature (ΔG_{poly} = 0) would be approximately -106 °C and any polymerization carried out at this temperature would be kinetically unfeasible. However, it is clear that average bond dissociation energies poorly estimate the enthalpy of ethylene homopolymerization, as this estimation suggests -14 kcal/mol, but the measured value is -22.348 kcal/mol.[41]

$$\Delta H_{poly} = \frac{[C(-10) + (E - C)(-14)]}{C + E} \qquad \text{Equation 2.1}$$

$$\Delta G = \Delta H - T\Delta S \qquad \text{Equation 2.2}$$
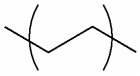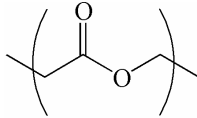
$$\Delta G_{poly} = \frac{[C(-10) + (E - C)(-14)]}{C + E} - T(-0.030) \qquad \text{Equation 2.3}$$

Table 2.1: Average bond dissociation energies (BDE) used to calculate the thermodynamics of ethylene/carbon dioxide copolymerizaion.

Reaction	BDE (kcal/mol) $\left(\begin{matrix}Bonds\\Broken\end{matrix}\right) - \left(\begin{matrix}Bonds\\Made\end{matrix}\right) =$ Total			
(ethylene → radical)	148	−	81	= 67
(radical → chain)	0	−	81	= -81
(ethylene → chain)	67	−	81	= -14
(ethylene → 2 :CH$_2$)	148	−	0	= 148
(CO$_2$ → diradical)	172	−	84	= 88
(2 :CH$_2$ + diradical → product)	0	−	(81+84)	= -165
(radical → polymer)	0	−	81	= -81
(ethylene + CO$_2$ → polymer)	(148+88)	−	(165+81)	= -10

Benson additivity thermodynamics. Generally, a more reliable thermodynamic method employs Benson's group additivity rules.[42] In the thermodynamic analysis of polymers, the Benson method can be modified to account for *supergroups* instead of simple groups. In the present case, the supergroups are taken to represent the insertion of ethylene (C–CH$_2$CH$_2$–C), and an isolated insertion of carbon dioxide (C–CH$_2$C(O)OCH$_2$–C) (Scheme 2.1). Table 2.2 shows the enthalpic Benson additivity values for these supergroups. This method yields ΔH_{poly} values of -22.5 for ethylene and -10.1 for an isolated carbon dioxide unit. It is reassuring to note that, for the homopolymerization of ethylene, the -22.5 kcal/mol that is predicted by the Benson additivity method correlates extremely well to the experimental value of -22.348 kcal/mol.[41] These supergroups simplify the resulting enthalpic formula for

Table 2.2: Enthalpic Benson Additivity Calculations Based on Supergroups[a]

Supergroup	Component Groups	Group Additivity ΔH	Supergroup Additivity ΔH	Supergroup ΔH_{poly} Calculation[b]
	C – (C)$_2$(H)$_2$ C – (C)$_2$(H)$_2$	-5.0 -5.0	-10.0	-10 – (12.5) = -22.5
	C – (H)$_2$(C)(CO) CO – (C)(O) O – (C)(CO) C – (H)$_2$(O)(C)	-5.2 -35.2 -43.1 -8.1	-91.6	-91.6 – (12.5 + -94.0) = -10.1
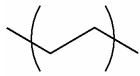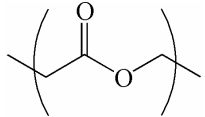
[a] In kcal/mol. [b] The following experimental data[43] are used for this calculation: $\Delta H°_f$ (ethylene) = 12.5 kcal/mol; $\Delta H°_f$ (CO$_2$) = -94.0 kcal/mol

copolymerization and predict the net enthalpy (in kcal/mol) *per monomer* incorporated as shown in Equation 2.4.

$$\Delta H_{\text{poly}} = \frac{[C(-10.1) + (E - C)(-22.5)]}{C + E} \qquad \text{Equation 2.4}$$

Another advantage of Benson additivities over BDE is the ability to calculate values for the entropy of polymerization, as opposed to using the estimated value of -0.030 kcal/(mol K), as was done above. The calculation of ΔS_{poly} using entropic Benson additivity values is shown in Table 2.3. This results in Equation 2.5, which predicts the net entropy (in kcal/(mol K) of polymerization per monomer incorporated.

Table 2.3: Entropic Benson Additivity Calculations Based on Supergroups[a]

Supergroup	Component Groups	Group Additivity S	Supergroup Additivity S	Supergroup ΔS_{poly} Calculation[b]
	C – (C)$_2$(H)$_2$	9.42	18.84	18.84 – (52.42) =
	C – (C)$_2$(H)$_2$	9.42		-33.6
	C – (H)$_2$(C)(CO)	9.6		
	CO – (C)(O)	14.78	43.07	43.07 – (52.42 + 51.10) =
	O – (C)(CO)	8.39		-60.5
	C – (H)$_2$(O)(C)	10.3		

[a] In cal/(mol K). [b] The following experimental data[43] are used for this calculation: $\Delta S°$(ethylene) = 52.42 cal/(mol K); $\Delta S°$(CO$_2$) = 51.10 cal/(mol K).

$$\Delta S_{\text{poly}} = \frac{[C(-0.0605) + (E - C)(-0.0336)]}{C + E} \qquad \text{Equation 2.5}$$

$$\Delta G_{poly} = \frac{[C(-10.1) + (E - C)(-22.5)]}{C + E} - \frac{T\,[C(-0.0605) + (E - C)(-0.0336)]}{C + E}$$

Equation 2.6

The value of ΔG_{poly} (per monomer) can be estimated by substituting Equations 2.4 and 2.5 into Equation 2.2. The result is Equation 2.6, and it shows that the formation of a perfectly alternating copolymer of ethylene and carbon dioxide is thermodynamically forbidden at room temperature.   The ceiling temperature is calculated to be -106 °C (agreeing with the BDE calculation), making the alternating copolymer unattainable due to kinetic reasons. However, copolymers with greater E/C quotients are thermodynamically possible at room temperature (298.15 K). The Benson additivity calculation predicts that the copolymerization is exergonic at room temperature for $E/C \geq 1.64$. Simply stated, the exergonic incorporation of ethylene into the polymer chain compensates for the endergonic incorporation of carbon dioxide, making the copolymerization of ethylene and carbon dioxide thermodynamically feasible.

Again, this model does not address the possibility of adjacent CO_2 monomers. This exclusion is valid because of the considerable endothermicity known for this kind of enchainment.[37-39] Using the Benson additivity method and the experimental value for the $\Delta H°_f$ of carbon dioxide[43], we can calculate the thermodynamics for the formation of hypothetical poly(carbon dioxide). These calculations show that the formation of

poly(carbon dioxide) is endothermic by 18.6 kcal/mol ($CO-(O)_2 + O-(CO)_2 - \Delta H^\circ_f(CO_2)$

$= (-29.2) + (-46.2) - (-94.0))$.

      DFT thermodynamics. In order to assess the quality of the Benson additivity approach, Density Functional Theory (DFT) calculations (B3LYP 6-31G†) were performed on polyethylene and ethylene/carbon dioxide copolymers of varying chain lengths. From these calculations, thermodynamic parameters were obtained for the insertion of one ethylene molecule or the insertion of one CO_2 molecule into a polyethylene chain (Figure 2.2). The results are summarized in Table 2.4 and Table 2.5, respectively.
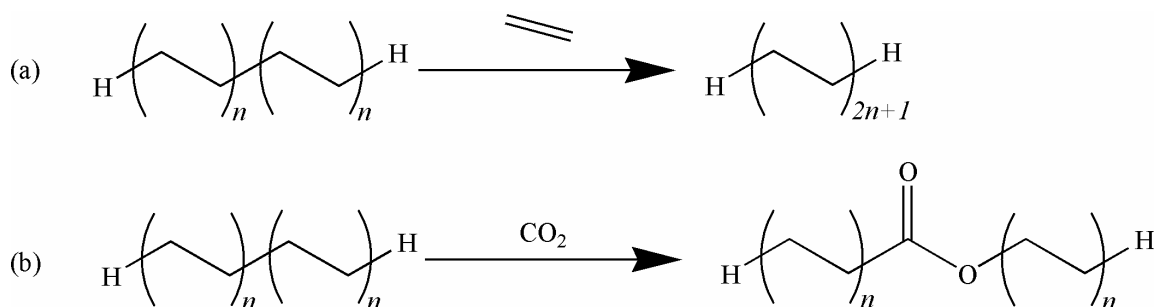
Figure 2.2: Reactions used in the DFT calculations of the thermodynamic parameters for the insertion of one ethylene (a) or one CO_2 (b) monomer into polyethylene chains of varying lengths.

Table 2.4: Summary of DFT Calculations for the Addition of One Ethylene Monomer.

n	Reactant Chain		Product Chain		Calculated Thermodynamic Parameters		
	H (kcal/mol)	S (cal/(mol K))	H (kcal/mol)	S (cal/(mol K))	ΔH^a (kcal/mol)	ΔS^a (cal/(mol K))	ΔG^b (kcal/mol)
1	-99345.32	73.138	-148646.71	88.308	-22.51	-39.935	-10.60
2	-197948.08	103.394	-247249.46	118.489	-22.51	-40.010	-10.58
3	-296550.83	133.381	-345852.15	146.851	-22.44	-41.635	-10.03
4	-395153.59	163.056	-444454.88	175.799	-22.42	-42.362	-9.79
5	-493756.35	192.712	-543057.61	204.641	-22.39	-43.176	-9.52
6	-592359.10	222.294	-641660.35	233.442	-22.38	-43.957	-9.27
7	-690961.71	247.814	-740263.08	262.191	-22.49	-40.728	-10.35
8	-789564.45	276.539	-838865.82	290.939	-22.49	-40.705	-10.36
9	-888167.18	305.323	-937468.55	319.690	-22.49	-40.738	-10.35
				Average for n = 1-9	-22.46	-41.472	-10.09

[a] Ethylene was calculated to have the following values for enthalpy and entropy: H = -492788 kcal/mol; S = 55.105 cal/(mol K). [b] At 298.15 K.

Table 2.5: Summary of DFT Calculations for the Addition of One Carbon Dioxide Monomer.

n	Reactant Chain		Product Chain		Calculated Thermodynamic Parameters		
	H (kcal/mol)	S (cal/(mol K))	H (kcal/mol)	S (cal/(mol K))	ΔH^a (kcal/mol)	ΔS^a (cal/(mol K))	ΔG^b (kcal/mol)
1	-99345.32	73.138	-217660.43	92.154	13.83	-32.122	23.41
2	-197948.08	103.394	-316263.07	122.138	13.96	-32.394	23.61
3	-296550.83	133.381	-414865.89	151.288	13.89	-33.231	23.80
4	-395153.59	163.056	-513468.66	180.224	13.87	-33.970	24.00
5	-493756.35	192.712	-612071.42	208.926	13.87	-34.924	24.28
6	-592359.10	222.294	-710674.18	237.432	13.85	-36.000	24.59
7	-690961.71	247.814	-809276.94	265.852	13.71	-33.100	23.58
8	-789564.45	276.539	-907879.51	293.454	13.88	-34.223	24.09
9	-888167.18	305.323	-1006482.46	322.468	13.66	-33.993	23.80
				Average for n = 1-9	13.84	-33.773	23.91

[a] Carbon dioxide was calculated to have the following values for enthalpy and entropy: H = -118328.94 kcal/mol; S = 51.138 cal/(mol K). [b] At 298.15 K.

The values in Table 2.4 provide an average ΔH_{poly} for ethylene of -22.46 kcal/mol, which correlates rather well to the published experimental value of -22.348 kcal/mol.[41] The calculated ΔS_{poly} for ethylene (-41.47 cal/mol K) is also a close match to the experimental value that includes the crystallization of the polyethylene chain (-41.6 cal/mol K).[44] This is expected, since the geometry optimized ethylene oligomers are all linear. The calculated thermodynamic parameters allow us to write Equation 2.7 and Equation 2.8, which give ΔH_{poly} and ΔG_{poly} (per monomer) for the copolymerization of ethylene and carbon dioxide according to this DFT investigation. It is important to note that the DFT calculations for the incorporation of carbon dioxide do not include one equivalent of ethylene as the BDE and Benson additivity methods do above. Thus, it is necessary to incorporate the ΔH_{poly} of ethylene into the first term of the equation, which represents the incorporation of C carbon dioxide monomers (-22.46 + 13.84 = -8.62). According to Equation 2.8, the copolymerization is expected to be exergonic for $E/C \geq$ 2.37 at room temperature. The ceiling temperature for the 1:1 copolymer is calculated to be -159°C.

$$\Delta G_{poly} = \frac{[C(-8.62) + (E - C)(-22.46)]}{C + E} - \frac{T\,[C(-0.03377) + (E - C)(-0.04147)]}{C + E}$$

Equation 2.7

$$\Delta H_{poly} = \frac{[C(-8.62) + (E - C)(-22.46)]}{C + E}$$

Equation 2.8

Figure 2.3 provides a graphical illustration of ΔG_{poly} versus the E/C ratio for each of the three calculational methods employed: bond dissociation energies, the Benson additivity method, and DFT. While these vary somewhat, they all suggest that the copolymerization thermodynamics are feasible at room temperature so long as a modest E/C quotient (1.64 - 2.56) is surpassed.
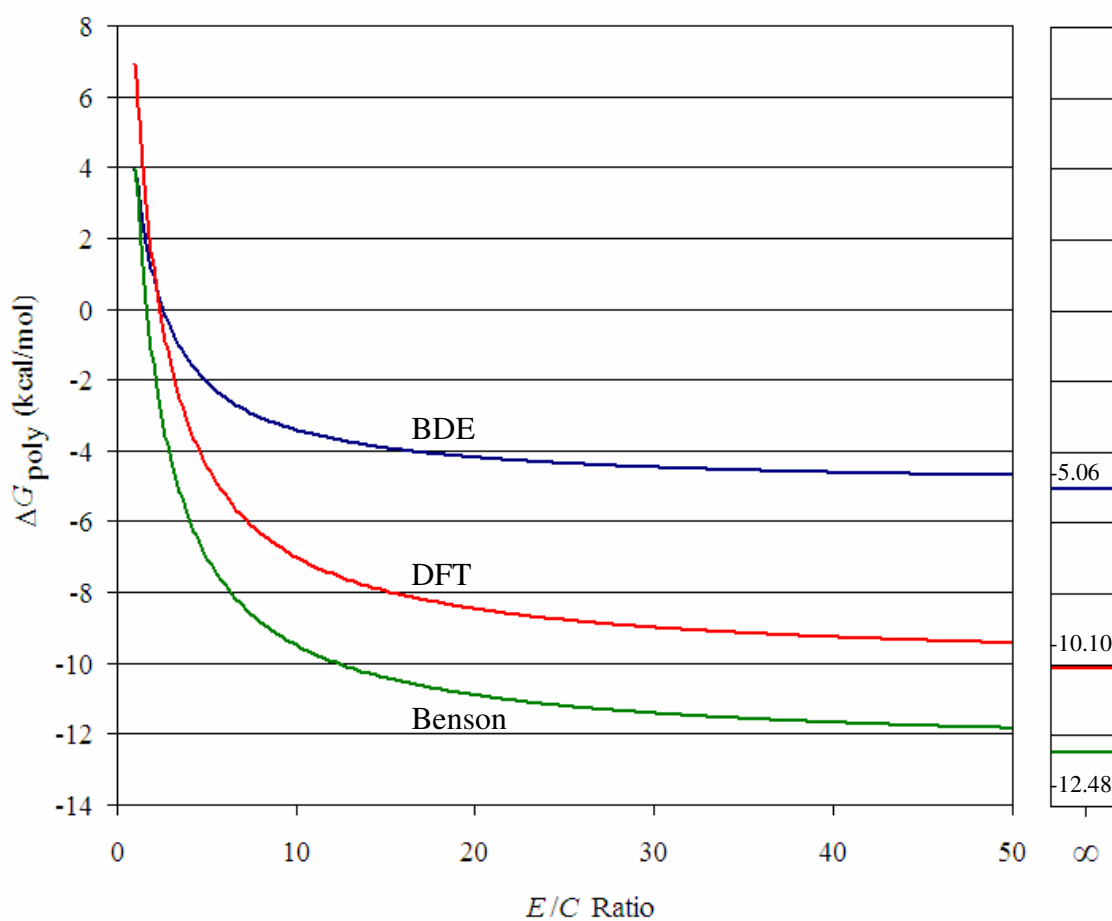
Figure 2.3: ΔG_{poly} per monomer (at 298.15 K) for varying ethylene/carbon dioxide ratios, as predicted by bond dissociation energy (BDE) calculations, the Benson additivity method and density functional theory (DFT) calculations.

Copolymerization results. Pyridine-diimine complexes **1**–**3** (Figure 2.4) were synthesized and activated with MAO (methylaluminoxane, 450-2000 equivalents), to test their activity towards ethylene/carbon dioxide copolymerization. Complexes of this type are known to be active for the homopolymerization of ethylene[19,45] and are reported to be active for the copolymerization of ethylene and CO_2.[35] Before attempting to repeat the ethylene/carbon dioxide copolymerization work of Zou et al., several successful control experiments were carried out, in which complexes were used to homopolymerize ethylene. A gas cylinder was charged with equimolar amounts of ethylene and carbon dioxide, and this gas mixture was used for the copolymerization attempts. Table 2.6 (entries 1–10) outlines the many polymerization reactions that were performed with various polymerization times, temperatures, and pressures. However, the resulting polymers contained only ethylene, as evidenced by the lack of a carbonyl peak in the ^{13}C NMR spectra (Figure 2.5), despite the fact that identical and more pressing conditions were used than those previously reported.[35]
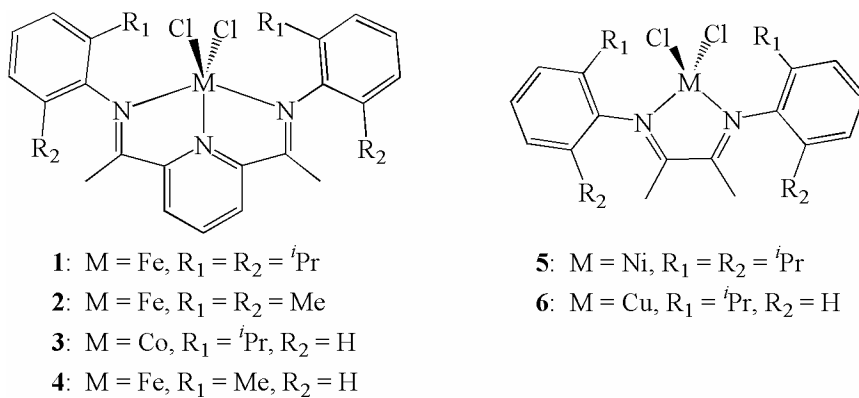
Figure 2.4: The late transition metal complexes investigated for ethylene/carbon dioxide copolymerizations, upon activation with MAO.

Table 2.6: Summary of Polymerization and Oligomerization Runs With **1-6**/MAO[a]

Entry	Precatalyst (mg)	Monomer(s)[b]	Time (min)	Temperature (°C)	Pressure (psi)
1	**1** (5)	E + C	60	25	75
2	**1** (4)	E + C	60	25	65
3	**1** (7)	E	45	25	105
4	**2** (5)	E + C	360	25	60
5[c]	**2** (5)	E + C	55	25	60
6	**2** (5)	E + C	120	25	88
7	**2** (5)	E + C	90	25	100
8	**2** (9)	E + C	60	25	100
9[d]	**2** (5)	E	25	25	105
10	**3** (10)	E + C	60	25	150
11[e]	**4** (10)	E + C	60	25	150
12[c]	**4** (20)	E + C	60	70	100
13	**4** (5)	E + C	60	25	60
14[c]	**5** (5)	E + C	80	25	60
15	**5** (5)	E + C	60	25	70
16	**6** (5)	E + C	60	25	60

[a] In 85 mL of toluene with 0.74 g MAO. [b] E = ethylene, C = CO_2, the E + C feed gas contained equimolar amounts of ethylene and CO_2. [c] In 85 mL of dichloromethane. [d] In 25 mL of toluene. [e] With 1.1 g of MAO.
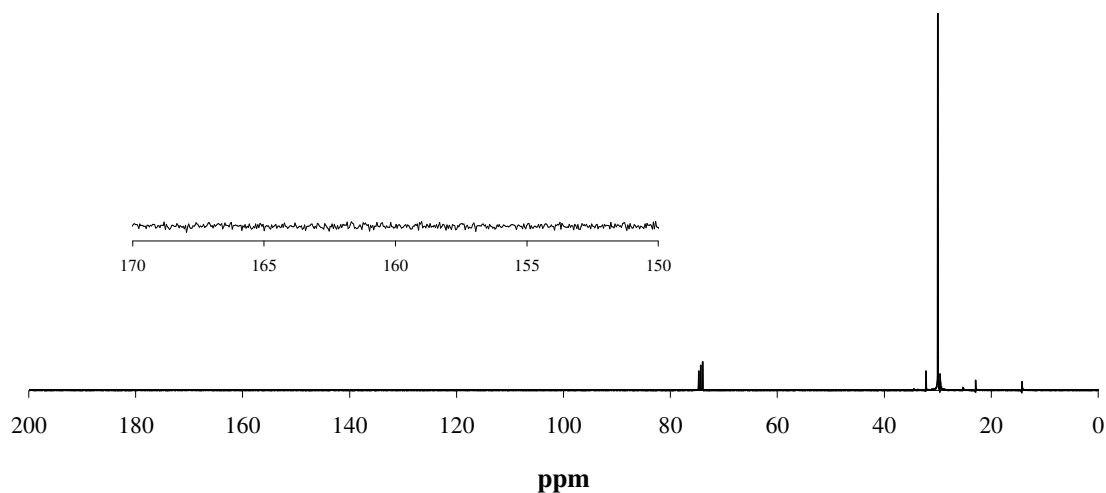
Figure 2.5: ^{13}C NMR spectrum of the polymer made by **1**/MAO (Table 2.6, entry 1) showing the absence of carbonyl peaks. For ^{13}C NMR spectra of all polymers produced, see Figures A.1 – A.10.

In an attempt to simplify the characterization of the products formed from the copolymerization reactions, catalyst systems were employed that are known to produce ethylene oligomers. It has been shown that by employing a less sterically-demanding ligand, the rate of chain transfer increases relative to the rate of propagation.[46-48] As a result, oligomers and low molecular weight polymers are formed, thereby easing characterization because of increased solubility in organic solvents compared to high molecular weight materials. We then synthesized complex **4**, which bears only a single methyl group on each aryl ring. After activation with MAO (450-1200 equivalents), **4** only produced toluene-soluble oligomers under various polymerization conditions with a 1:1 ethylene:carbon dioxide monomer feed (Table 2.6, entries 11-13). These oligomers were subjected to GC-MS analysis in an attempt to detect any CO_2 incorporation. A typical chromatogram, along with the representative mass for each GC peak, is shown in Figure 2.6. The masses correspond to the expected masses for $C_{10} - C_{36}$ oligomers with unsaturated end groups. No carbon dioxide incorporation was detected by GC-MS.
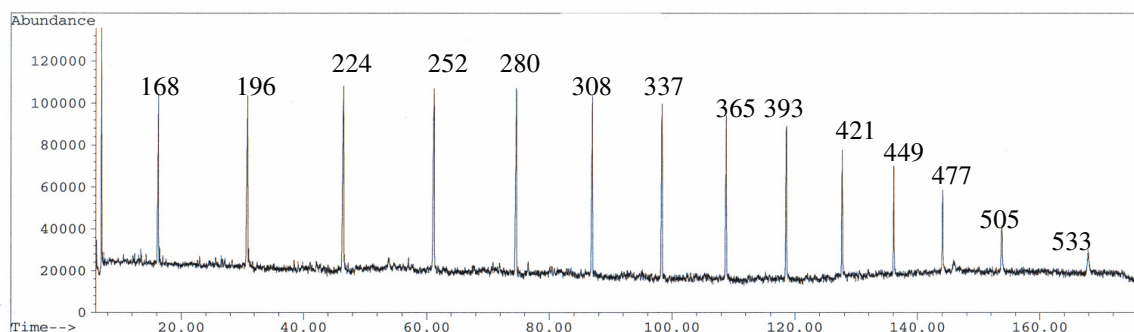
Figure 2.6: GC–MS of the oligomers produced by **4**/MAO (Table 2.6, entry 11) with the masses for each peak. Found were unsaturated ethylene oligomers, no CO_2 incorporation is evident.

In addition, α-diimine complexes of late transition metal have been shown to be active for the polymerization and oligomerization of ethylene.[49,50] Complexes **5** and **6** were synthesized in order to test their ability to incorporate CO_2 into a growing polyethylene chain. Again, lower molecular weight products were desired because their increased solubility facilitates characterization. After activation with MAO (1100-1300 equivalents), complexes **5** and **6** produced waxy solids and toluene-soluble oligomers, respectively. Neither high-temperature NMR nor GC-MS provided any evidence of CO_2 incorporation (see Appendix A).

CONCLUSIONS

The thermodynamic parameters for the incorporation of ethylene and the incorporation of carbon dioxide into a polyethylene chain were calculated using average bond dissociation energies, the Benson additivity method, and DFT calculations. These calculations indicate that a perfectly alternating ethylene/CO_2 copolymer is thermodynamically impossible above -167 °C, and is therefore inaccessible. However, the favorable thermodynamics for ethylene can offset the unfavorable thermodynamics of carbon dioxide and polymers with ethylene/carbon dioxide quotients greater than 2.37 (less than 29.7 mol% CO_2) should be possible at room temperature (DFT analysis). There are two major implications of these thermodynamic results on small molecule catalysis: 1) the 1:1 coupling of olefins (or alkynes) with carbon dioxide should be thermodynamically restricted; and 2) the 1:1 coupling of dienes (or enynes or diynes) with carbon dioxide should be feasible – and in several cases, this has been demonstrated.[51-55]

All attempts to reproduce the copolymerization results by Zou et al. have failed. Using identical and similar catalysts under identical and more stringent conditions, we were unable to detect any CO_2 incorporation into the polymeric and oligomeric products by ^{13}C NMR or GC-MS. These results are not surprising given that supercritical CO_2 can be used as the solvent in polymerizing olefins to the expected polyolefins using similar palladium complexes.[56,57]
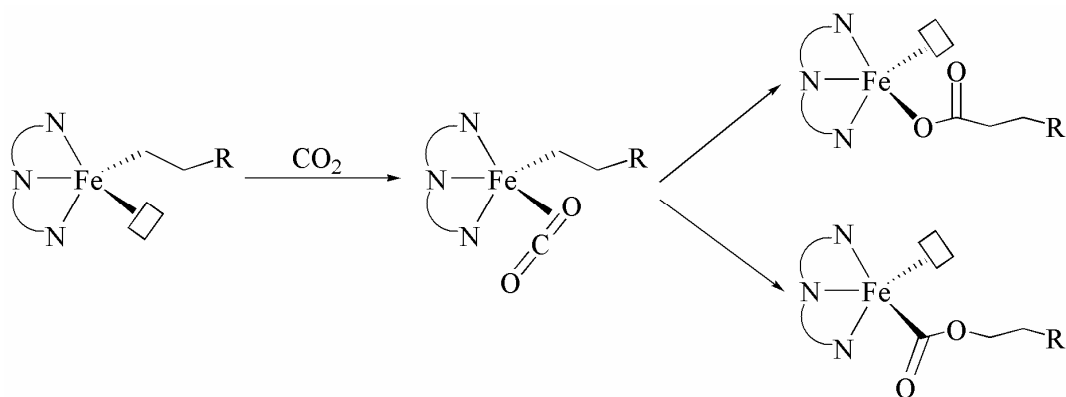
Figure 2.7: The normal (top) and inverse (bottom) insertion of CO_2 in to a metal-carbon bond.

While the thermodynamics of ethylene and carbon dioxide copolymerization are feasible for sufficiently large ethylene/CO_2 quotients, an effective kinetic pathway has yet to be found. Given our current understanding of organometallic chemistry, it is difficult to envisage a mechanism that would allow such an enchainment process, as normal CO_2 insertion would result in a metal-oxygen bond. We propose a pathway that relies on the inverse insertion of carbon dioxide into a metal-carbon bond – thus allowing maintenance of a metal-carbon bond throughout the propagation (Figure 2.7) – as a possible mechanism for the copolymerization. The motivations for achieving this copolymer are numerous and include the prospect of readily producing aliphatic polyesters that exhibit the mechanical properties of polyethylene, but are biodegradable because of the ester functionality located in the polymer backbone.

EXPERIMENTAL

General considerations. All air-sensitive procedures were performed under a purified nitrogen atmosphere in a glove box or by using standard Schlenk line and vacuum line techniques. Methylaluminoxane (MAO) (Albemarle, 30% in toluene) was concentrated to dryness and used as a solid. When required, solvents were distilled from an appropriate drying agent into oven-dried Straus flasks: ethanol and methanol from magnesium sulfate, tetrahydrofuran (THF) from sodium/benzophenone, and toluene from elemental sodium. All other chemicals and solvents were used as received. All compounds were prepared according to literature procedures. The general procedures are as follows.

Theoretical calculations. All calculations were performed using the Gaussian 03 suite of programs.[58] Geometry optimizations and frequency calculations were performed using Density Function Theory (DFT) employing Becke's 3-parameter hybrid functional (B3)[59] with the correlation functional of Lee, Yang and Parr (LYP)[60,61] starting from the extended chain conformation. Pople-style, double-ζ split polarized basis sets with pure d orbitals (6-31G(d') = 6-31G†) was used.[62,63] All energies include zero-point energies.

Pyridyl-diimine ligand synthesis. *Method A:* To a solution of 2,6-diacetylpyridine (3.00 g, 18.4 mmol) in 30 mL dry ethanol was added the appropriate amount (46 mmol, 2.5 eq.) of a substituted aniline and 5 drops of glacial acetic acid. The resulting solution was refluxed for 18 hours and then concentrated to approximately half the original volume. The mixture was cooled to 0°C and then filtered to isolate the

solid product. *Method B:* To a solution of 2,6-diacetylpyridine (3.00 g, 18.4 mmol) in 200 mL dry toluene was added the appropriate amount (46 mmol, 2.5 eq.) of a substituted aniline and 0.1 g *p*-toluene sulfonic acid. The resulting solution was azeotropically distilled using a Dean-Stark trap until 90% of the calculated amount of water was collected. The solution was poured into a separatory funnel and the organic layer was rinsed with 100 mL of a dilute aqueous sodium bicarbonate solution (3.0 g in 100 mL water). The aqueous layer was rinsed with diethyl ether (2 x 100 mL). All organic layers were combined and concentrated to dryness.

α-**diimine ligand synthesis.** To a solution of 2,3-butanedione (43.05 g, 0.50 mol) in 250 mL of dry methanol was added the appropriate amount of a substituted aniline (1.1 mol, 2.2 eq.). The resulting solution was shaken at room temperature for 36 hours, after which time a solid precipitate formed. The reaction was heated until homogeneous, then slowly cooled to 0°C. It was then filtered to isolate the solid product.

Precatalyst synthesis. Inside the glove box, 10 mmol of the ligand and 10 mmol of the metal dichloride were combined in a 100 mL round bottom flask and a swivel frit apparatus was attached. The apparatus was brought out of the box and evacuated. Approximately 70 mL of an appropriate solvent (dry ethanol or THF) were condensed in at -196°C, and the reaction mixture was slowly warmed to room temperature. The resulting slurry was either stirred at room temperature for 16 hours *or* refluxed for 30 minutes. The swivel frit apparatus was flipped and all soluble material was washed to the lower collection flask. The solvent was reduced to approximately half its original

volume. The swivel frit was flipped again and the solution was filtered to isolate the solid product.

General polymerization and oligomerization procedures. *CAUTION!* All polymerizations should be carried out in a fume hood behind a blast shield. Polymerizations were carried out in an 85 mL glass Lab-Crest® (Andrews Glass Co.) cylindrical polymerization reactor equipped with a 2 inch cylindrical stir bar able to provide ample surface agitation while stirring. In the glove box, the vessel was charged with the appropriate amount of precatalyst, MAO, and solvent. The reactor was assembled and brought out of the box. Rapid stirring was begun and the reactor was pressurized with ethylene or a 1:1 mixture of ethylene and CO_2. The reaction was quenched by slowly venting the vessel and adding ~5 mL of an acidic methanol solution (methanol plus 10% aqueous concentrated HCl). The insoluble polymer was collected by filtration. For oligomerizations, the quenched reaction mixture was poured into a separatory funnel and the aqueous layer was removed. The organic layer was washed with a 10% sodium bicarbonate solution, dried over $MgSO_4$, and subjected to GC-MS analysis.

CHAPTER III

ELECTRONIC DIFFERENCES IN A SERIES OF STERICALLY-EXPANDED CYCLOPENTADIENYL-BASED LIGANDS

SYNOPSIS

The octamethyloctahydrodibenzofluorenyl ligand has profound steric consequences when incorporated into metallocene and constrained geometry olefin polymerization catalysts. However, its electronic effects are less understood than the role played by the steric environment. The electronic nature of this ligand has been compared to a series of cyclopentadienyl analogues via DFT calculations, as well as NMR, UV-visible, and IR spectroscopies. Both metallocene and non-metallocene complexes of early- and mid-transition metals have been prepared and investigated. The octamethyloctahydrodibenzofluorenyl ligand is measurably more electron-rich than fluorenyl and other cyclopentadienyl analogues. These electronics are readily conveyed to the transition metal and perturb its static and catalytic behavior.

INTRODUCTION

Since their discovery, *ansa*-metallocenes have received considerable attention as olefin polymerization catalysts.[20,64,65] In the early 1990s, a new type of catalyst was reported that contained a cyclopentadienyl-based bridged η^1-amido ligand.[66-71] These catalysts, termed "constrained geometry catalysts" (CGCs), have been extensively studied because their ability to produce high molecular weight polymers at high polymerization temperatures makes them ideally suited for industrial use. Recent work in the areas of *ansa*-metallocenes[72-75] and CGCs[76] has utilized a sterically expanded ligand based on fluorene – 2,2,5,5,8,8,11,11-octamethyl-2,3,4,5,8,9,10,11-octahydrodibenzo[*b*,*e*]fluorene (OctH) – as a component in a highly active catalyst for olefin polymerization. OctH was first reported in 1980[77] and can now easily be synthesized in >200 g batches (92% yield). Recently, there have been numerous reports focusing on how the steric environment of the ligand affects the polymerization catalyst.[78-82] In particular, the addition of steric bulk to the fluorene plane – in the form of the Oct group – greatly increases the syndioselectivity of both *ansa*-metallocene[75] and CGC[83] propylene polymerization catalysts. However, there are relatively few attempts to elucidate the *electronic* consequences of incorporating sterically expanded ligands into transition metal-based catalysts.[84,85]

This chapter discusses explorations of the electronic differences in symmetric cyclopentadienyl-based ligands (Figure 3.1), via density functional theory (DFT) calculations, as well as NMR, UV-Vis and IR spectroscopies. We have synthesized both

metallocene and non-metallocene transition metal complexes of these ligands using early-, and mid-transition metals to show that the trend is specific to the ligands only.

Cyclopentadienyl
(**Cp**)

Pentamethylcyclopentadienyl
(**Cp***)

Fluorenyl
(**Flu**)

Octamethyloctahydrodibenzofluorenyl
(**Oct**)
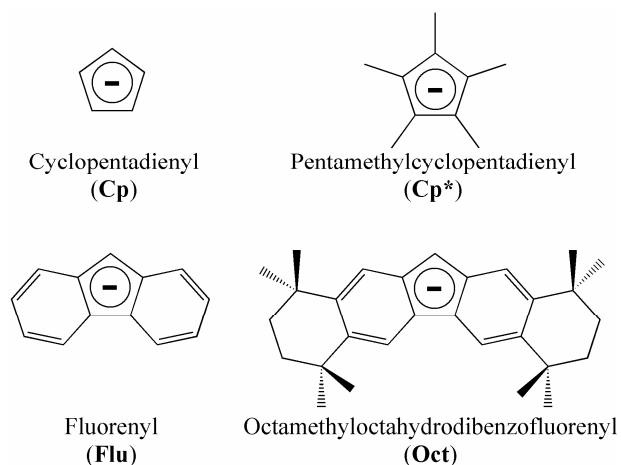
Figure 3.1. The series of sterically-expanded ligands explored.

RESULTS AND DISCUSSION

NMR studies. One simple indication of the electronic nature of molecules is their NMR chemical shifts. As the electron density on an atom increases, it becomes more shielded. As a result, its NMR resonance shifts upfield (to lower δ values). Of particular interest is the doubly benzylic CH_2 group of both FluH and OctH. The ^{13}C NMR spectra of OctH and FluH show a difference of 0.66 ppm for this carbon atom (δ 36.17 for OctH versus 36.83 for FluH). In addition, the proton NMR show the same effect. In the ^{1}H NMR spectra, the difference between OctH and FluH is nearly 0.1 ppm (δ 3.85 versus 3.94 for FluH).

In addition, the competitive deprotonation of OctH and FluH by *tert*-butyl lithium was followed by ^{1}H NMR (Figure 3.2) and the results are outlined in Table 3.1. Starting from a 1:1 mixture of OctH and FluH in THF-d_8, 1 μL aliquots of *tert*-butyl

lithium (1.5 M in pentane) were added. NMR spectra were taken after each addition, and the deprotonation was followed by observing the benzylic protons for the four possible species. The peaks colored blue correspond to Oct-based species (OctH at 3.75 ppm and OctLi at 5.44 ppm), while the peaks attributed to Flu-based species are colored red (3.84 ppm for FluH and 5.90 ppm for FluLi). After the fourth addition of base, all four species were observed in the ^{1}H NMR spectrum (Table 3.1, entry 5). The reaction was allowed to stand at room temperature for 150 minutes without adding additional aliquots of base in order to ensure that the reaction was at equilibrium. Another NMR spectrum taken after this time showed almost identical integrations for the four species, indicating that the reaction was indeed at equilibrium (Table 3.1, entry 6). Using Equation 3.1, we were able to calculate a K_{eq} of 7500 for the reaction shown in Scheme 1 from the integrations of these peaks. We were also able to calculate that the pK_a of OctH as 26.8, given a value of 23 for FluH (in DMSO) – an increase of almost 4 pK_a units. Since OctH contains four tertiary alkyl groups on the fluorene ring, this result correlates well with previous experiments that indicate that the addition of one t-butyl group to an aryl ring should increase the pK_a of a benzylic proton by almost 1 unit.[86]

$$pK_{a\ OctH} = pK_{a\ FluH} + log\left[\frac{\dfrac{I_{OctH}}{2}\ \ I_{FluLi}}{\dfrac{I_{FluH}}{2}\ \ I_{OctLi}}\right] \qquad \text{Equation 3.1}$$

Table 3.1: Percent of Each Species Present in the Competitive Deprotonation of OctH and FluH.[a]

Entry	Total Volume of Base Added (μL)[b]	FluH	OctH	FluLi	OctLi
1	0	49.85	50.15	0.00	0.00
2	1	45.91	51.63	2.46	0.00
3	2	43.35	52.60	4.04	0.00
4	3	10.69	64.81	24.50	0.00
5	4	0.23	66.19	32.35	1.22
6	4	0.23	66.79	31.77	1.21
7	5	0.00	53.86	35.15	10.99
8	6	0.00	48.41	36.98	14.61
9	7	0.00	41.91	38.57	19.52

[a] By ^{1}H NMR. [b] Each addition is 1 μL of t-butyllithium (1.5 M in pentane).
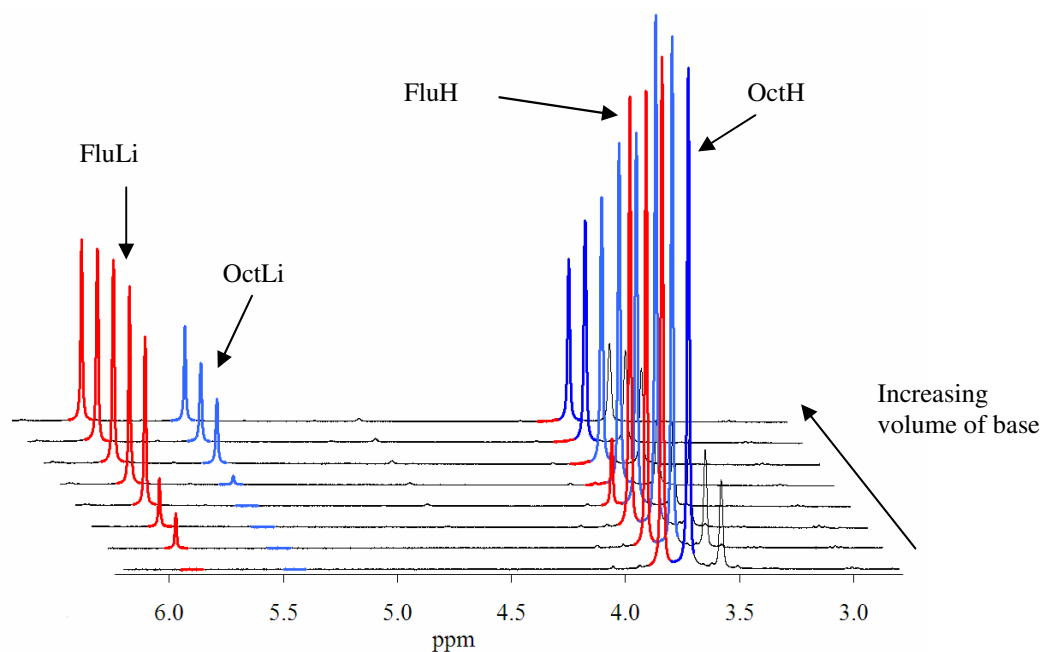
Figure 3.2. The competitive deprotonation of FluH and OctH by *tert*-butyl lithium. The small peak at 3.58 ppm is residual 2-proteo-solvent.
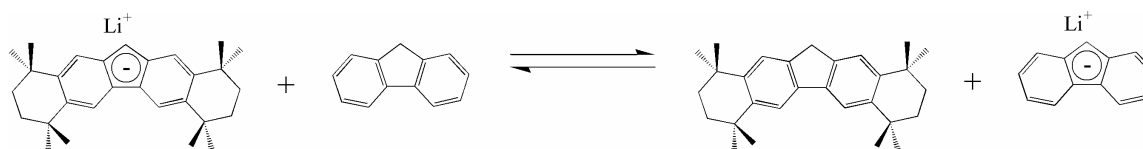
Figure 3.3. The isodesmic reaction studied by NMR and DFT calculations.

In addition to the NMR studies above, DFT calculations (B3LYP/6-31G†) were carried out on the isodesmic reaction shown in Figure 3.3. From these calculations, we determined a ΔH of -2.6 kcal/mol and a ΔG of -2.65 kcal/mol (at 298.15 K) indicating that the reaction favors the products. From this value for ΔG, we calculate a K_{eq} of 87.5, compared to 7500 for the NMR experiment. The discrepancy is likely due to the fact that the DFT calculations were carried out in the gas phase, without considering solvent effects. This over-estimates the stability of the large OctLi species, thereby placing too much emphasis on the starting materials. It is presumed that ΔH is actually more negative than these calculations predict.

Differences in *ansa*-metallocenes. To assess the electronic ramifications of the sterically expanded Oct-based ligands on transition metal complexes, a series of *ansa*-metallocenes were synthesized which utilize the Flu and Oct moieties (Figure 3.4). UV-Vis spectroscopy was employed to probe the ligand-to-metal charge transfer (LMCT) in these metallocene complexes, which is generally accepted to be responsible for the colors observed.[87] As the *ansa* ligand becomes more electron rich, the LMCT should become more facile, thereby shifting the LMCT bands to higher wavelengths (lower energy). Figure 3.5 shows the UV-Vis absorption spectra for a series of sterically expanded *ansa*-metallocenes. The addition of steric bulk to the fluorene plane shifts the

λ_{max} of the metallocene by approximately 22 nm. For the isopropylidine-bridged metallocene, the λ_{max} increases from 493 to 516 nm when Oct is substituted for Flu, which corresponds to a 2.59 kcal/mol decrease in energy for the LMCT. The energy of the LMCT is decreased by 2.30 kcal/mol (500 to 521 nm) for the diphenylmethylidine bridge upon the same substitution.

1: R = Me
2: R = Ph

3: R = Me
4: R = Ph
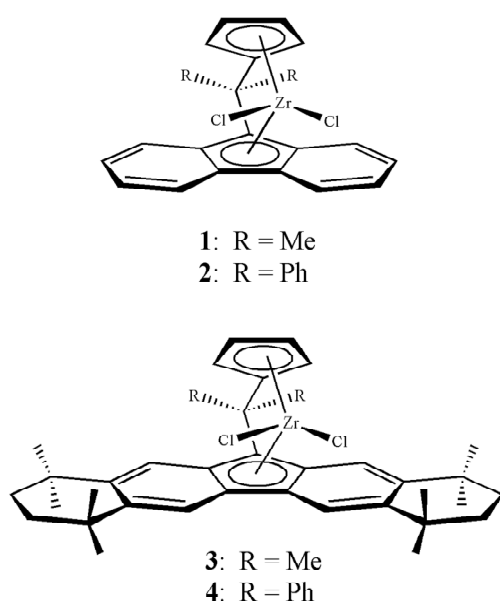
Figure 3.4: *ansa*-metallocenes investigated via UV-Vis spectrophotometry.
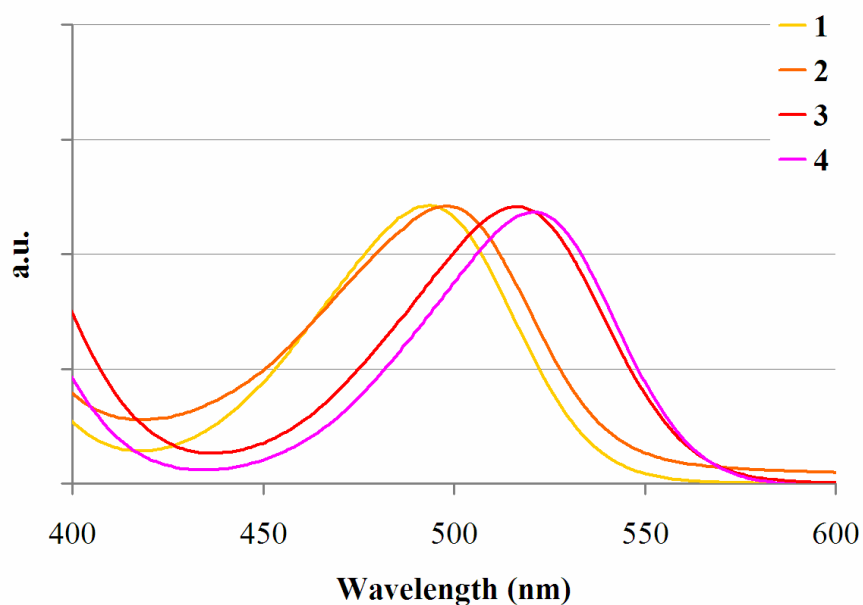
Figure 3.5: UV-Vis spectra of metallocenes **1-4**.

In addition, density functional theory (DFT) calculations (B3LYP 6-31G**/LanL2DZ) were performed on *ansa*-metallocenes **1** and **3**. From these calculations, pictures of the molecular orbitals were generated (Figure 3.6), and the HOMO-LUMO gaps were determined. The HOMO-LUMO gaps are of interest because the LMCT occurs from the HOMO to the LUMO. Our calculations show that the HOMOs of both metallocenes are largely ligand based, with approximately 64% on the fluorenyl portion of the ligand, and only a small contribution from the zirconium atom (Table 3.2). However, for the LUMOs, our calculations shows that the contribution from the zirconium atom has increased significantly (to ~33%) while the contribution from the Flu/Oct system has decreased substantially to approximately 16%. Flu-based **1** and Oct-based **2** were calculated to have HOMO-LUMO gaps of 35.77 and 33.89

kcal/mol respectively. This indicates that the LMCT is a lower energy transition for the Oct-based metallocene, **2** (by 1.88 kcal/mol), as the electron-rich Oct portion of the ligand facilitates the LMCT. This calculated difference of 1.88 kcal/mol correlates rather well with the 2.58 kcal/mol difference observed in the λmax from the UV-Vis spectra of the two metallocenes.

Table 3.2. Breakdown of MO Distribution for **1** and **3**.[a]

	Metallocene **1**		Metallocene **3**	
	HOMO (%)	LUMO (%)	HOMO (%)[b]	LUMO (%)
Zr	16.6	33.6	18.3	33.5
Flu/Oct ring system	64.8	15.6	63.4	16.8
^{i}Propylidene	0.4	6.7	0.4	6.6
Cyclopentadienyl	10.9	39.8	10.0	38.7
Chloride	7.3	4.3	8.0	4.4

[a] DFT calculations (B3LYP 6-31G**/LanL2DZ). [b] Values do not sum to 100% due to rounding.
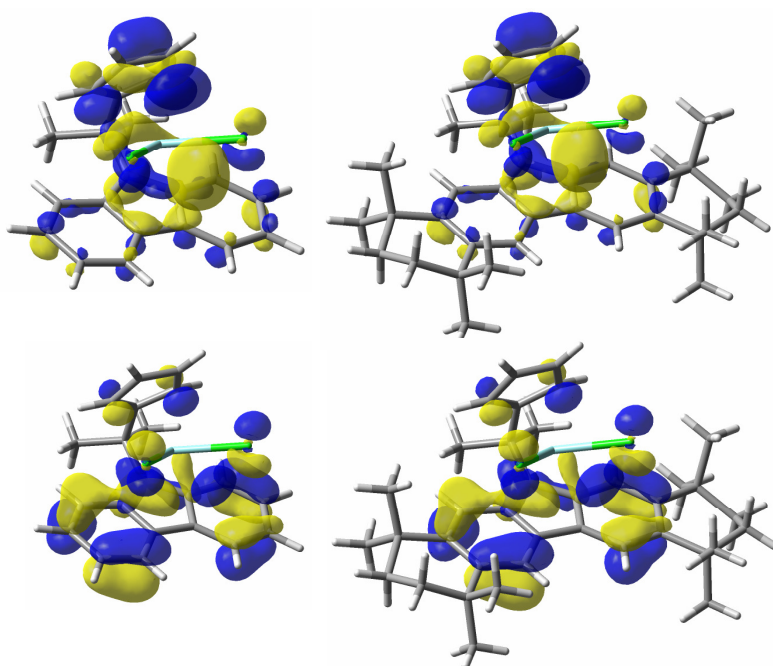
Figure 3.6: Calculated HOMO (bottom) and LUMO (top) for metallocenes **1** and **3**.

Infrared studies.[88] Manganese tricarbonyl compounds of Cp, Cp*, Flu, and Oct were synthesized (Figure 3.7) in order to further quantify the electronic differences between the ligands and to show that these differences are specific to the ligands. The electronic environment imparted by the organic ligands was assessed by infrared spectroscopy. Representative spectra are shown in Figure 3.8, and all carbonyl stretching frequencies are outlined in Table 3.3. Compared to the Cp analogue (**5**), the manganese center in **7** is slightly electron poor, owing to the electron withdrawing ability of the aryl rings. However, of the four compounds studied, the Oct-based species (**8**) is the most electron rich, due to the four electron-donating alkyl groups. Although the steric consequences of Oct likely prohibit the formation of a bis(Oct) zirconocene,

Parkin and coworkers have recently shown that the pentamethyl derived Cp is one of the

most electron donating cyclopentadienes available in a large series of zirconocenes.[89]
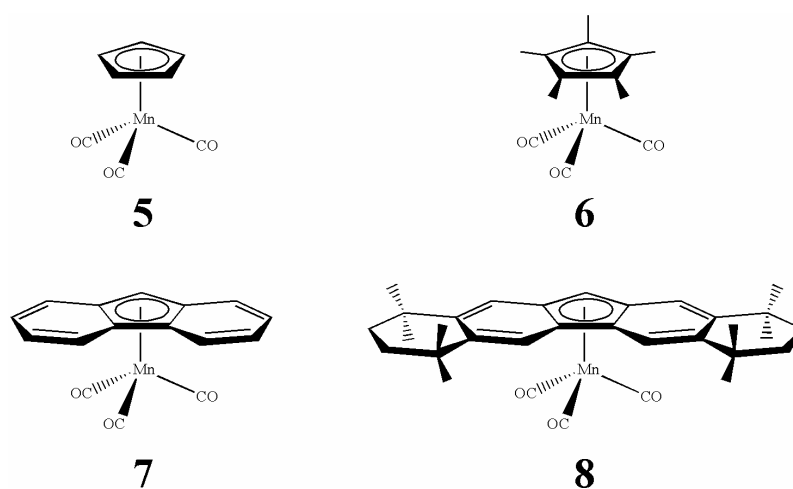
Figure 3.7: Manganese tricarbonyl compounds investigated via IR spectroscopy.

Table 3.3: Manganese Carbonyl Stretching Frequencies.[a]

		v_{CO} (cm^{-1})	
Compound	Substituent	Symmetric	Asymmetric
5	Cp	2022	1933
6[b]	Cp*	2001	1917
7	Flu	2016	1933
8	Oct	2009	1924

[a] Recorded as a THF solution. [b] Literature value,[90] recorded in CH_2Cl_2.

CONCLUSIONS

Oct has been compared to several symmetric cyclopentadienyl-based ligands in both metallocene and non-metallocene complexes via DFT calculations, UV-Vis and IR. In addition, the free protonated ligand was compared to fluorene by NMR and DFT calculations. In all cases, Oct is measurably more electron rich than the other ligands studied, as well as any other cyclopentadiene based ligands reported.

The competitive deprotonation of OctH and FluH was followed via ^{1}H NMR. From this, the pK_a of OctH was found to be 26.8, an increase of nearly one unit for each of the four tertiary alkyl groups attached to the fluorene ring. In addition, metallocenes that contain Oct are more electron rich than those containing Flu, as evidenced by the relatively low energy required for the LMCT. the molecular orbitals of metallocenes based on Oct and Flu were calculated using DFT.

EXPERIMENTAL

General considerations. All air-sensitive procedures were performed under a purified nitrogen atomsphere in a glovebox or by using standard Schlenk line and vacuum line techniques. Solvents were sparged with nitrogen and dried over molecular sieves using an M. Braun MB-SPS solvent purification system, dispensed into oven-dried and evacuated Straus flasks. All other chemicals were used as received. Metallocenes **1-4** were synthesized according to literature procedures. CpMn(CO)$_3$ is commercially available from Strem. Unless otherwise noted, compounds **5-7** were synthesized using procedures analogous to the previously published routes for the

synthesis of the Cp*,[91] Flu,[92] or Oct[93] complexes. Solution infrared spectra were recorded in THF on a Bruker Tensor 27 FTIR spectrometer using 0.1 mm NaCl sealed cells.

Theoretical calculations. DFT calculations were carried out with the Gaussian 03 suite of programs[58] using the gradient-corrected Becke exchange functional[59] and the correlation functional of Lee, Yang and Parr[60,61] (B3LYP). Full geometry optimization calculations were carried out on OctH, FluH, OctLi and FluLi using a 6-31G† basis set.[63] The reaction enthalpy (ΔH) was derived from the energy of each molecule (from the single-point calculation) corrected to enthalpy by the "thermal correction to enthalpy term" obtained from the frequency calculation. Single-point calculations were carried out on **7** and **9** using the geometries obtained from the crystal structures using a LanL2DZ basis set[94,95] for the Zr atom and 6-31G** for all other atoms.[96,97]

2,5-dichloro-2,5-dimethylhexane. A 3 L Erlenmeyer flask was charged with 200.00 g of 2,5-dimethyl-2,5-hexanediol and 1.0 L of concentrated aqueous HCl. The resulting slurry, which was periodically shaken by hand, sat at room temperature for 48 hours. Water was added (~800 mL) and the slurry was extracted with diethyl ether (3 x 250 mL). The combined ether layers were dried over MgSO$_4$ and concentrated to ~200 mL. The flask was heated to redissolve the formed precipitate, then slowly cooled to recrystallize the product. The white crystalline solid was isolated via vacuum filtration and dried overnight on the filter (237.6 g, 94.7%). ^{1}H NMR (CDCl$_3$): δ, 1.98 (s, 4H, CH_2) 1.58 (s, 12H, CH_3). ^{13}C NMR (CDCl$_3$): δ 70.4, 41.4, 32.9.

Synthesis of OctH. A nitrogen purged 1 L round bottom flask was charged with fluorene (22.65 g, 136.3 mmol) and 2,5-dichloro-2,5-dimethylhexane (50.00 g, 273.2 mmol) and the solids were dissolved in ~450 mL of nitromethane. A solution of $AlCl_3$ (22.30 g in 50 mL nitromethane) was added via syringe over 20 minutes. The resulting dark blue solution was stirred at room temperature for 48 hours. The reaction mixture was poured into 1 L of ice water and the resulting light green precipitate was collected via vacuum filtration. The solid was triturated in dry ethanol for 24 hours, filtered and recrystalized from toluene to yield 48.3 g (92.1 %) of a white crystalline solid. ^{1}H NMR (CDCl$_3$): δ 7.63 (s, 2H, CH_1), 7.41 (s, 2H, CH_1), 3.75 (s, 2H, Ar$_2$CH_2), 1.72 (apparent s, 8H, CH_2), 1.38 (s, 12H, CH_3), 1.32 (s, 12H, CH_3). ^{13}C {^{1}H} NMR (C$_6$D$_6$): δ 143.6, 143.5, 141.2, 139.8, 123.2, 117.6, 36.6, 35.8, 35.7, 34.95, 34.93, 32.7, 32.6.

Synthesis of (C$_{29}$H$_{37}$)Li (OctLi). In a nitrogen filled glove box, octamethyloctahydrodibenzofluorene (4.133 g, 10.69 mmol) was dissolved in toluene (50 mL) and *n*-butyllithium (5.13 mL of a 2.5 M solution in hexanes, 13 mmol) was added via syringe. The flask was attached to a swivel frit and the apparatus was affixed to the vacuum line. After heating to 75 ˚C for 14 hours, the precipitated solid was collected by filtration. Drying *in vacuo* afforded the pink product in 97.0% yield (4.070 g).

Synthesis of (C$_{13}$H$_9$)Li (FluLi). In a nitrogen filled glove box, fluorene (45.050 g, 271.03 mmol) was charged to a 500 mL round bottom flask and assembled to a swivel frit. The frit was then evacuated on the vacuum line and diethyl ether (300 mL) condensed in at 77 K. As the reaction was warming to room temperature, *n*-butyllithium

(120 mL of a 2.5 M solution in hexanes, 300 mmol) was then added via syringe. After 16 hr the solvent was removed *in vacuo*. Heptane (250 mL) and diethyl ether (100 mL) are vacuum transferred in at 77 K. The mixture is warmed to room temperature and stirred for 1 hr, at which time the solid product is collected by filtration. The ether is then removed *in vacuo* and the product washed with heptane (2 x 25 mL). Drying *in vacuo* afforded the yellow product in 95.3% yield (44.472 g).

Synthesis of (η^5-C$_{29}$H$_{37}$)Mn(CO)$_3$ (7). In a nitrogen filled glove box, OctLi (0.786 g, 2.00 mmol) and BrMn(CO)$_5$ (0.550 g, 2.00 mmol) were combined in a 100 mL receiving flask and sealed with a 180˚ needle valve. The flask was then evacuated on the vacuum line and THF (50 mL) was condensed in at 77 K. The reaction was slowly warmed to room temperature and stirred for 24 hours, at which time the solvent was removed *in vacuo*. The resulting yellow solid was extracted into pentane (60 mL) and filtered through a pad of celite inside a swivel frit. Concentration to 20 mL and stirring overnight afforded the title compound as a yellow powder. The precipitated solid was then collected by filtration, washed with pentane and dried *in vacuo* to yield 180 mg. A second crop is obtained from subsequent concentration of the filtrate to 6 mL to yield 0.319 g. The yield for two crops is 0.499 g (47.6%). Yellow needle-like crystals were grown from a saturated solution in pentane being slowly evaporated into a surrounding solution of toluene at -36 ˚C. Crystals can also be grown by cooling a saturated solution in pentane to -36 ˚C. ^{1}H NMR (C$_6$D$_6$): δ 1.21 (s, 6H, Oct-C*H*$_3$), 1.23 (s, 6H, Oct-C*H*$_3$), 1.29 (s, 6H, Oct-C*H*$_3$), 1.30 (s, 6H, Oct-C*H*$_3$), 1.52 (apparent s, 8H, Oct-C*H*$_2$), 5.22 (s, 1H, Oct-C^9*H*$_1$), 7.33 (s, 2H, Oct-C*H*$_1$), 8.09 (s, 2H, Oct-C*H*$_1$). ^{13}C {^{1}H} NMR (C$_6$D$_6$):

δ 227.1, 147.5, 144.0, 122.4, 121.6, 106.3, 95.5, 58.2, 35.5, 35.40, 35.36, 35.36, 33.0, 32.94, 32.92, 32.7.

Synthesis of (η^5-C$_{13}$H$_9$)Mn(CO)$_3$ (6). In a nitrogen filled glove box, FluLi (0.344 g, 2.00 mmol) and BrMn(CO)$_5$ (0.550 g, 2.00 mmol) were combined in a 100 mL receiving flask and sealed with a 180° needle valve. The flask was then evacuated on the vacuum line and THF (50 mL) was condensed in at 77 K. The reaction was slowly warmed to room temperature and stirred for 23 hours, at which time the solvent was removed *in vacuo*. The resulting yellow solid was extracted into pentane (60 mL) and filtered through a pad of celite inside a swivel frit. Concentration to 5 mL afforded the title compound as a yellow powder. The precipitated solid was then collected by filtration, washed with pentane and dried *in vacuo* to yield 0.258 g (42.4%). ^{1}H NMR (C$_6$D$_6$): δ 7.57 (d, $^3J_{HH}$ = 8.7 Hz, 2H, Ar-*H*), 7.04 (d, $^3J_{HH}$ = 8.4 Hz, 2H, Ar-*H*), 6.81 (td, $^3J_{HH}$ = 6.6 Hz, $^4J_{HH}$ = 1.2 Hz, 2H, Ar-*H*), 6.74 (td, $^3J_{HH}$ = 6.6 Hz, $^4J_{HH}$ = 1.2 Hz, 2H, Ar-*H*), 4.93 (s, 1H, Ar-*H*-Ar). ^{13}C {^{1}H} NMR (C$_6$D$_6$): δ 22.62, 127.4, 125.3, 125.0, 124.8, 106.7, 95.7, 60.4.

CHAPTER IV

PROBING THE ACTIVATION OF METALLOCENES VIA

UV-VISIBLE SPECTROSCOPY

SYNOPSIS

Prior to activation with methylaluminoxane (MAO), the metallocenes studied exhibit a ligand-to-metal charge transfer (LMCT) proportional to the number of electron-donating substituents attached to the fluorenyl ring. However, upon activation with MAO, the steric bulk of the ligands dominate the LMCT by influencing the distance between the cationic zirconium center and the anionic MAO. Time-dependent changes in the observed λ_{max} and the catalytic activity are attributed to the changing distance between the zirconocenium cation and the MAO anion as the MAO changes structure in solution. Evidence is presented that MAO slowly changes structure after activation so that it can form a closer-contact ion pair with the zirconocenium cation – likely through a bridging methyl group. Polymerization and UV-Vis experiments run with increasing amounts of MAO show that the catalysts reach their maximum activity and maximum λ_{max} with the same MAO:Zr ratio, and the activity decreases at greater MAO:Zr ratios – although the optimum ratio is not the same for all catalysts. The decrease in activity at high MAO concentrations is likely due to excess trimethyl aluminum (TMA). However, experiments contradict the generally-accepted belief that TMA binds to the catalytically-active zirconocenium cation.

INTRODUCTION

In the recent past, *ansa*-metallocenes have received much attention as homogeneous catalysts for olefin polymerization.[98-102] A great deal of the work in this area has focused on compounds based on the original $(CH_3)_2C(\eta^5\text{-}C_5H_4)(\eta^5\text{-}C_{13}H_8)MX_2$ *ansa*-metallocenes of Ewen.[27,103] The activity of these compounds is due to the generation of an electron-deficient cationic species with an open coordination site at the metal center. This is usually accomplished through the use of a co-catalyst/activator such as methylaluminoxane (MAO) (for X = halogen), $[C(Ph)_3]^+[(B(Ar^F)_4]^-$ or $B(Ar^F)_3$ (for X = alkyl).[104] Once activated, the cationic metallocene and the anionic activator are in equilibrium between the close-contact ion pair and the solvent-separated ion pair, which is generally accepted to be the active catalytic species (Figure 4.1). Fluorenyl-based catalysts (**1**, Figure 4.2) are generally less active than the sterically-expanded homologues.[75] It is believed that sterically expanded catalysts, such as **4**, which is based on octamethyloctahydrodibenzofluorenyl (Oct), are more active because they make the close contact ion pair less favorable.[75]
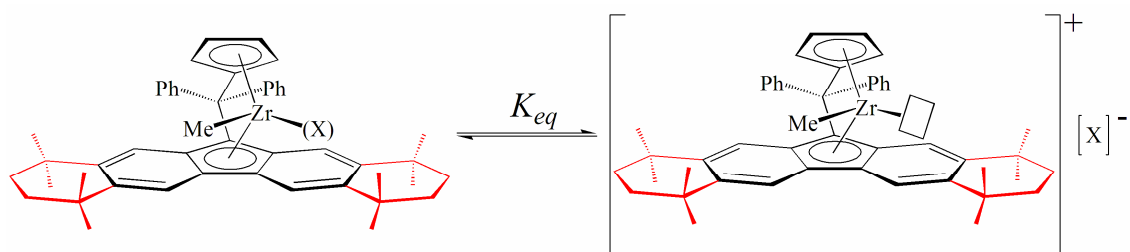
Figure 4.1: Equilibrium established upon activation of *ansa*-metallocenes, generating the catalytically active metallocenium cation.
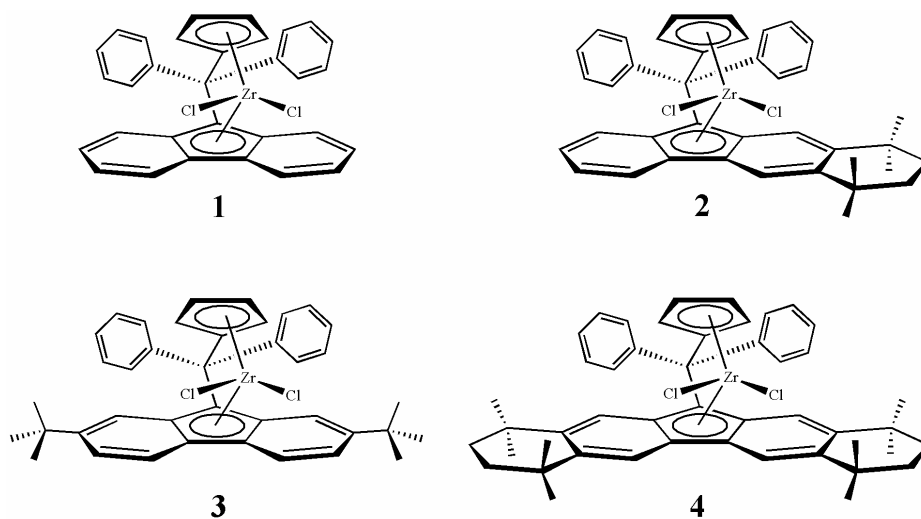
Figure 4.2: The *ansa*-metallocenes precatalysts studied upon activation with MAO.

The intense absorption bands of these metallocenes strongly indicate that the observed colors are due to ligand to zirconium (IV) charge transfer transition.[105] As the average metal center becomes more cationic in nature (that is, K_{eq} increases for the equilibrium in Figure 4.1), the ligand-to-metal charge transfer (LMCT) should become more facile, thereby leading to a shift in the observed absorption spectra.[87] It has been

suggested that UV-Vis spectrophotometry could be a powerful tool to probe the nature of the active structures in zirconocene-mediated olefin polymerization.[106] To this end, we have used UV-Vis spectrophotometry to observe the LMCT for **1**-**4** – both in the pre-catalyst and upon activation. We have rationalized changes in the absorption spectra over time, and we have correlated these changes to changes in the catalytic activity for the production of polyethylene (PE).

RESULTS AND DISCUSSION

      Time-dependent activation.   The generally-accepted mechanism for the activation of metallocenes with MAO involves replacing one chloride with a methyl group and abstracting the other chloride to form a cationic metal center with an open coordination site. Upon activation with MAO, metallocenes **1**-**4** exhibit an immediate bathachromic shift (red shift), indicating a lower barrier to the LMCT, which correlates to the formation of the cationic metal center.   In addition, sterically-expanded metallocenes **2**-**4** undergo a time-dependent hypsochromic shift (blue shift) following the initial activation.

      Upon activation with MAO, metallocene **1** undergoes an immediate red shift from 500 nm to 552 nm (ΔE = -4.26 kcal/mol). This indicates that the LMCT has become more facile, which corresponds to the formation of the metallocenium cation. However, unlike metallocenes **2**-**4**, the fluorenyl-based metallocene does not show a time-dependent blue shift after activation (Figure 4.3), instead exhibiting a constant λ_{max} of 552 nm. By comparison, **4** also exhibits an immediate red shift upon activation with

MAO. Upon addition of MAO to a solution of **4** in toluene, the observed λ_{max} shifts from 521 nm to 622 nm (ΔE = -8.91 kcal/mol); again corresponding to the generation of the metallocenium cation (Figure 4.4). The initial LMCT is measured to be more facile for **4** than for **1** ($\Delta\Delta E$ = -4.65 kcal/mol).
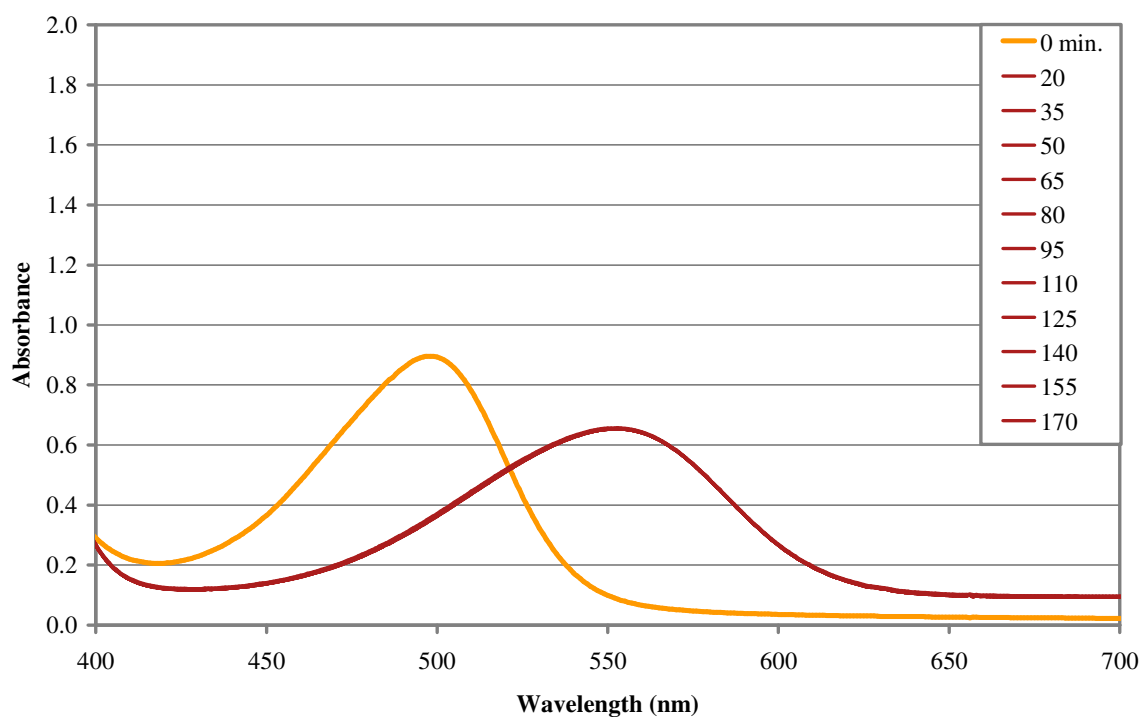
Figure 4.3: UV-Vis spectra of **1**/MAO over three hours. 0.25 mM in toluene, activated with 5000 eq. MAO at t = 0 min. ε_0 = 3573, ε_i = ε_f = 2215 $M^{-1}cm^{-1}$. All spectra taken 5-170 minutes are identical in the range 400-700 nm.
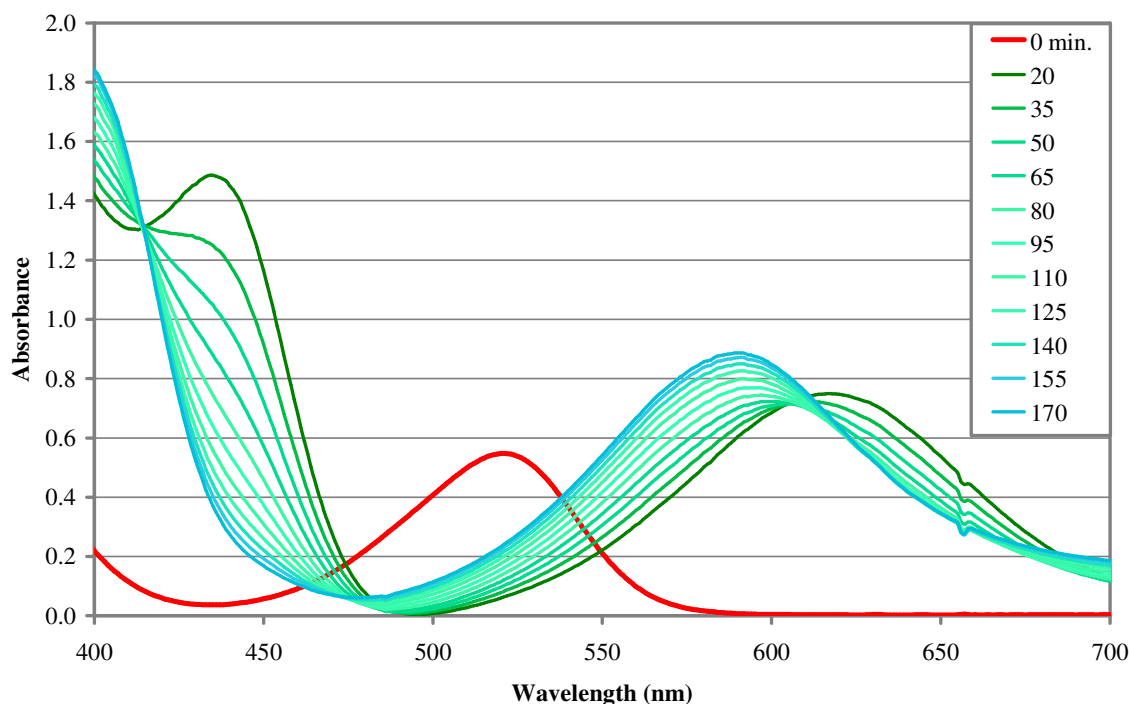
Figure 4.4: UV-Vis spectra of **4**/MAO over three hours. 0.25 mM in toluene, activated with 5000 eq. MAO at t = 0 min. $\varepsilon_0 = 2549$, $\varepsilon_i = 3194$, $\varepsilon_f = 3582$ M^{-1}cm^{-1}.

These observations can be explained in two ways. The energy required for the LMCT can be overcome more easily if the ligand is more electron rich, or if the metal is more electron poor. With four electron-donating tertiary alkyl groups, the ligand for metallocene **4** is more electron rich, which explains the difference observed in the UV-Vis spectra before activation. Before the addition of MAO, **1** has a λ_{max} of 500 nm compared to 521 nm for **4** – a difference of 2.3 kcal/mol. Therefore, the electronic differences in the two metallocene ligands can account for some, but not all of the 4.65 kcal/mol difference we observe in the λ_{max} of the species after activation. The remainder must be attributed to the zirconium center in metallocene **4** being more cationic than that

of **1** after activation. This can be explained by examining the proposed structure of MAO, which calculations[107-110] and NMR studies[111] indicate has a complex cage-like structure consisting of approximately 10-30 [AlOMe] units.[108,112,113] After activation, the added steric bulk of metallocene **4** is more efficient at holding the large counter anion away from the metallocenium cation as compared to the sterically-open metallocene **1**. As a result, the average metal center in **4** is more cationic than in **1**, further decreasing the energy barrier for LMCT. However, over the course of 3 hours, metallocene **4** undergoes a slow blue shift down to 587 nm. This indicates that the LMCT is becoming more difficult over time. Presumably, the electron-donating ability of the ligand does not change over this time period. Therefore, the change must be attributed to the average zirconium center becoming less cationic. This indicates that the MAO counter anion forms a closer contact ion pair with the zirconocenium cation (that is, K_{eq} is decreasing for Figure 4.1). Initially, the steric bulk imposed by the ligand of **4** is able to hold the MAO counteranion at bay, leading to an average zirconium center with significant cationic character. However, over time, the MAO anion is able to rearrange in order to come to a structure that is "pointier" and better able to form the close contact ion pair with the zirconium center.

For the metallocenes **2** and **3**, which have intermediate amounts of steric bulk, intermediate energies are observed for the LMCT in the UV-Vis spectra, as well as intermediate times required to reach an equilibrium λ_{max} (Figures 4.5 and 4.6, respectively). Since both metallocenes have two electron donating tertiary alkyl groups, one might expect for the energies associated with the LMCT for these two metallocenes

to be between that observed for **1**, which has no electron donating groups; and **4**, which has four. Indeed, before activation, both metallocenes have a λ_{max} of 510 nm, which indicates that the energy barrier associated with the LMCT for these two metallocenes is 1.12 kcal/mol lower than that observed for **1** and 1.18 kcal/mol higher than the barrier observed for the LMCT in **4** – putting metallocenes **2** and **3** directly in the middle.
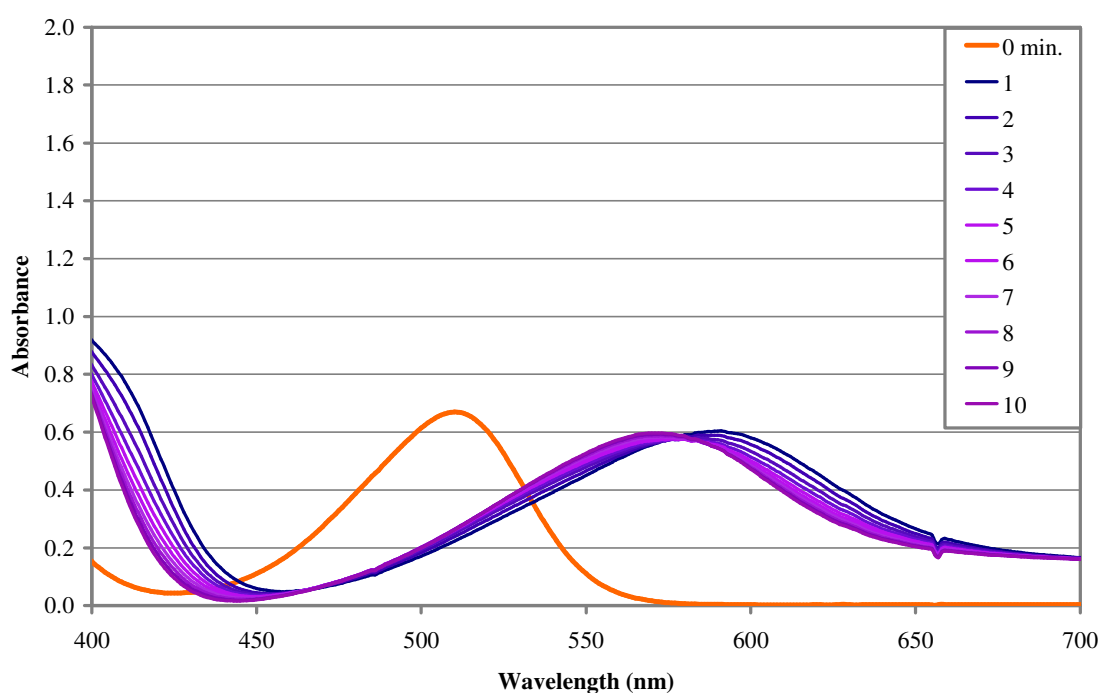
Figure 4.5: UV-Vis spectra of **2**/MAO over 10 minutes. 0.25 mM in toluene, activated with 5000 eq. MAO at t = 0 min. ε_0 = 2677, ε_i = 2455, ε_f = 2384 $M^{-1}cm^{-1}$.
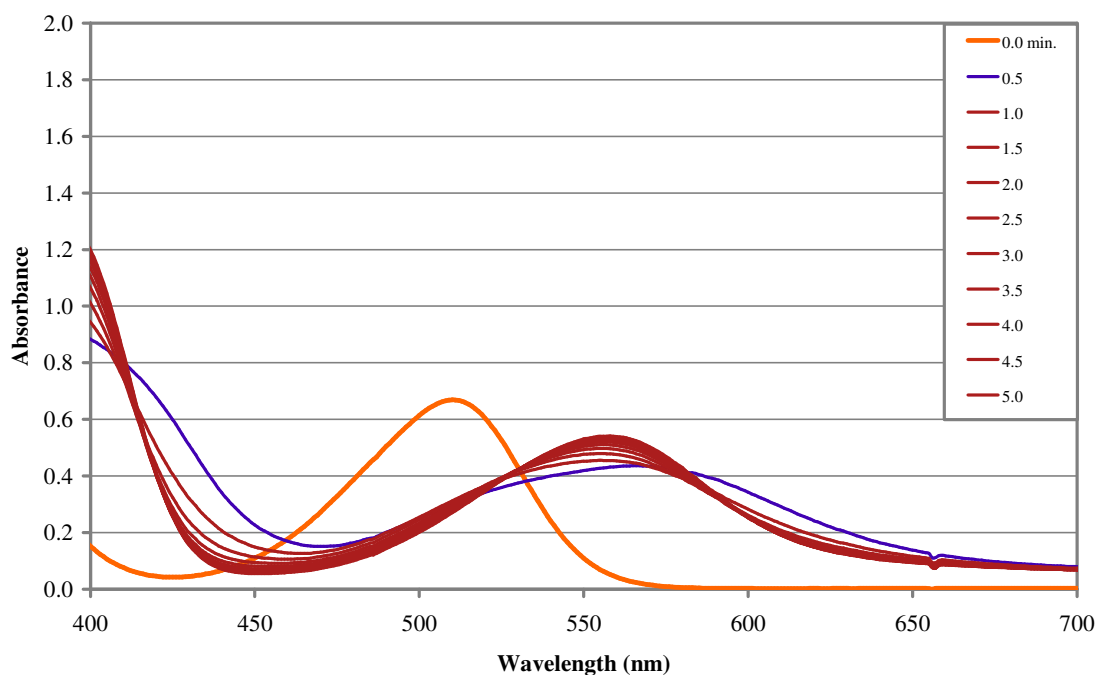
Figure 4.6: UV-Vis spectra of **3**/MAO over 5 minutes. 0.25 mM in toluene, activated with 5000 eq. MAO at t = 0 min. $\varepsilon_0 = 2677$, $\varepsilon_i = 1836$, $\varepsilon_f = 1990$ M^{-1}cm^{-1}.

Like **4**, metallocenes **2** and **3** also undergo a time-dependent blue shift after activation, although the time required to reach the equilibrium λ_{max} is much shorter. This indicates that the MAO counteranion requires less time in order to rearrange into a geometry that can bind to the cationic zirconium center. Since the ligands for these two metallocenes are much less sterically-demanding when compared to **4**, the MAO counteranion has to undergo a less extensive geometry rearrangement in order to be able to reach the zirconocenium cation.

Previous theoretical studies on the activation of metallocenes have focused on methide abstraction from substituted bis(cyclopentadienyl) zirconocenes by B(C$_6$F$_5$)$_3$.[114] These studies indicated that in all cases, the enthalpy of activation of the pre-catalyst is

negative and the magnitude of ΔH is influenced by both the steric and electronic contributions of the ligand. However, according to those reports, the electron-donating ability of the ligand was the predominating factor, with the steric environment of the ligand contributing to a much lesser extent. This is contrary to what we have observed for the abstraction a chloride from *ansa*-metallocenes by MAO. In particular, **2** and **3** both have two tertiary alkyl groups attached to the fluorenyl portion of the ligand. Therefore, if they followed the model proposed by Ziegler, the two metallocenes should behave almost identically. However, we observe a difference of several minutes in the amount of time required to reach their respective equilibrium λ_{max} values, as well as a difference in the λ_{max} values themselves. This leads us to conclude that not only is the amount of steric bulk important in this series of metallocenes, but the location of the sterically-demanding groups is also very important.

Overall, the effect of time on the λ_{max} of the various catalysts studied is summarized in Figure 4.7. As the steric environment around the zirconium center increases in the order **1** < **2** ≈ **3** < **4**, the effects are observed in the LMCT both before and after activation with MAO. Before activation (time < 0 min.), the ease of the LMCT is controlled by the electronics of the metallocene. With four tertiary alkyl groups, **4** is the most electron rich metallocene in the series. As such, the absorption associated with the LMCT is observed at an energy lower than the other three metallocenes. Metallocene **1** has no electron donating groups on the ligand, making the metallocene relatively electron-poor. Accordingly, the LMCT absorption is located at the highest energy of any of the metallocenes in this series. Both **2** and **3** have two tertiary alkyl

groups attached to the fluorenyl portion of the ligand. As expected, the energy associated with the LMCT for these two metallocenes is equally spaced between the energies observed for **1** and **4**.

However, after activation (time > 0 minutes), the steric environment of the ligand dominates. The four bulky tertiary alkyl groups of metallocene **4** are able to hold the MAO counteranion farther away from the cationic zirconium center. As a result, the average zirconium center is more electron deficient, thereby decreasing the energy required for the LMCT. However, over the course of three hours, the MAO is able to change geometries in order to "fit" into the zirconium center. This results in a less electron deficient metal center and raises the energy required for the LMCT. Metallocene **1**, which has no added steric bulk, does not exhibit any time-dependence in the energy barrier to LMCT. Presumably, this means that the MAO counteranion does not need to undergo any geometry changes in order to form the close-contact ion pair. The two metallocenes with intermediate amounts of steric bulk, **2** and **3**, exhibit a very rapid change to the equlibrium λ_{max} values. This is consistent with the MAO counteranion having to only slightly change its geometry in order to be able to form the close-contact ion pair.
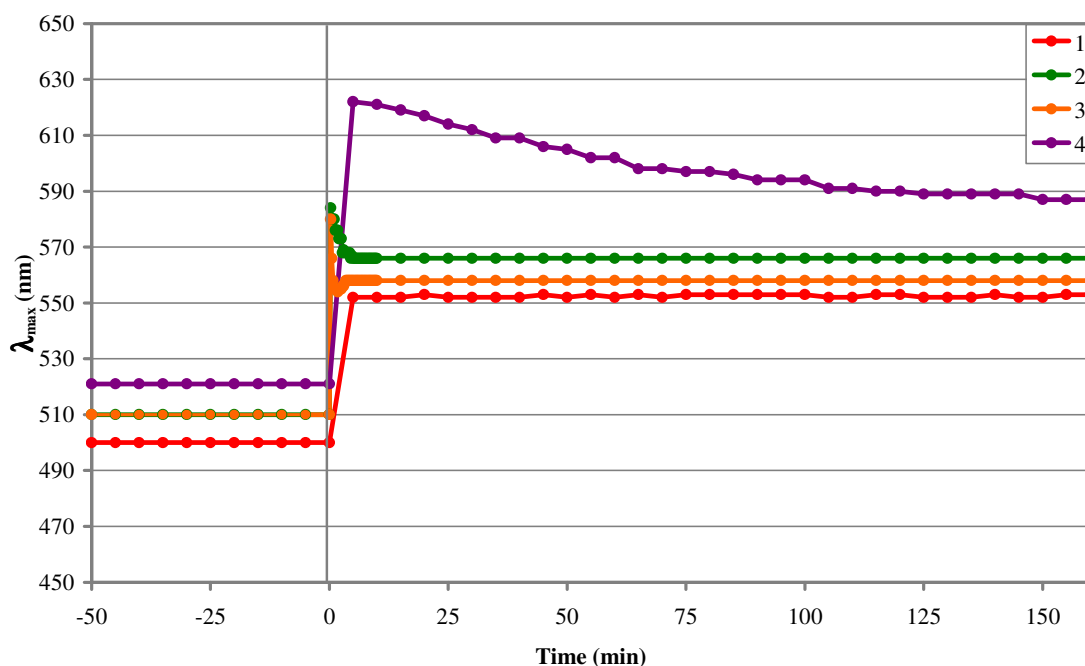
Figure 4.7: The effect of time on the observed λ_{max} of metallocenes **1**-**4**.

In order to further elucidate the cause of the time-dependent shifts observed in the UV-Vis spectra, dimethyl metallocenes **5** and **6** (Figure 4.8) were synthesized and their activation with MAO and with $B(C_6F_5)_3$ was followed by UV-Vis spectrophotometry. Upon activation with $B(C_6F_5)_3$, **5** and **6** undergo immediate red shifts, with the newly observed λ_{max} values remaining essentially constant for the next three hours (Figure 4.9). This is expected since the discrete counteranion – $[MeB(C_6F_5)_3]^-$ – has a static structure and, unlike MAO, cannot change geometries in order to form a closer-contact ion.
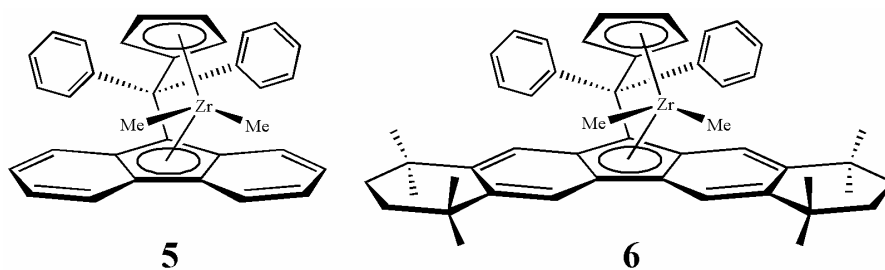
Figure 4.8: The dimethyl analogues studied upon activation with MAO or $B(C_6F_5)_3$.
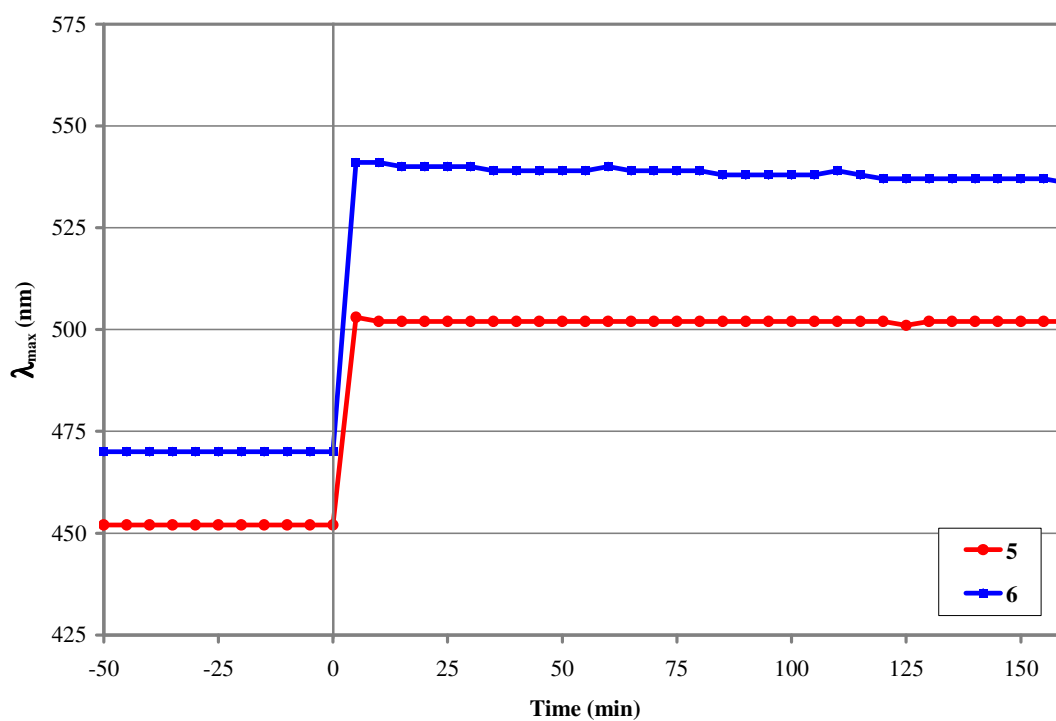
Figure 4.9: The observed λ_{max} values for **5** and **6** upon activation with $B(C_6F_5)_3$. 0.25 mM in toluene, activated with 1.0 eq. $B(C_6F_5)_3$ at t = 0 min.

However, **5** and **6** can also be activated using MAO, presumably forming the same methyl zirconocenium cations[21] which result from the activation of **1** and **4** with MAO, respectively. Upon activation of **6** with MAO, an immediate red shift is observed, as it was for the dichloride (**4**). However, unlike the activation of **4** with MAO, **6**/MAO showed no time-dependent blue shift following the initial red shift (Figure 4.10). It is also noteworthy that the final λ_{max} values observed upon activation with MAO are the same for both species (585 nm), with the only difference between **4** and **6** being the time need to reach this λ_{max} value. In addition, upon activation of either the dicholoro (**1**) or dimethyl (**5**) metallocene with MAO, the same λ_{max} value is observed (552 nm). This indicates that the final species is similar when MAO is employed as an activator, regardless of the metallocene used– most likely the close-contact ion pair between zirconium and MAO. The only difference is the time required to reach such a structure for the sterically-expanded metallocenes. This is most easily explained by rationalizing the structure of the final close-contact ion pair, which most likely contains bridging methyl groups,[108] as depicted in Figure 4.11. When a methyl group is abstracted from **6**, this close-contact ion pair is formed almost immediately; whereas with the abstraction of a chloride from **4**, the MAO must change geometries in order to have a methyl group protruding from the cage structure capable of binding to the metal.
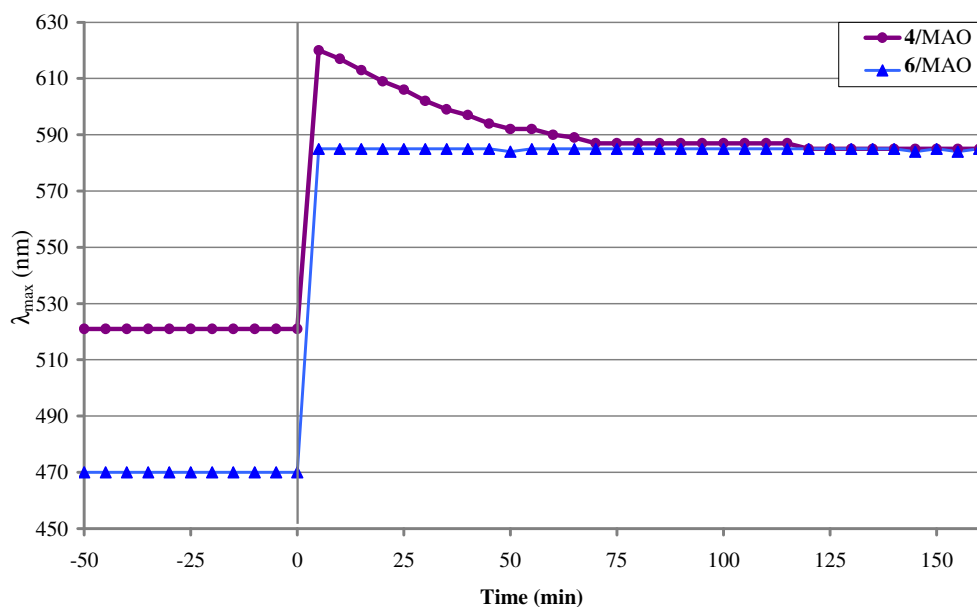
Figure 4.10: The activation of a zirconocene-dichloride (**4**) and -dimethide (**6**) with MAO, as followed by UV-Vis spectrophotometry. 0.25 mM in toluene, activated with 5000 eq. MAO at t = 0 min.
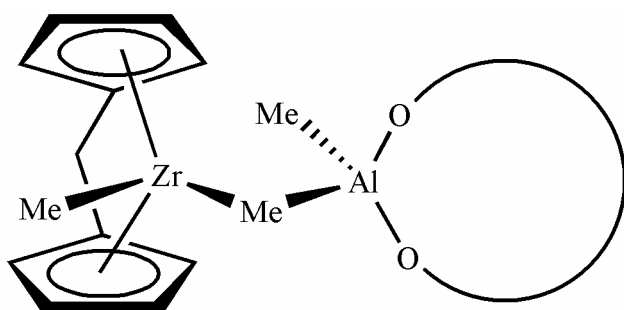
Figure 4.11: Proposed structure of the close-contact ion pair between metallocenes and MAO. The metallocene ligand and the cage structure of MAO have been simplified for clarity.

Solvent-dependent activation. The time-dependent activation studies described above were carried out on **4**/MAO in several solvents of differing polarity in order to ascertain what effect this had on the activation of the metallocene. In all cases, the length of time required to reach an equilibrium λ_{max} was decreased significantly when polar solvents were used (Figure 4.12). When non-polar solvents were used, the relaxation times were at least 120 minutes. However, when polar solvents were used – such as dichloromethane or halogenated benzenes – the relaxation times were decreased to between 5 and 60 minutes. This indicates that the reorganization of the MAO cage structure most likely involves a charge-separated transition state. When a polar solvent is employed, this transition state is stabilized, which allows the MAO counteranion to undergo the geometry rearrangement much faster. The faster the MAO counteranion can undergo this rearrangement, the faster it will bind to the zirconocenium cation and effect the observed blue shift. When non-polar solvents are used, this transition state is not stabilized, leading to a slower reorganization.
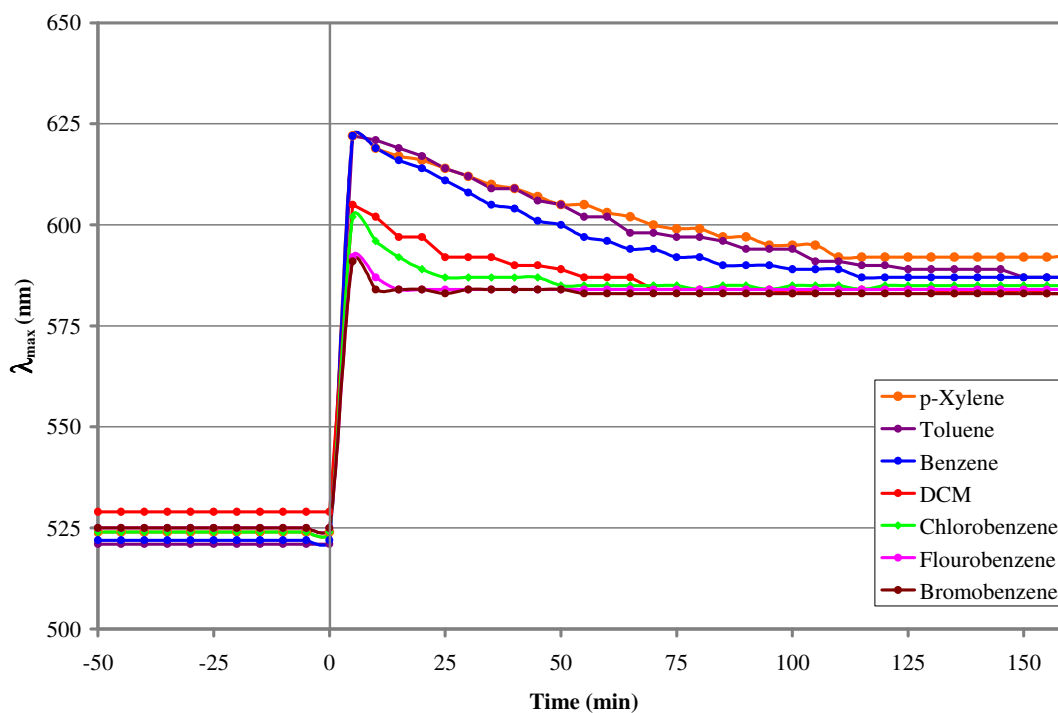
Figure 4.12: The time-dependent λ_{max} of **4**/MAO in solvents of different polarity. 0.25 mM in various solvents, activated with 5000 eq. MAO at t = 0 min.

Activity/λ_{max} correlation. In the past, UV-Vis spectrophotometry has been used to correlate catalytic activity with the observed λ_{max} for metallocenes,[115,116] although it is most frequently used to study the catalyst's dependence on Al:Zr ratios.[117-122] There are a few reports of using UV-Vis to monitor olefin polymerization catalysts with respect to time. However, these reports have focused on the monitoring the reaction of zirconocenes with trimethyl aluminum (TMA) prior to the polymerization reaction[123] or have followed the decomposition of nickel (II) bisimine catalysts to Ni^0.[124] To the extent

that the red shift is proportional to the distance between the catalytically active zirconocenium cation and the MAO anion, one would expect the activity of the catalyst to be related to the observed color change. This observation has been reported for similar *ansa*-metallocenes, although only the initial polymerization rate was considered.[75] In order to help validate the hypothesis that the changes observed in the UV-Vis spectra for the above metallocenes are due to differences in the zirconocenium cation-MAO anion distances, polymerizations were performed with metallocenes **1**-**4** at various times following activation with MAO. As explained above, the extremely facile LMCT observed for **4** immediately after activation is attributed to the fact that the MAO counteranion is separated from the active catalytic zirconocenium cation. Over the course of three hours, the MAO anion is able to undergo changes in geometry that allow it to form a closer-contact ion pair, thereby increasing the energy required for the LMCT. If this is the case, one would expect to observe a greater catalytic activity for polymerizations run at times when the solvent separated ion pair dominates (soon after activation with MAO), compared to polymerizations performed at times when the close-contact ion pair is favored (after the MAO counter anion has had time to form a closer-

contact ion pair). To this end, we have performed polymerizations with metallocenes **1**-**4** after allowing them to stir with MAO for various amounts of time, thereby "aging" the active catalysts (see Experimental Section).

As expected, the activity of metallocenes **1**-**4** tracked extremely well with the observed λ_{max} values (Figures 4.13-4.16) and the data are summarized in Table 4.1. Polymerizations performed with **1** exhibited a constant activity towards ethylene (350 kg PE/(mol Zr • hr)), regardless of how long the active catalyst was aged (Figure 4.13). This was expected since the λ_{max} observed for **1**/MAO does not change over the time periods studied, indicating a constant zirconium cation-MAO anion distance. Although both **2** and **3** do exhibit a time-dependent blue shift following their initial red shift, the blue shift is mostly completed by the beginning of the earliest polymerization run (with an aging time of 5 minutes) and a constant λ_{max} is observed during any of the times when polymerizations were carried out. As a result, **2** and **3** also provided constant polymerization activities toward ethylene, regardless of aging time (Figures 4.14 and 4.15 respectively), with **2** producing 2750 kg PE/(mol Zr • hr) and **3** producing 2250 kg PE/(mol Zr • hr).

Table 4.1: Polymerization Results for **1**-**4** Aged with MAO.[a]

Entry	Precatalyst	Aging Time (min.)	Yield (g)[b]	Activity[c]
1	**1**	5	0.0147	352 ± 204
2	**1**	35	0.0173	416 ± 113
3	**1**	70	0.0127	304 ± 28
4	**1**	110	0.0123	296 ± 37
5	**1**	150	0.0160	384 ± 63
6	**2**	5	0.0760	3040 ± 80
7	**2**	35	0.0687	2747 ± 450
8	**2**	70	0.0697	2786 ± 101
9	**2**	110	0.0687	2747 ± 266
10	**2**	150	0.0733	2933 ± 405
11	**3**	5	0.0590	2360 ± 592
12	**3**	35	0.0580	2320 ± 183
13	**3**	70	0.0637	2546 ± 335
14	**3**	110	0.0597	2387 ± 441
15	**3**	150	0.0523	2093 ± 272
16	**4**	5	0.0477	5720 ± 970
17	**4**	35	0.0243	2920 ± 703
18	**4**	70	0.0190	2280 ± 240
19	**4**	110	0.0187	2240 ± 367
20	**4**	150	0.0143	1720 ± 183

[a] 40 psi ethylene, 0.5 μmol catalyst, and 1000 eq. MAO in 25.0 mL toluene at 25.0 °C, 5 minute polymerization runs for **1**, 3 minute polymerization runs for **2** and **3**, 1 minute polymerization runs for **4**. [b] Average of three runs.
[c] In kg PE/(mol Zr • hr), ± one standard deviation.
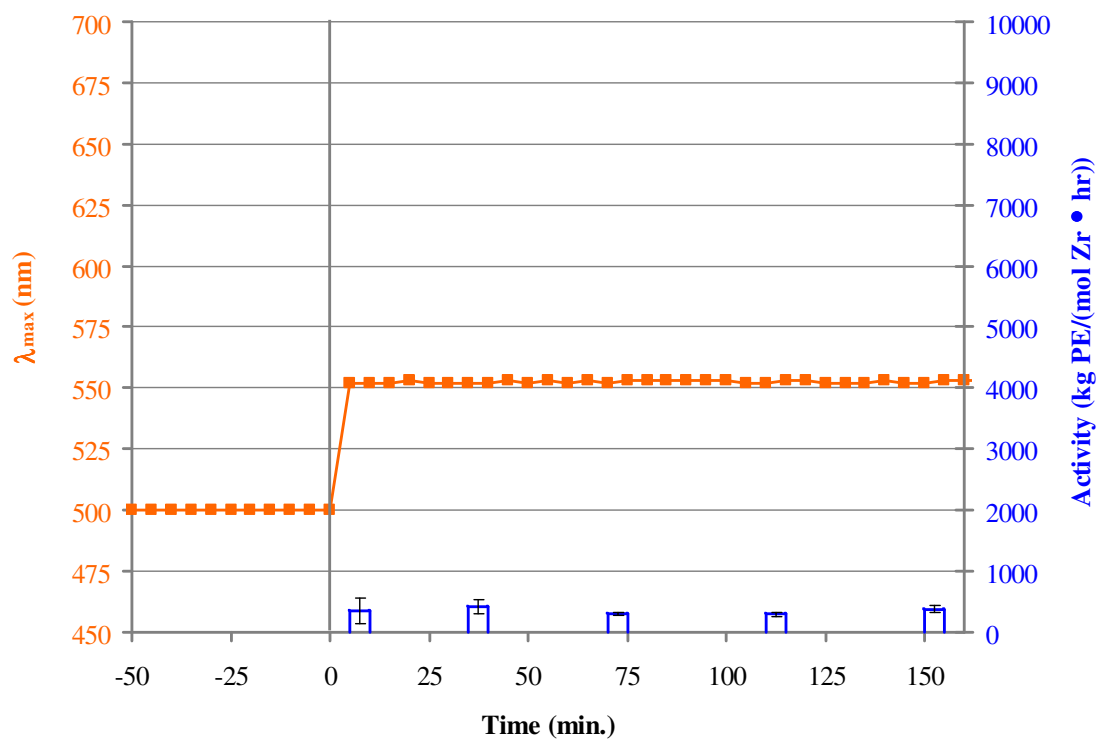
Figure 4.13: Activity/λ_{max} correlation for **1** with various aging times. Activities are an average of three runs, error bar is ±1 standard deviation.
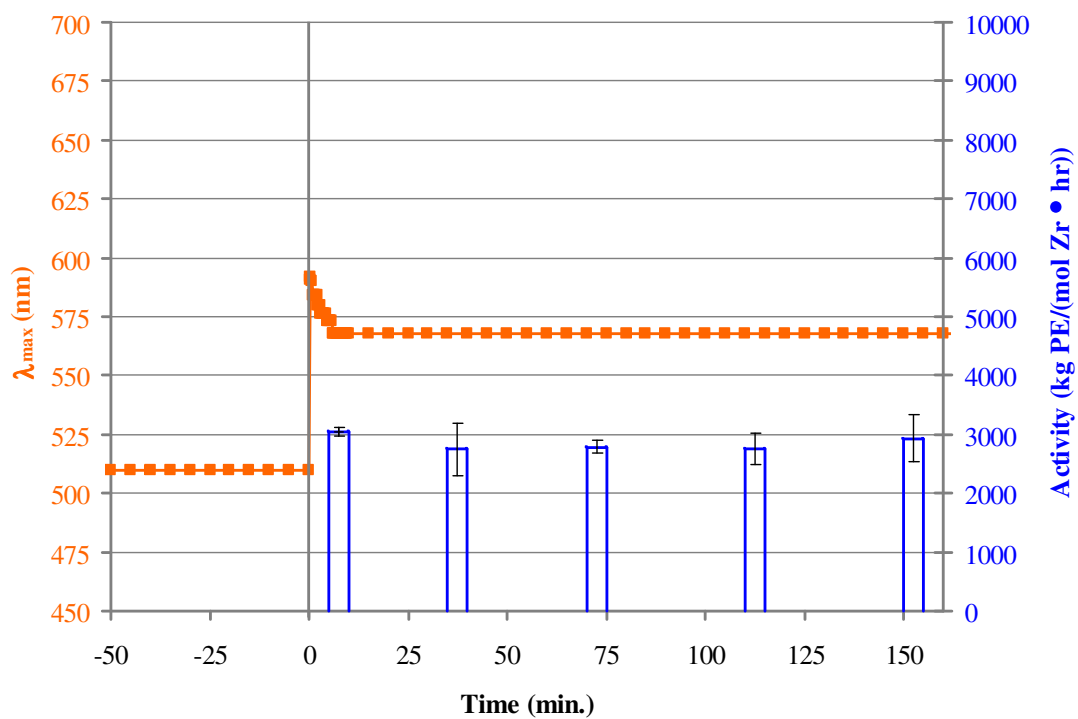
Figure 4.14: Activity/λ_{max} correlation for **2** with various aging times. Activities are an average of three runs, error bar is ±1 standard deviation.
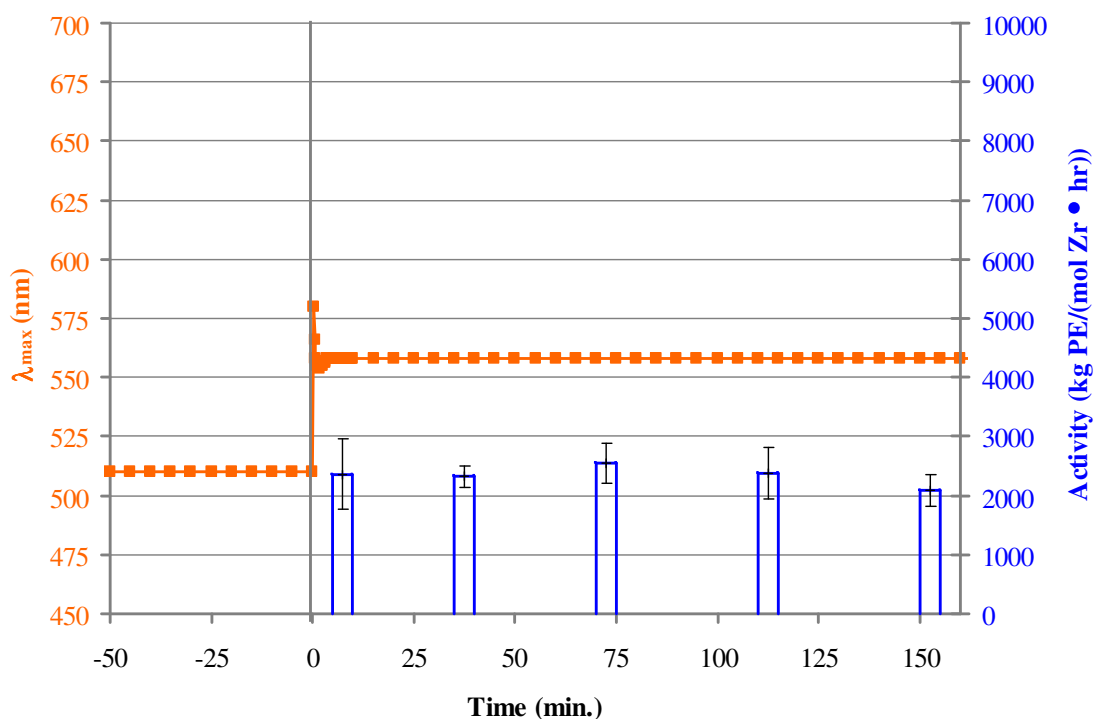
Figure 4.15: Activity/λ_{max} correlation for **3** with various aging times. Activities are an average of three runs, error bar is ±1 standard deviation.

However, when polymerizations are performed with **4**/MAO after various aging times, changes in the activity of the catalyst are observed. These changes in the activity track with the slow blue shift observed in the UV-Vis spectra of the **4**/MAO (Figure 4.16). When polymerizations are run with short aging times (5 or 35 minutes), a greater catalytic activity is observed. This is presumably due to the increased zirconium cation-MAO anion distance, leaving the coordination sphere of the metal relatively open. However, for longer aging times we see a decrease in activity as well as a decrease in the observed λ_{max} for the activated metallocene. Both of these observations can be explained

by the slow rearrangement of MAO to form a closer-contact ion pair with the active zirconocenium cation – increasing the energy required for the LMCT and hindering the ability of the metal center to coordinate monomer.
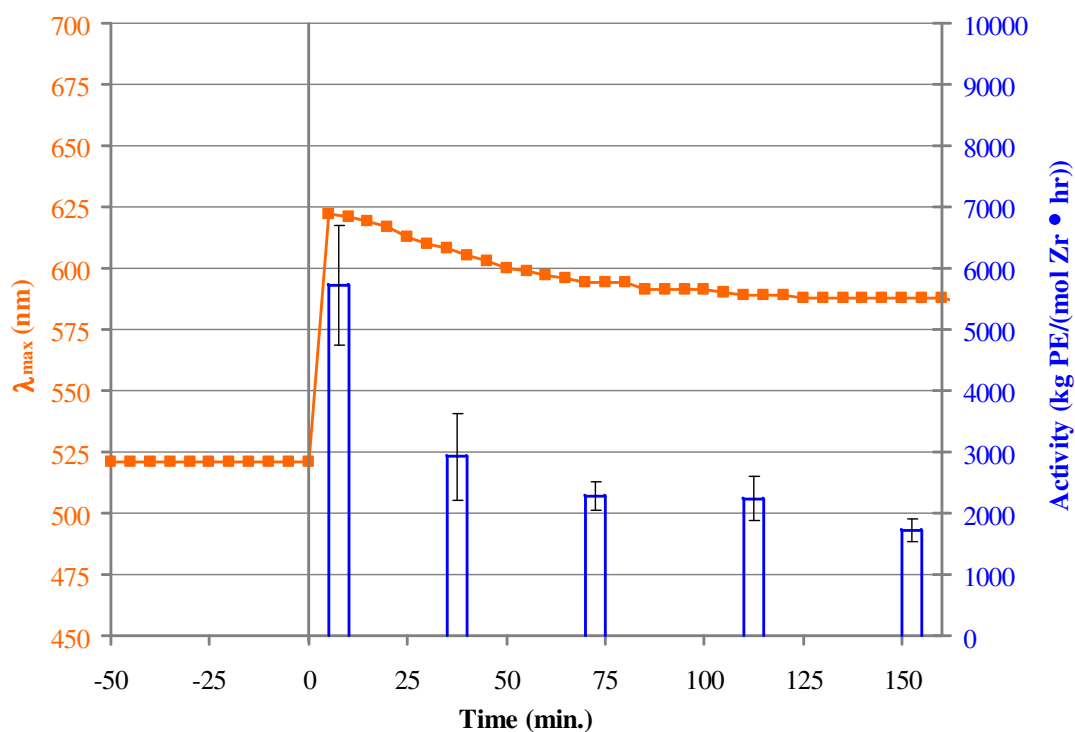
Figure 4.16: Activity/λ_{max} correlation for **4** with various aging times. Activities are an average of three runs, error bar is ±1 standard deviation.

In addition to studying the effect of aging time on the metallocenes, we also employed UV-Vis spectroscopy to study the activation of **1** and **4** with various amounts of MAO. In doing so, we were able to observe the minimum amount of MAO required

to fully activate the catalysts – that is, the smallest Al:Zr ratio that provided for a complete red shift – and we were able to correlate these observations in the UV-Vis spectra to the catalytic activity. Figures 4.17 and 4.18 show the observed λ_{max} values and the catalytic activity for **1** and **4**, respectively, with various amounts of MAO. It is interesting to note that **1** and **4** reach their maximum activity with the same Al:Zr ratio that is required to reach the maximum red shift, and that **4** required much less MAO than **1** to become fully activated. That is, **1** requires 2500 equivalents of MAO to reach the maximum red shift and the maximum activity, while **4** requires 1000 equivalents.
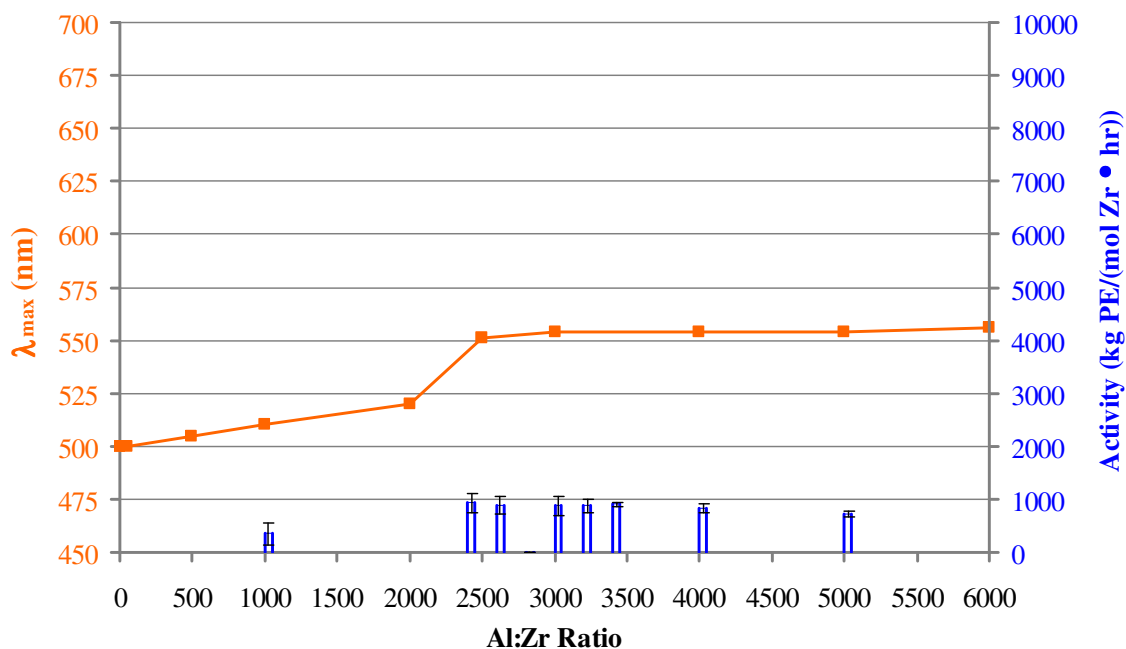
Figure 4.17: Observed λ_{max} values and catalytic activity for **1**/MAO at various Al:Zr ratios. Activities are an average of three runs, error bar is ±1 standard deviation.
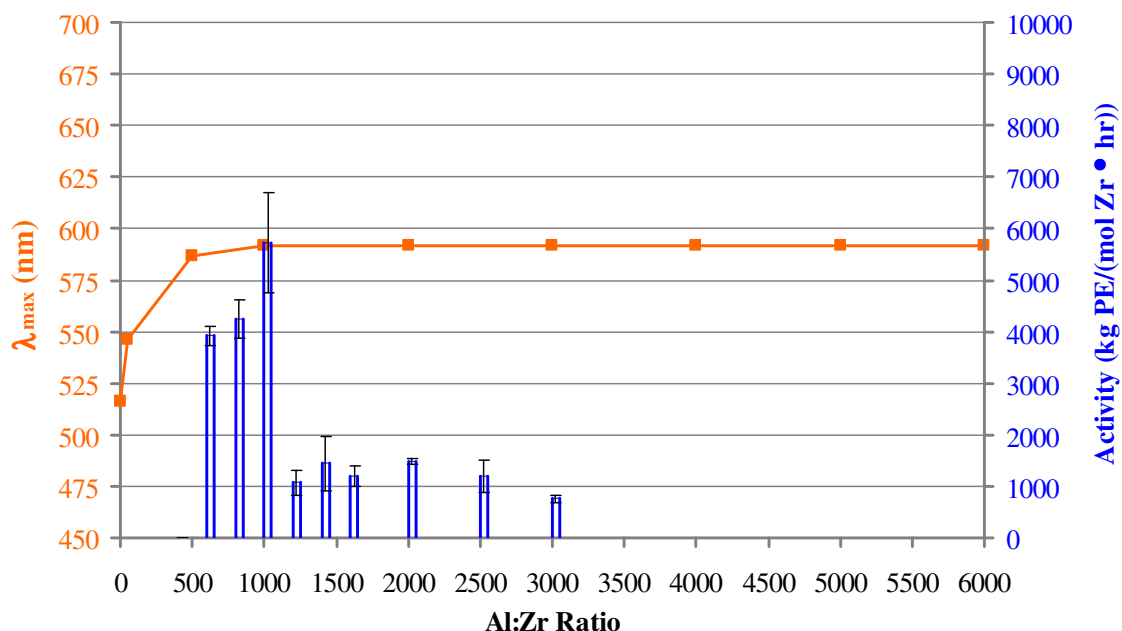
Figure 4.18: Observed λ_{max} values and catalytic activity for **4**/MAO at various Al:Zr ratios. Activities are an average of three runs, error bar is ±1 standard deviation.

For **4**, there is a drastic reduction in catalytic activity for any MAO above 1000 equivalents. This is generally attributed to residual trimethyl aluminum (TMA) left over from the synthesis of MAO, which poisons the active catalyst.[122,125-127] However, not all catalysts are affected by excess TMA, and there have been several reports of TMA having no effect on the catalytic activity,[126,128] although it is thought that even in theses cases, TMA does alter the termination mechanism.[128] This seems to be the case with **1**, which shows only a slight decrease in catalytic activity, even at very high concentrations of MAO. To test this hypothesis, we performed polymerizations near the catalysts' optimal MAO concentrations (3000 eq. MAO for **1** and 1000 eq. for **4**) and spiked the reaction with excess TMA. The results are summarized in Table 4.2.

Table 4.2: Polymerization Results for **1** and **4** with TMA Added.[a]

Entry	Pre-catalyst	MAO (eq.)	TMA (eq.)	Yield (g)	Activity[c]	% Change
1[b]	**1**	3000	0	0.0367	880	–
2	**1**	3000	440	0.0180	432	-50%
3[b]	**4**	1000	0	0.0477	5720	–
4	**4**	1000	440	0.0020	240	-96%

[a] 40 psi ethylene, 0.5 μmol catalyst, in 25.0 mL toluene at 25.0 °C, 5 minute polymerization runs for **1**, 1 minute polymerization runs for **4**. [b] Average of three runs. [c] In units of kg PE/(mol Zr • hr).

It has been suggested that TMA is responsible for the methylation of zirconocene dichlorides, which corresponds to the first step of the activation process.[129] TMA has been even considered as the actual zirconocene activator[130] although this has been contradicted.[131] In fact, it is reported that a mixture of TMA and zirconocene dichloride do not react with each other in solution.[132] In the generally-accepted mechanism by which TMA poisons the catalyst, free TMA binds to the zirconium center,[126,133-135] usually through bridging methyl groups. To this end, we have recorded the UV-Vis spectra of **4**/MAO/TMA over the course of 3 hours and have observed very little change in the λ_{max} of the species (Figure 4.19). From the data in Table 4.2, it is clear that TMA adversely affects the catalytic activity of **4**. However, the UV-Vis data seems to contradict the previously held belief that the TMA binds to the metal, shutting down the catalytic activity. If this were the case, the LMCT should increase in energy as the electronic nature of the zirconocenium cation changes. Since there is very little

difference in the observed red shift, our results indicate that TMA shuts down the polymerization by some other mechanism.
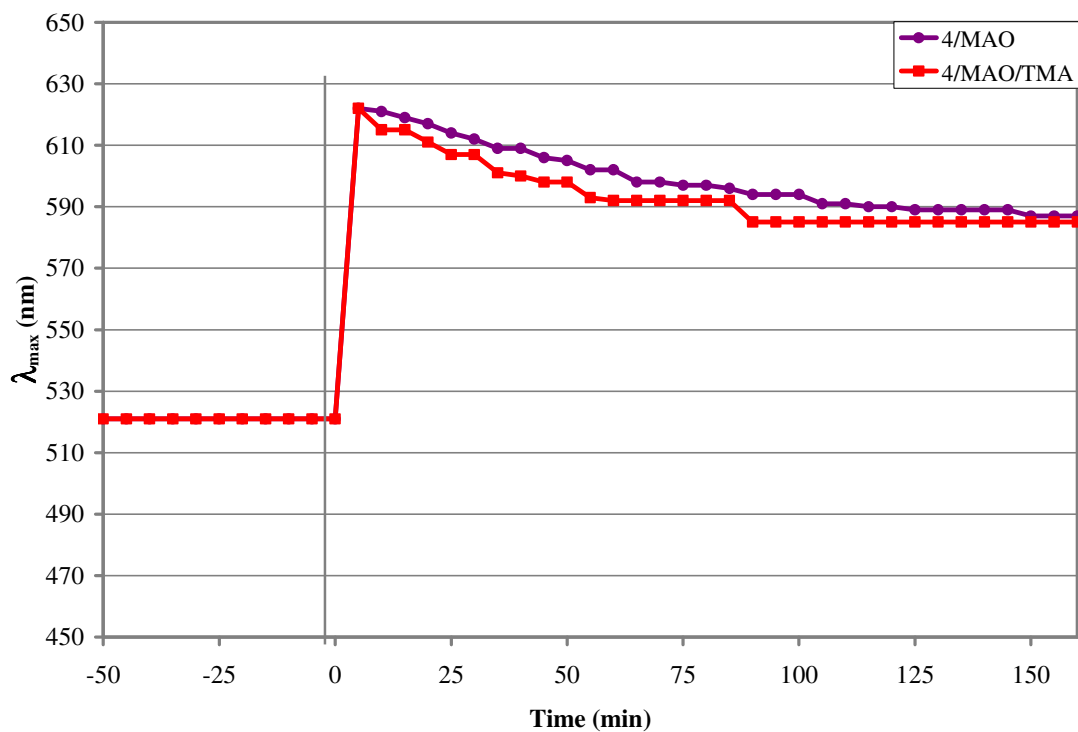
Figure 4.19: The time-dependent λ_{max} values of **4**/MAO with and without added TMA. 0.25 mM in toluene, activated with 1000 eq. MAO or 1000 eq. MAO + 440 eq. TAM at t = 0 min.

CONCLUSIONS

Prior to activation with MAO, metallocenes **1-4** show a predictable trend in the energy required for the LMCT, with the required energy for those metallocenes containing two electron-donating tertiary alkyl groups equally spaced between the metallocene with no tertiary alkyl groups (**1**), and that with four groups (**4**). After activation with MAO, an immediate red shift is observed, indicating that the metal has become more cationic as the active catalytic center is formed. After activation, the steric environment of the ligand dominates the LMCT. By physically holding the large MAO counteranion away from the zirconocenium center, ligands such as those employed in **4** make the metal more cationic and lower the barrier for LMCT. The subsequent time-dependent blue shift observed for the sterically-expanded metallocenes correlates to an increase in the energy required for the LMCT. Larger metallocenes, such as **4**, are able to hold the MAO at bay until the MAO rearranges its geometry to be able to fit past the steric bulk and reach the cationic zirconium – a observation supported by the fact that the slow blue shift for **4** is solvent-dependent. Smaller metallocenes, such as **1**, are unable to hold the MAO at bay. Therefore, MAO forms the close-contact ion pair almost immediately and there is no time-dependent blue shift observed in the UV-Vis spectra. While comparing **2** and **3**, it becomes apparent that the metallocenes are not only influenced by the steric bulk of the ligands, but also by the location of the sterically demanding tertiary alkyl groups. This is evidenced by the differences in the UV-Vis spectra of the activated species as well as the activities of the catalysts. In addition, the Zr-MAO distances observed in the UV-Vis spectra correlate very well with the catalytic

activities of **1**-**4**, with the greatest catalytic activities corresponding to the greatest Zr-MAO distance.

The activation of dimethyl metallocenes **5** and **6** with $B(C_6F_5)_3$ provides an initial red shift as the zirconium center becomes more cationic. As expected, there is no time-dependent blue shift after activation as the discrete $[MeB(C_6F_5)_3]^-$ counteranion has a static structure which provides for a constant cation-anion distance. Upon activation of **5** or **6** with MAO, the UV-Vis spectra show absorbences equal to the equilibrium λ_{max} values observed for **1** and **4** respectively (552 nm for **1**, 587 nm for **2**). This indicates that the close-contact ion pair is formed almost immediately.

Polymerizations performed with varying amounts of MAO show that metallocenes **1** and **4** reach their maximum catalytic activity with the same MAO:Zr ratios required to effect a maximum red shift in the UV-Vis spectra. Increasing the MAO:Zr ratio adversely affects both metallocenes, presumably by introducing more TMA into the polymerization reaction, although the effect is much more pronounced with metallocene **4**. UV-Vis data contradicts the generally-accepted belief that TMA poisons metallocene catalysts by binding to the active zirconocenium center – although it does not provide evidence for an alternate mechanism.

EXPERIMENTAL

General considerations. All air-sensitive procedures were performed under a purified nitrogen atomsphere in a glovebox or by using standard Schlenk line and vacuum line techniques. Methylaluminoxane (MAO) (Albemarle, 30% in toluene) was concentrated to dryness and used as a solid. Solvents used for UV-Vis measurements and for polymerizations were dried before use: toluene was distilled from sodium/benzophenone; dichloromethane, benzene, xylene, and halogenated benzenes were vacuum-transferred from calcium hydride and then degassed by three freeze-pump-thaw cycles. Solvents for the synthesis of ligands and precatalysts were sparged with nitrogen and dried over molecular sieves using an M. Braun MB-SPS solvent purification system, dispensed into oven-dried Straus flasks and degassed by stirring under reduced pressure for 20 minutes. All other chemicals were used as received. All UV-Vis spectra were recorded on an Agilent Technologies 8453 UV-Vis spectrophotometer using an airtight 1.0 cm cuvette equipped with a 100 mL round bottom flask and a magnetic stir bar. All compounds were prepared according to literature procedure, and the characterization data matched that previously reported. The general procedures are as follows.

Synthesis of 2,5-dichloro-2,5-dimethylhexane. 2,5-dimethyl-2,5-hexanediol (200.0 g) was charged to a 4 L Erlenmeyer flask and 1L of concentrated aqueous hydrochloric acid was added. The resulting slurry was periodically shaken by hand. After 48 hours, 800 mL of water was added and the slurry was extracted with diethyl ether (4 x 200 mL). The combined ether layers were dried over $MgSO_4$, filtered and

concentrated to ~150 mL. The reaction was heated to redissolve the formed precipitate, slowly cooled and filtered to isolate 237.6 g (94.7 %) of a white crystalline solid.

Synthesis of 2,2,5,5-tetramethyl-2,3,4,5-tetrahydro-benzo[*b*]fluorene (TetH).[136] Fluorene (100.00 g, 602.41 mmol), 2,5-dichloro-2,5-dimethylhexane (13.00 g, 71.04 mmol) and ~400 mL of nitromethane were charged to a 1L round bottom flask that had been purged with nitrogen. The reaction was heated to 60 °C until homogeneous. To this, a solution of aluminum trichloride (5.0 g in ~50 mL nitromethane) was added dropwise via syringe over 10 minutes. The reaction was stirred for an additional 15 minutes, and was quenched by slowly adding ~10 mL of water, followed by an additional 150 mL of water. The mixture was cooled to room temperature and filtered to remove unreacted fluorene. The filtrate was extracted with hexanes (4 x 100 mL) and the combined hexanes layers were dried over $MgSO_4$ and evacuated to dryness. The resulting solid (20:80 TetH:FluH by GC) was subjected to Kugelrohr distillation under dynamic vacuum at 100 °C to remove unreacted fluorene. The residue (58:42 TetH:FluH by GC) was taken up in hot ethanol, cooled and filtered to isolate a solid. This solid (60:40 TetH:FluH by GC) was again subjected to Kugelrohr distillation as above. The residue was again taken up in hot ethanol, cooled and filtered to isolate 6.98 g of pure TetH (35.6 %).

Synthesis of 2,7-ditertbutylfluorene. Fluorene (50.0 g, 299.4 mmol) and 2-chloro-2-methylpropane (48.24 g, 598.8 mmol) were charged to a 2 L round bottom flask and dissolved in 700 mL nitromethane. A solution of $AlCl_3$ (10.0 g in 60 mL of nitromethane) was slowly added via syringe. Reaction stirred at room temperature for

two days, after which time it was poured into 1 L of ice water. The green solid was collected via vacuum filtration, and triturated in ethanol. The white solid was collected via vacuum filtration and recrystallized from toluene to yield 35.99 g (43.2%).

Synthesis of 2,2,5,5,8,8,11,11-octamethyl-2,3,4,5,8,9,10,11-octahydro-dibenzo[*b,e*]fluorene (OctH).[77] Fluorene (22.65 g, 136.25 mmol) and 2,5-dichloro-2,5-dimethylhexane (50.0 g, 273.22 mmol) were charged to a 1 L round bottom flask and dissolved in ~400 mL of nitromethane. To this, a solution of aluminum trichloride (22.3 g in ~100 mL of nitromethane) was added via syringe over 20 minutes and the resulting blue slurry was stirred at room temperature. After 48 hours, the reaction mixture was slowly poured into 1 L of ice water and the green precipitate was collected via vacuum filtration. The solid was triturated in dry ethanol for 24 hours, filtered and recrystallized from toluene to yield 48.29 g of a white solid (92.1 %).

Synthesis of 6,6-diphenylfulvene.[137] Benzophenone (170.0 g, 0.933 mol) and sodium methoxide (55.8 g) were dissolved in ~700 mL of dry ethanol. To this, was added 134 mL of freshly distilled cyclopentadiene. The orange reaction stirred at room temperature overnight. It was filtered to isolate a deep orange powder which was then triturated in methanol, filtered and dried to yield 198.1 g (92.2 %) of an orange powder

Synthesis of *ansa*-ligands. On the benchtop, the desired fluorene (35.0 mmol) was charged to a round bottom flask equipped with a magnetic stir bar and a 180° needle valve. Diethyl ether (~100 mL) was condensed in at 77 K. As the reaction was slowly warming to room temperature, *n*-butyllithium was added via syringe (15.3 mL of a 2.77 M solution in hexanes, 1.2 eq.). The reaction stirred for 24 hours open to a mercury

bubbler. The solvent was removed *in vacuuo* and brought into the glove box where 6,6-dimethylfulvene was added (3.73 g, 35.0 mmol). The flask was attached to the vacuum line and again, ~100 mL of diethyl ether were condensed in at 77 K. The reaction was allowed to slowly warm to room temperature and stirred for four days. Then, ~10 mL of a saturated aqueous solution of NH_4Cl was slowly added, followed by an additional 50 mL. The aqueous layer was washed with diethyl ether (2 x 50 mL). All organic layers were combined and washed with water (2 x 50 mL) and dried over $MgSO_4$. After filtering, the solvent was removed via rotary evaporation to afford a sold, and the desired product was recrystallized from diethyl ether or hexanes.

Synthesis of *ansa*-metallocene dichloride complexes. On the benchtop, 25 mmol of the desired ligand was charged to a 100 mL recovery flask and a 180° needle valve was attached. The apparatus was attached to the vacuum line and ~50 mL of dry diethyl ether were condensed in at -196 °C. While the reaction was warming to room temperature, 18.2 mL of *n*-butyllithium (2.77 M in hexanes, 50.5 mmol) were added via syringe over 10 minutes. The reaction mixture was stirred at room temperature for 24 hours, then evacuated to dryness. The flask was sealed and brought into the glovebox where $ZrCl_4$ was added (5.83 g, 25 mmol) and the needle valve was replaced with a swivel frit apparatus. The apparatus was attached to the vacuum line and ~50 mL of diethyl ether were condensed in at -196 °C. The reaction was allowed to slowly warm to room temperature and was then stirred for 24 hours. The solvent was removed on the vacuum line and ~50 mL of toluene were condensed in at -196 °C. The frit was flipped to filter off LiCl and the cake was extracted until colorless by condensing toluene from

the lower collection flask. The resulting metallocene solution was concentrated to ~10 mL and placed in an ice-water bath to precipitate the product. The frit was flipped again and the solid product collected via filtration.

Synthesis of *ansa*-metallocene dimethyl complex 5. In the box, **1** (0.331 g, 0.595 mmol) was charged to a 50 mL recovery flask and dissolved in ~20 mL of diethyl ether. Methylmagnesium chloride (0.43 mL of a 22 wt% solution, 2.2 eq.) was added via syringe and a swivel frit apparatus was assembled. The reaction stirred at room temperature for 3 days, during which time the reaction changed from orange-red to yellow as a white precipitate formed. The swivel frit was flipped and the reaction was filtered to remove the insoluble salt. The filtrate was concentrated to ~5 mL and the frit was flipped again to collect 0.127 g (38.4%) of a bright yellow powder.

Synthesis *ansa*-metallocene dimethyl complex 6. In the box, **4** (0.332 g, 0.427 mmol) was charged to a 50 mL recovery flask and dissolved in ~20 mL of diethyl ether. Methylmagnesium chloride (0.31 mL of a 22 wt% solution, 2.2 eq.) was added via syringe and a swivel frit apparatus was assembled. The reaction stirred at room temperature for 3 hours, during which time the reaction changed from pink to yellow as a white precipitate formed. The swivel frit was flipped and the reaction was filtered to remove the insoluble salt. The filtrate was concentrated to ~5 mL and the frit was flipped again to collect 0.182 g (57.8%) of a bright yellow powder.

General UV-Vis procedure. For metallocenes **1** and **4-6**: Inside the glove box, the round bottom portion of the air-tight cuvette apparatus was charged with the appropriate amount of a toluene stock solution of the chosen activator (MAO or

$B(C_6F_5)_3$), enough toluene to bring the volume to 7.0 mL, and 1.0 mL of a 2.0 mM stock solution of the chosen metallocene. The apparatus was sealed with a teflon valve and brought out of the glovebox. The spectrophotometer was blanked using toluene in a matched cuvette. The apparatus was tipped to allow the activated catalyst solution to flow into the cuvette portion and UV-Vis spectra were recorded every 5 minutes for 180 minutes.

For metallocenes **2** and **3**: Inside the glove box, the round bottom portion of the air-tight cuvette apparatus was charged with the appropriate amount of a MAO stock solution and enough toluene to bring the volume to 7.0 mL. The openings were capped with septa and the apparatus was brought out of the glovebox. The spectrophotometer was blanked using toluene in a matched cuvette. Then, 1.0 mL of a 2.0 mM precatalyst stock solution was injected with rapid stirring. The apparatus was tipped to allow the activated catalyst solution to flow into the cuvette portion and UV-Vis spectra were recorded every 15 seconds for 15 minutes, then every 5 minutes for the next 165 minutes.

General polymerization procedure. *CAUTION!* All polymerizations should be carried out in a fume hood and behind a blast shield. Polymerizations were carried out in an 85 mL glass Lab-Crest (Andrews Glass Company) cylindrical polymerization reactor equipped with a 2 in. octagonal stir bar able to provide ample surface agitation wile stirring. In the glovebox, the vessel was charged with the appropriate amount of a 1.0 M MAO stock solution, enough toluene to bring the total volume in the reactor to 24.0 mL, and 1.0 mL of a 0.5 mM solution of the appropriate pre-catalyst. The addition

of the precatalyst represents $t = 0$ minutes. The reactor was assembled and was allowed to stir inside the glovebox until 5 minutes before the polymerization run was to begin (in the case of the polymerization runs beginning at $t = 5$ minutes, the reactor was brought out of the box immediately). It was then taken out of the box, placed in a 25 °C thermostatic water bath and rapid stirring was begun. At the appropriate time, the reactor was pressurized to 40 psi with a continuous supply of ethylene. After the appropriate time (5 minutes for **1**, 3 minutes for **2** and **3** and 1 minute for **4**), the reaction was quenched by slowly venting the vessel and adding ~8 mL of an acidic methanol solution (methanol plus 10% aqueous concentrated HCl). The insoluble polymer was collected by vacuum filtration.

CHAPTER V

CONCLUSIONS

The ongoing desire to produce polymers from renewable feedstocks remains, despite our inability to reproduce previously published reports on the copolymerization of ethylene and carbon dioxide. The thermodynamic parameters for the copolymerization show that an alternating copolymer is thermodynamically impossible at any reasonable polymerization temperatures. However, the copolymer is thermodynamically feasible at room temperature as long as the molar ratio of ethylene/CO_2 exceeds 2.37 (less than 29.7 mol% CO_2). Despite the thermodynamic possibility of a copolymer between ethylene and CO_2, it is difficult to imagine a suitable mechanism that would allow for a feasible kinetic pathway.

Octamethyloctahydrodibenzofluorenyl has profound steric consequences when incorporated into metallocene ligands for olefin polymerization – including increased activity and stereoselectivity. However, its electronic contributions to the metallocene are less understood. The electron-donating ability of the four tertiary alkyl groups on Oct has been studied by DFT calculations, and UV-Vis spectroscopy of the pre-catalysts. OctH was found to have a pK_a of 26.8, an increase of nearly 4 pK_a units compared to fluorene.

Data from UV-Vis and catalytic activity studies support the theory that the increased activity of Oct-containing metallocenes is due to the ability of the steric bulk to influence the counteranion distance. In addition, it was found that TMA is detrimental

to the catalytic activity of the metallocenes studied. However, the effect is varies depending on the metallocene. UV-Vis data also contradicts the generally-accepted belief that TMA poisons metallocene catalysts by binding so the active zirconium center, although it does not provide evidence for an alternative mechanism.

REFERENCES

(1)   von Pechmann, H. *Ber.* **1898**, *31*, 2640-2646.

(2)   Fawcett, E. W.; Gibson, R. O.; Perrin, M. W. U.S. Patent 2,153,553, 1939.

(3)   Fawcett, E. W.; Gibson, R. O.; Perrin, M. W.; Paton, J. G.; Williams, E. G. British Patent 471,590, 1938.

(4)   Perrin, M. W.; Paton, J. G.; Williams, E. G. U.S. Patent 2,188,465, 1940.

(5)   Perrin, M. W. *Research (London)* **1953**, *6*, 111.

(6)   Ziegler, K.; Holzkamp, H. B.; Martin, H. *Angew. Chem.* **1955**, *67*, 541-547.

(7)   Natta, G. *J. Polym. Sci.* **1960**, *48*, 219-239.

(8)   Stevens, M. P. *Polymer Chemistry: An Introduction*; Oxford: New York, 1999.

(9)   Dawans, F.; Teyssié, P. *Bull. Soc. Chim. Fr.* **1963**, *10*, 2376-2392.

(10)   Boor, J. J. *Ziegler-Natta Catalysts and Polymerizations*; Academic Press: New York, 1979.

(11)   Keii, T. *Kinetics of Ziegler-Natta Polymerization*; Halsted Press: New York, 1972.

(12)   Zakharov, V. A.; Bukatov, G. D.; Ermakov, Y. I. *Adv. Polym. Sci.* **1983**, *51*, 61-100.

(13)   Guyot, A.; Spitz, R.; Journaud, C.; Eisenstein, O. *Macromol. Chem. Phys.* **1995**, *89*, 39-54.

(14)   Sinn, H.; Kaminsky, W.; Vollmer, H. J.; Woldt, R. *Angew. Chem.* **1980**, *92*, 396-402.

(15)   Huang, J.; Rempel, G. L. *Prog. Polym. Sci.* **1995**, *20*, 459-526.

(16)   Kaminsky, W. *Macromol. Chem. Phys.* **1996**, *197*, 3907-3945.

(17)   Jordan, D. O. In *The Stereochemistry of Macromolecules*, Ketley, A. D., Ed.; Marcel Dekker: New York, 1967.

(18)   Zambelli, A.; Locatelli, P.; Provasoli, A.; Ferro, D. R. *Macromolecules* **1980**, *13*, 267-270.

(19)   Ittel, S. D.; Johnson, L. K.; Brookhart, M. *Chem. Rev.* **2000**, *100*, 1169-1203.

(20)   Coates, G. W. *Chem. Rev.* **2000**, *100*, 1223-1252.

(21)   Chen, M. C.; Marks, T. J. *Chem. Rev.* **2000**, *100*, 1391-1434.

(22)   Karol, F. J.; Johnson, R. N. *J. Polym. Sci., Polym. Chem.* **1975**, *13*, 1607-1617.

(23)   Arthur, S. D.; Brookhart, M. S.; Cotts, P. M.; Guan, Z.; Johnson, L. K.; Killian, C. M.; McCord, E. F.; McLain, S. J. World Patent Application WO 9947572, 1988.

(24)   Guan, Z.; Cotts, P. M.; McCord, E. F.; McLain, S. J. *Science (Washington, D. C.)* **1999**, *283*, 2059-2062.

(25)   Guan, Z. *Polym. Mater. Sci. Eng.* **1999**, *80*, 50.

(26)   Guan, Z.; Cotts, P. M.; McCord, E. F. *Polym. Prepr. (Am. Chem. Soc., Div. Polym. Chem.)* **1998**, *39*, 402-403.

(27)   Ewen, J. A.; Jones, R. L.; Razavi, A.; Ferrara, J. D. *J. Am. Chem. Soc.* **1988**, *110*, 6255-6256.

(28)   Shamshoum, E.; Schardl, J. In *Metallocene-Catalyzed Polymers - Materials, Properties, Processing and Markets*, Benedikt, G. M.; Goodall, B. L., Eds.; Plastic Design Library: New York, 1998.

(29)   Andrews, A. E.; Bruhwiler, L.; Crotwell, A.; Dlugokencky, E. J.; Hahn, M. P.; Hirsch, A. I.; Kitzis, D. R.; Lang, P. M.; Masarie, K. A.; Michalak, A. M.; Miller, J. B.; Novelli, P. C.; Peters, W.; Tans, P. P.; Thoning, K. W.; Vauchn, B. H.; Zhao, C. In *Climate Monitoring and Diagnostic Laboratory Summary Report No. 27*; Conway, T. J., Ed.; National Oceanographic and Atmospheric Administration, U.S. Department of Commerce: Boulder, CO, 2003; p 32.

(30)   Inoue, S.; Koinuma, H.; Tsuruta, T. *J. Polym. Sci., Polym. Lett. Ed.* **1969**, *7*, 287-292.

(31)   Coates, G. W.; Moore, D. R. *Angew. Chem., Int. Ed.* **2004**, *43*, 6618-6639.

(32)   Kuran, W.; Rokicki, A.; Romanowska, D. *J. Polym. Sci., Part A: Polym. Chem.* **1979**, *17*, 2003-2011.

(33)   Ihata, O.; Kayaki, Y.; Ikariya, T. *Macromolecules* **2005**, *38*, 6429-6434.

(34)   Ikeda, S.; Soga, K.; Hosoda, S.; Tazuke, Y.; Uenishi, K.; Hyakkoku, K.; Toshida, Y. *Asahi Garasu Kogyo Gijutsu Shoreikai Kenkyu Hokoku* **1977**, *31*, 87-104.

(35)   Zou, F.; Li, Y.; Zou, X.; Qian, C.; Chen, R.; Song, Y. Chinese Patent CN1334279, February 6, 2002.

(36)   Lowry, T. H.; Richardson, K. S. *Mechanism and Theory in Organic Chemistry*; Harper Collins: New York, 1987; p 162.

(37)   Markevich, M. A.; Pavlinov, L. I.; Lebedev, Y. A. *Dokl. Akad. Nauk SSSR* **1982**, *262*, 652-655.

(38)   Liu, Z.; Torrent, M.; Morokuma, K. *Organometallics* **2002**, *21*, 1056-1071.

(39)   Darensbourg, D. J.; Yarbrough, J. C.; Ortiz, C.; Fang, C. C. *J. Am. Chem. Soc.* **2003**, *125*, 7586-7591.

(40)   Odian, G. *Principles of Polymerization*, 4th. ed.; Wiley-Interscience: New York, 2004; p 275.

(41)   Jessup, R. S. *J. Chem. Phys.* **1948**, *16*, 661-664.

(42)   Cohen, N.; Benson, S. W. *Chem. Rev.* **1993**, *93*, 2419-2438.

(43)   Chase, M. W., Jr. NIST-JANAF Thermochemical Tables, 4th ed., *J. Phys. Chem. Ref. Data*, **1998**, *Monograph 9*, pp 1-1951.

(44)   Leonard, J. In *Polymer Handbook*, 4th. ed.; Brandup, J.; Immergut, E. H.; Grulke, E. A., Eds.; Wiley-Interscience: New York, 1999; pp 363-414.

(45)   Britovsek, G. J. P.; Gibson, V. C.; Wass, D. F. *Angew. Chem., Int. Ed.* **1999**, *38*, 429-447.

(46)   Svejda, S. A.; Brookhart, M. *Organometallics* **1999**, *18*, 65-74.

(47)   Shultz, L. H.; Tempel, D. J.; Brookhart, M. *J. Am. Chem. Soc.* **2001**, *123*, 11539-11555.

(48)   Leatherman, M. D.; Svejda, S. A.; Johnson, L. K.; Brookhart, M. *J. Am. Chem. Soc.* **2003**, *125*, 3068-3081.

(49)   Johnson, L. K.; Killian, C. M.; Brookhart, M. *J. Am. Chem. Soc.* **1995**, *117*, 6414-6415.

(50)   Canich, J. A. M.; Vaughan, G. A.; Matsunaga, P. T.; Gindelberger, D. E.; Shaffer, T. D.; Squire, K. R. PCT Int. Appl. WO 9,748,735, 1997.

(51)   Hoberg, H.; Gross, S.; Milchereit, A. *Angew. Chem.* **1987**, *99*, 567-9.

(52)   Hoberg, H.; Peres, Y.; Milchereit, A.; Gross, S. *J. Organomet. Chem.* **1988**, *345*, C17-C19.

(53)   Tsuda, T.; Morikawa, S.; Sumiya, R.; Saegusa, T. *J. Org. Chem.* **1988**, *53*, 3140-3145.

(54)   Louie, J.; Gibby, J. E.; Farnworth, M. V.; Tekavec, T. N. *J. Am. Chem. Soc.* **2002**, *124*, 15188-15189.

(55)   Tekavec, T. N.; Arif, A. M.; Louie, J. *Tetrahedron* **2004**, *60*, 7431-7437.

(56)   de Vries, T. J.; Kemmere, M. F.; Keurentjes, J. T. F. *Macromolecules* **2004**, *37*, 4241-4246.

(57)   de Vries, T. J.; Vorstman, M. A. G.; Keurentjes, J. T. F.; Duchateau, R. *Chem. Commun.* **2000**, 263-264.

(58)   Frisch, M. J.; Trucks, G. W.; Schlegel, H. B.; Scuseria, G. E.; Robb, M. A.; Cheeseman, J. R.; Montgomery, J. A., Jr.; Vreven, T.; Kudin, K. N.; Burant, J. C.; Millam, J. M.; Iyengar, S. S.; Tomasi, J.; Barone, V.; Mennucci, B.; Cossi, M.; Scalmani, G.; Rega, N.; Petersson, G. A.; Nakatsuji, H.; Hada, M.; Ehara, M.; Toyota, K.; Fukuda, R.; Hasegawa, J.; Ishida, M.; Nakajima, T.; Honda, Y.; Kitao, O.; Nakai, H.; Klene, M.; Li, X.; Knox, J. E.; Hratchian, H. P.; Cross, J. B.; Bakken, V.; Adamo, C.; Jaramillo, J.; Gomperts, R.; Stratmann, R. E.; Yazyev, O.; Austin, A. J.; Cammi, R.; Pomelli, C.; Ochterski, J. W.; Ayala, P. Y.; Morokuma, K.; Voth, G. A.; Salvador, P.; Dannenberg, J. J.; Zakrzewski, V. G.; Dapprich, S.; Daniels, A. D.; Strain, M. C.; Farkas, O.; Malick, D. K.; Rabuck, A. D.; Raghavachari, K.; Foresman, J. B.; Ortiz, J. V.; Cui, Q.; Baboul, A. G.; Clifford, S.; Cioslowski, J.; Stefanov, B. B.; Liu, G.; Liashenko, A.; Piskorz, P.; Komaromi, I.; Martin, R. L.; Fox, D. J.; Keith, T.; Al-Laham, M. A.; Peng, C. Y.; Nanayakkara, A.; Challacombe, M.; Gill, P. M. W.; Johnson, B.; Chen, W.; Wong, M. W.; Gonzalez, C.; Pople, J. A. *Gaussian 03*, revision C.02; Gaussian, Inc.: Wallingford, CT, 2004.

(59)   Becke, A. D. *J. Chem. Phys.* **1993**, *98*, 5648-5652.

(60)   Lee, C.; Yang, W.; Parr, R. G. *Phys. Rev.* **1988**, *B37*, 785-789.

(61)   Miehlich, B.; Savin, A.; Stoll, H.; Preuss, H. *Chem. Phys. Lett.* **1989**, *157*, 200-206.

(62)   Ditchfield, R.; Hehre, W. J.; Pople, J. A. *J. Chem. Phys.* **1971**, *54*, 724-728.

(63)   Petersson, G. A.; Al-Laham, M. A. *J. Chem. Phys.* **1991**, *94*, 6081-6090.

(64)   Brintzinger, H. H.; Fischer, D.; Müelhaupt, R.; Rieger, B.; Waymouth, R. M. *Angew. Chem., Int. Ed. Engl.* **1995**, *34*, 1143-1170.

(65)   Resconi, L.; Cavallo, L.; Fait, A.; Piemontesi, F. *Chem. Rev.* **2000**, *100*, 1253-1345.

(66)   Shapiro, P. J.; Bunel, E.; Schaefer, W. P.; Bercaw, J. E. *Organometallics* **1990**, *9*, 867-869.

(67)   Shapiro, P. J.; Cotter, W. D.; Schaefer, W. P.; Labinger, J. A.; Bercaw, J. E. *J. Am. Chem. Soc.* **1994**, *116*, 4623-4640.

(68)   Okuda, J. *Chem. Ber.* **1990**, *123*, 1649-1651.

(69)   Stevens, J. C.; Timmers, F. J.; Wilson, D. R.; Schmidt, G. F.; Nickias, P. N.; Rosen, R. K.; Knight, G. W.; Lai, S. Y. European Patent 416815-A2, August 30, 1991.

(70)   Canich, J. A. M. US Patent 5026798, September 13, 1991.

(71)   Turner, H. W.; Hlatky, G. G.; Canich, J. A. M. World Patent WO 9319103, March 16, 1993.

(72)   Kawai, K.; Yamashita, M.; Tohi, Y.; Kawahara, N.; Michiue, K.; Kaneyoshi, H.; Mori, R. PCT Int. Appl. WO 01/27124, 2001.

(73)   Miller, S. A.; Bercaw, J. E. U.S. Pattent 6469188, 2002.

(74)   Miller, S. A.; Bercaw, J. E. U.S. Patent 6693153, 2004.

(75)   Miller, S. A.; Bercaw, J. E. *Organometallics* **2004**, *23*, 1777-1789.

(76)   Irwin, L. J.; Reibenspies, J. H.; Miller, S. A. *J. Am. Chem. Soc.* **2004**, *126*, 16716-16717.

(77)   Guilhemat, R.; Pereyre, M.; Pétraud, M. *Bull. Soc. Chim. Fr.* **1980**, *2*, 334-344.

(78)   Schmid, M. A.; Alt, H. G.; Milius, W. *J. Organomet. Chem.* **1995**, *501*, 101-106.

(79)   Alt, H. G.; Zenk, R. *J. Organomet. Chem.* **1996**, *522*, 39-54.

(80)   Alt, H. G.; Zenk, R. *J. Organomet. Chem.* **1996**, *518*, 7-15.

(81)   Schmid, M. A.; Alt, H. G.; Milius, W. *J. Organomet. Chem.* **1996**, *525*, 9-14.

(82)   Schertl, P.; Alt, H. G. *J. Organomet. Chem.* **1999**, *582*, 328-337.

(83)   Irwin, L. J.; Miller, S. A. *J. Am. Chem. Soc.* **2005**, *127*, 9972-9973.

(84)   Möhring, P. C.; Coville, N. J. *J. Molec. Catal.* **1992**, *77*, 41-50.

(85)   Möhring, P. C.; Vlachakis, N.; Grimmer, N. E.; Coville, N. J. *J. Organomet. Chem.* **1994**, *483*, 159-166.

(86)   Gau, G.; Marques, S. *J. Am. Chem. Soc.* **1976**, *98*, 1538-1541.

(87)   Loukova, G. V. *Chem. Phys. Lett.* **2002**, *353*, 244-252.

(88)   I would like to thank Paul Zeits in our research group who synthesized the Mn complexes and recorded their IR spectra.

(89)   Zachmanoglou, C. E.; Docrat, A.; Bridgewater, B. M.; Parkin, G.; Brandow, C. G.; Bercaw, J. E.; Jardine, C. N.; Lyall, M.; Green, J. C.; Keister, J. B. *J. Am. Chem. Soc.* **2002**, *124*, 9525-9546.

(90)   Bencze, É.; Mink, J.; Németh, C.; Herrmann, W. A.; Lokshin, B. V.; Kühn, F. E. *J. Organomet. Chem.* **2002**, *642*, 246-258.

(91)   Hemond, R. C.; Hughes, R. P.; Locker, H. B. *Organometallics* **1986**, *5*, 2392-2395.

(92)   Decken, A.; MacKay, A. J.; Brown, M. J.; Bottomley, F. *Organometallics* **2002**, *21*, 2006-2009.

(93)   Irwin, L. J.; Zeits, P. D.; Reibenspies, J. H.; Miller, S. A. *Organometallics* **2007**, *26*, 1129-1133.

(94)   Dunning Jr., T. H.; Hay, P. J. In *Modern Theoretical Chemistry*, Schaefer III, H. F., Ed.; Plenum: New York, 1976; Vol. 3, pp 1-28.

(95)   Hay, P. J.; Wadt, W. R. *J. Chem. Phys.* **1985**, *82*, 270-283.

(96)   Krishnan, R.; Binkley, J. S.; Seeger, R.; Pople, J. A. *J. Chem. Phys.* **1980**, *72*, 650-654.

(97)   Spintzagel, G. W.; Clark, T.; Schleyer, P. v. R. *J. Comp. Chem.* **1987**, *8*, 1109-1116.

(98)   Longo, P.; Grassi, A.; Pellecchia, C.; Zambelli, A. *Macromolecules* **1987**, *20*, 1015-18.

(99)   Cavallo, L.; Guerra, G.; Vacatello, M.; Corradini, P. *Macromolecules* **1991**, *24*, 1784-1790.

(100) Guerra, G.; Corradini, P.; Cavallo, L.; Vacatello, M. *Macromol. Symp.* **1995**, *89*, 307-319.

(101) Gilchrist, J. H.; Bercaw, J. E. *J. Am. Chem. Soc.* **1996**, *118*, 12021-12028.

(102) Waymouth, R. M.; Leclerc, M. K. *J. Am. Chem. Soc.* **2001**, *123*, 9555-9563.

(103) Ewen, J. A.; Elder, M. J. Eur. Patent Appl. EP0426637, 1991.

(104) Razavi, A.; Thewalt, U. *J. Organomet. Chem.* **1993**, *445*, 111-114.

(105) Mulliken, R. S.; Person, W. B. *J. Am. Chem. Soc.* **1969**, *91*, 3409-3413.

(106) Cavillot, V.; Champagne, B. *Chem. Phys. Lett.* **2002**, *354*, 449-457.

(107) Ystenes, M.; Eilertsen, J. L.; Liu, J.; Ott, M.; Rytter, E.; Stovneng, J. A. *J. Polym. Sci., Part A: Polym. Chem.* **2000**, *38*, 3106-3127.

(108) Zurek, E.; Woo, T. K.; Firman, T. K.; Ziegler, T. In *Organometallic Catalysts and Olefin Polymerization*, Blom, R.; Follestad, A.; Rytter, E.; Tilset, M.; Ystenes, M., Eds.; Springer: Berlin, 2001; pp 109-123.

(109) Zurek, E.; Ziegler, T. *Prog. Polym. Sci.* **2004**, *29*, 107-148.

(110) Negureanu, L.; Hall, R. W.; Butler, L. G.; Simeral, L. A. *J. Am. Chem. Soc.* **2006**, *128*, 16816-16826.

(111) Babushkin, D. E.; Semikolenova, N. V.; Panchenko, V. N.; Sobolen, A. P.; Zakharov, V. A.; Talsi, E. P. *Macromol. Chem. Phys.* **1997**, *198*, 3845-3854.

(112) Barron, A. R. In *Metallocene-Based Polyolefins*, Scheirs, J.; Kaminsky, W., Eds.; John Wiley & Sons Ltd.: Chichester, UK, 2000; pp 33-67.

(113) Talsi, E. P.; Semikolenova, N. V.; Panchenko, V. N.; Sobolev, A. P.; Babushkin, D. E.; Shubin, A. A.; Zakharov, V. A. *J. Molec. Catal. A, Chem.* **1999**, *139*, 131-137.

(114) Chan, M. S. W.; Vanka, K.; Pye, C. C.; Ziegler, T. *Organometallics* **1999**, *18*, 4624-4636.

(115) Pieters, P. J. J.; van Beek, J. A. M.; van Tol, M. F. H. *Macromol. Rapid Commun.* **1995**, *16*, 463-467.

(116) Paczkowski, N.; Gregorius, H.; Kristen, M. O.; Süling, C.; Suhm, J.; Brintzinger, H.-H.; Wieser, U. International Patent WO 03/006961 A1, 2003.

(117) Coevoet, D.; Cramail, H.; Deffieux, A. *Macromol. Chem. Phys.* **1998**, *199*, 1451-1457.

(118) Coevoet, D.; Cramail, H.; Deffieux, A. *Macromol. Chem. Phys.* **1998**, *199*, 1459-1464.

(119) Pédeutour, J.-N.; Coevoet, D.; Cramail, H.; Deffieux, A. *Macromol. Chem. Phys.* **1999**, *200*, 1215-1221.

(120) Wieser, U.; Brintzinger, H.-H. In *Organometallic Catalysts and Olefin Polymerization*, Blom, R.; Follestad, A.; Rytter, E.; Tilset, M.; Ystenes, M., Eds.; Springer: Berlin, 2001; pp 3-13.

(121) Mäkelä, N. I.; Knuuttila, H. R.; Linnolahti, M.; Pakkanen, T. A.; Leskelä, M. A. *Macromolecules* **2002**, *35*, 3395-3401.

(122) Pédeutour, J.-N.; Radhakrishnan, K.; Cramail, H.; Deffieux, A. *Polym. Int.* **2002**, *51*, 973-977.

(123) Seraidaris, T.; Löfgren, B.; Helaja, T.; Vanne, T.; Mäkelä-Vaarne, N. *J. Polym. Sci., Part A: Polym. Chem.* **2005**, *43*, 6455-6464.

(124) Peruch, F.; Cramail, H.; Deffieux, A. *Macromolecules* **1999**, *32*, 7977-7983.

(125)   Coevoet, D.; Cramail, H.; Deffieux, A. *Macromol. Chem. Phys.* **1999**, *200*, 1208-1214.

(126)   Liu, J.; Støvneng, J. A.; Rytter, E. *J. Polym. Sci., Part A: Polym. Chem.* **2001**, *39*, 3566-3577.

(127)   Pédeutour, J.-N.; Radhakrishnan, K.; Cramail, H.; Deffieux, A. *J. Molec. Catal. A, Chem.* **2002**, *185*, 119-125.

(128)   Bruaseth, I.; Bahr, M.; Gerhard, D.; Rytter, E. *J. Polym. Sci., Part A: Polym. Chem.* **2005**, *43*, 2584-2597.

(129)   Cam, D.; Giannini, U. *Makromol. Chem.* **1992**, *193*, 1049-1055.

(130)   Resconi, L.; Bossi, S.; Abis, L. *Macromolecules* **1990**, *23*, 4489-4491.

(131)   Tritto, I.; Li, S.; Sacchi, M. C.; Zannoni, G. *Macromolecules* **1993**, *26*, 7111-7115.

(132)   Eilertsen, J. L.; Støvneng, J. A.; Ystenes, M.; Rytter, E. *Inorg. Chem.* **2005**, *44*, 4843-4851.

(133)   Bochmann, M.; Lancaster, S. J. *Angew. Chem. Int. Ed. Engl.* **1994**, *33*, 1634-1637.

(134)   Babushkin, D. E.; Semikolenova, N. V.; Zakharov, V. A.; Talsi, E. P. *Macromol. Chem. Phys.* **2000**, *201*, 558-567.

(135)   Pédeutour, J.-N.; Cramail, H.; Deffieux, A. *J. Molec. Catal. A, Chem.* **2001**, *176*, 87-94.

(136)   Gverdtsiteli, D. D.; Revazishvili, N. S.; Tsitsishvili, V. G.; Kikoladze, V. S. *Soobshch. Akad. Nauk. Gruz. SSR* **1989**, *133*, 77-80.

(137)   Stone, K. J.; Little, R. D. *J. Org. Chem.* **1984**, *49*, 1849-1853.

APPENDIX A

KINETIC AND THERMODYNAMIC CONSIDERATIONS IN THE COPOLYMERIZATION OF ETHYLENE AND CARBON DIOXIDE

SPECTRA OF POLYMER AND OLIGOMER SAMPLES

General Considerations and Instrumentation. The insoluble polymer was collected by filtration. Approximatly 100 mg of polymer was dissolved in ~1 mL of 1,1,2,2-tetrachloroethane-d_2. All ^{13}C NMR spectra of polymer samples were recorded on an Inova-300 spectrometer (^{13}C, 75.424 MHz) at 100°C using at least 6100 transients. The methylene peak was used as an internal standard (30.0 ppm). After quenching with acidic methanol, reactions that produced only toluene-soluble oligomers were poured into a separatory funnel and the aqueous layer was removed. The organic layer was washed with a 10% sodium bicarbonate solution then dried over $MgSO_4$ and subjected to GC-MS analysis.

¹³C Spectra of Polymer Samples.
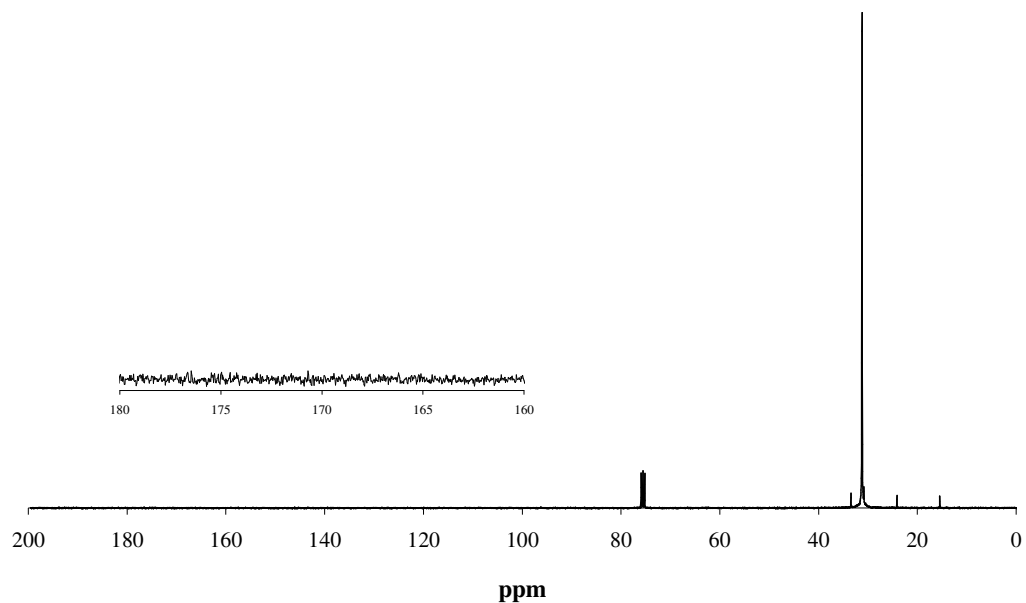
Figure A.1: Polymer produced by the homopolymerization of ethylene with **1**/MAO (Table 2.6, entry 3) showing the necessary absence of carbonyl peaks.
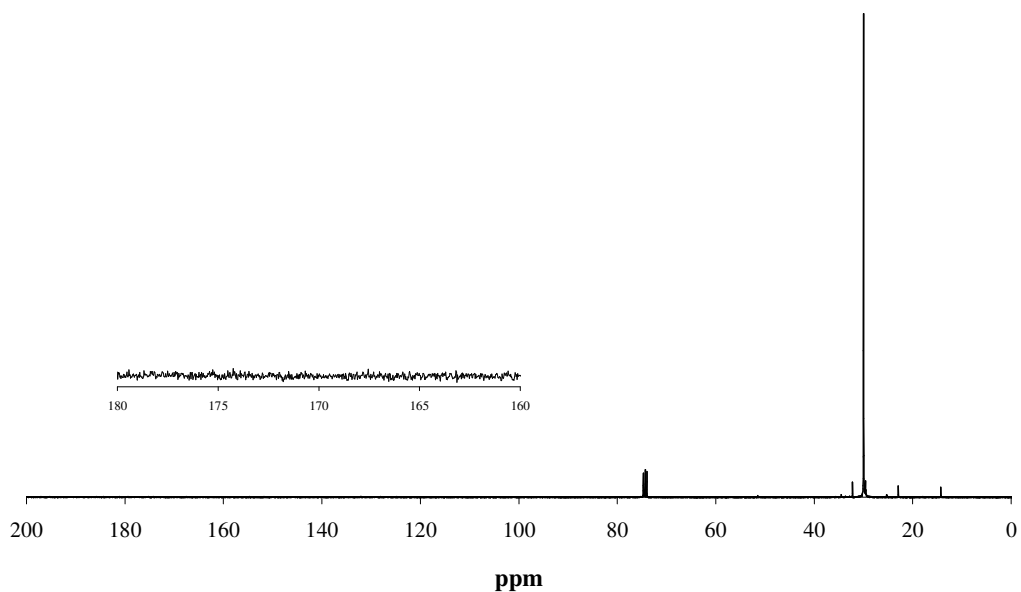
Figure A.2: Polymer produced by **2**/MAO (Table 2.6, entry 4) showing the absence of carbonyl peaks.
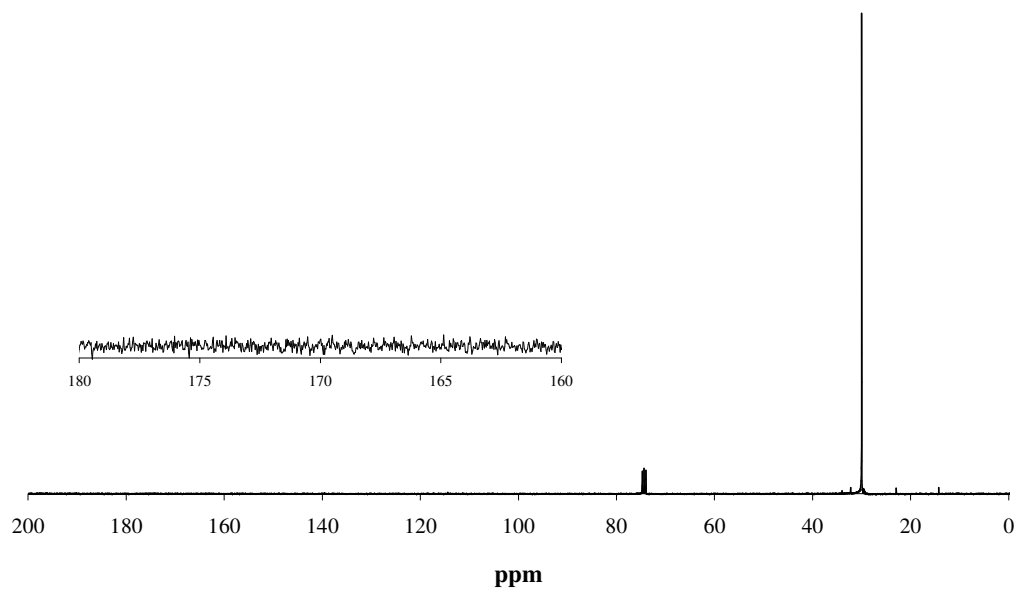
Figure A.3: Polymer produced by **2**/MAO (Table 2.6, entry 5) showing the absence of carbonyl peaks.
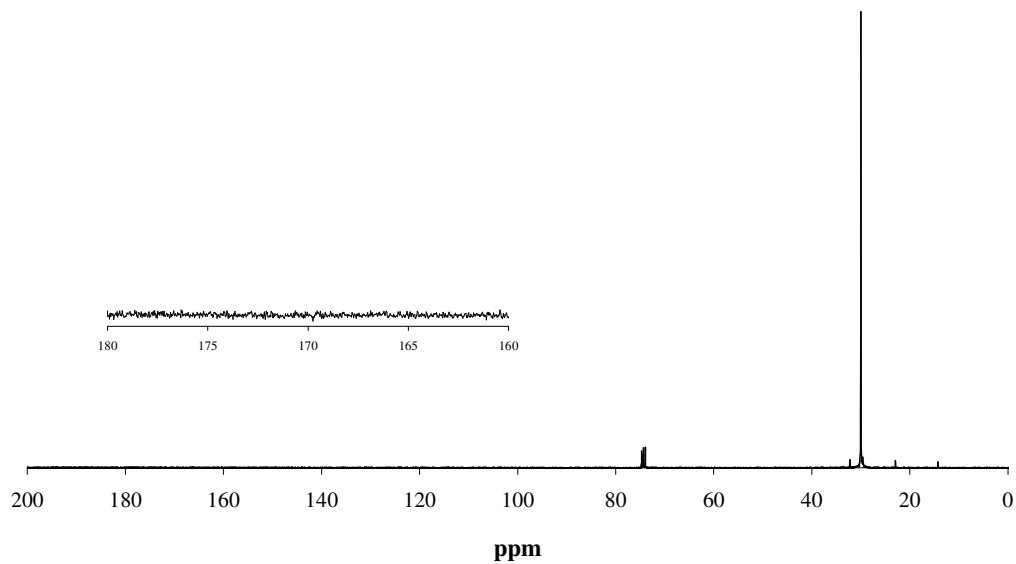
Figure A.4: Polymer produced by **2**/MAO (Table 2.6, entry 6) showing the absence of carbonyl peaks.
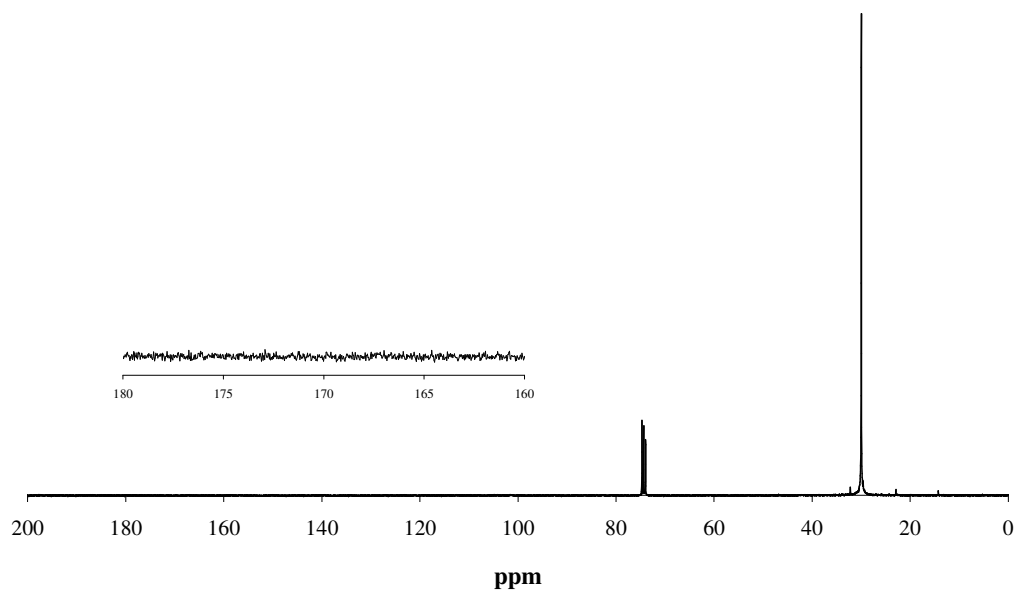
Figure A.5: Polymer produced by **2**/MAO (Table 2.6, entry 7) showing the absence of carbonyl peaks.
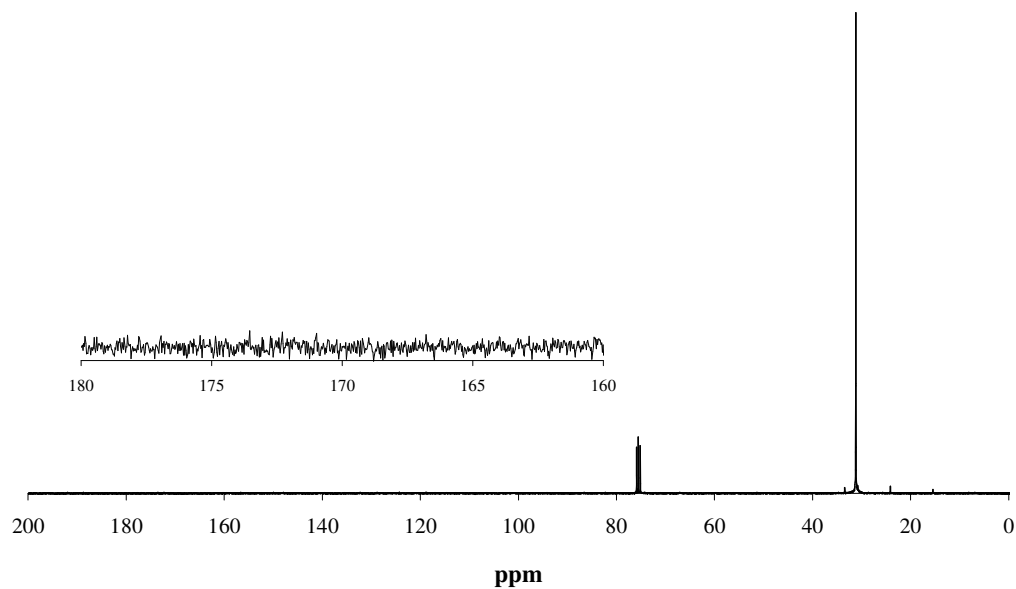
Figure A.6: Polymer produced by **2**/MAO (Table 2.6, entry 8) showing the absence of carbonyl peaks.
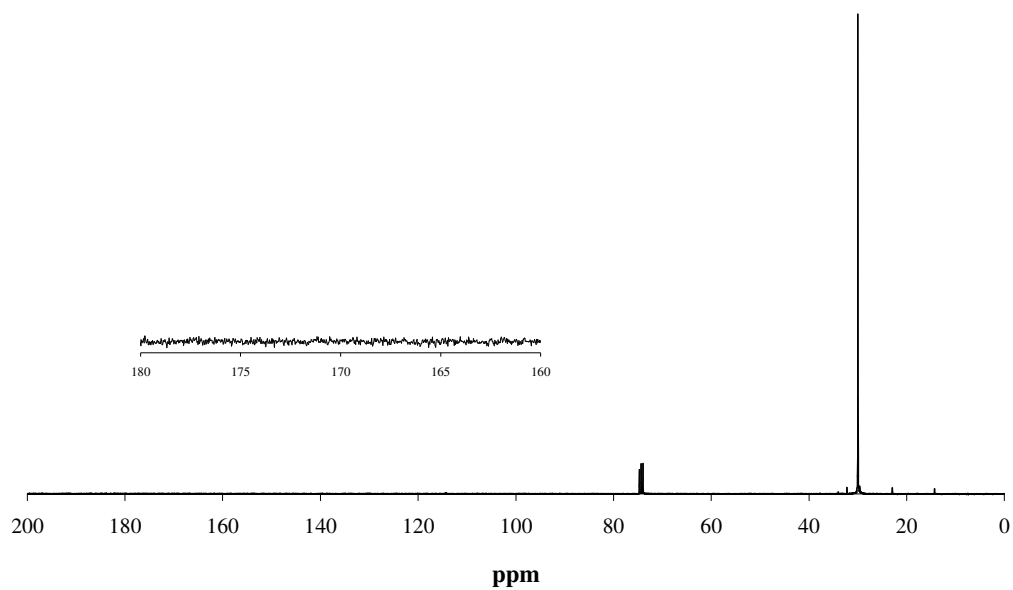
Figure A.7: Polymer produced by the homopolymerization of ethylene with **2**/MAO (Table 2.6, entry 9) showing the necessary absence of carbonyl peaks.
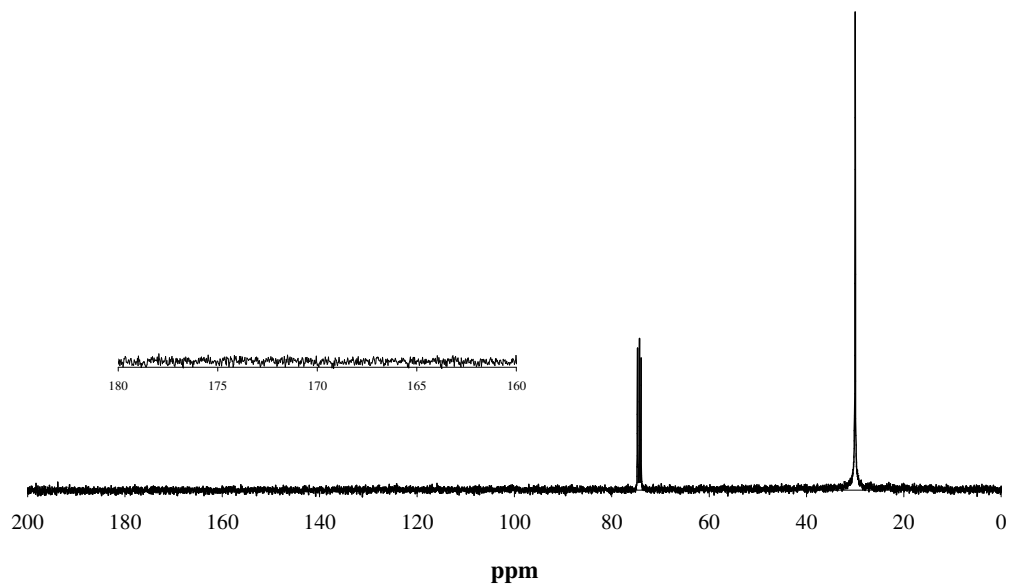
Figure A.8: Polymer produced by **3**/MAO (Table 2.6, entry 10) showing the absence of carbonyl peaks.
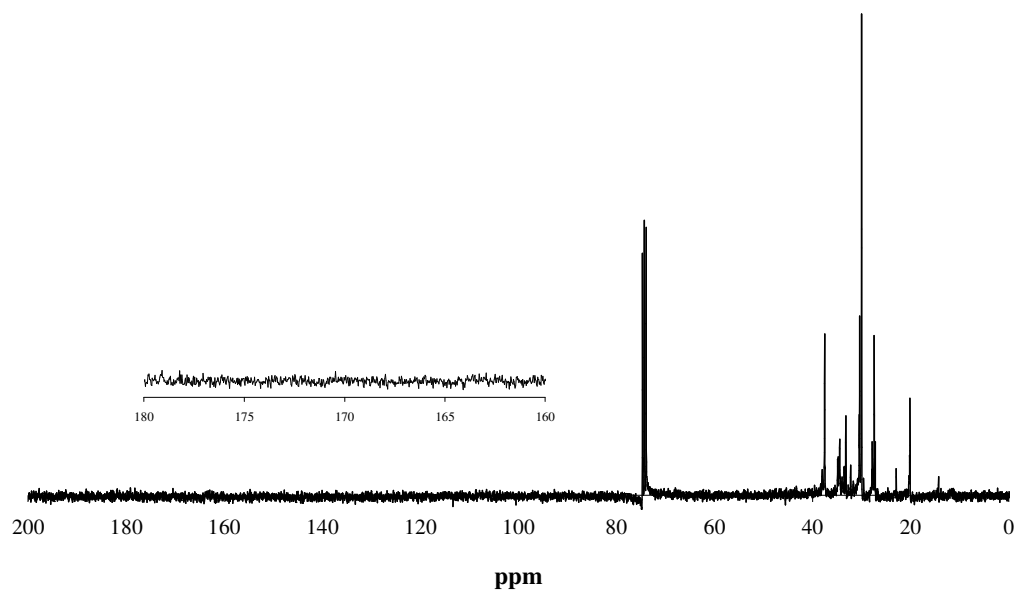
Figure A.9: Polymer produced by **5**/MAO (Table 2.6, entry 14) showing the absence of carbonyl peaks.
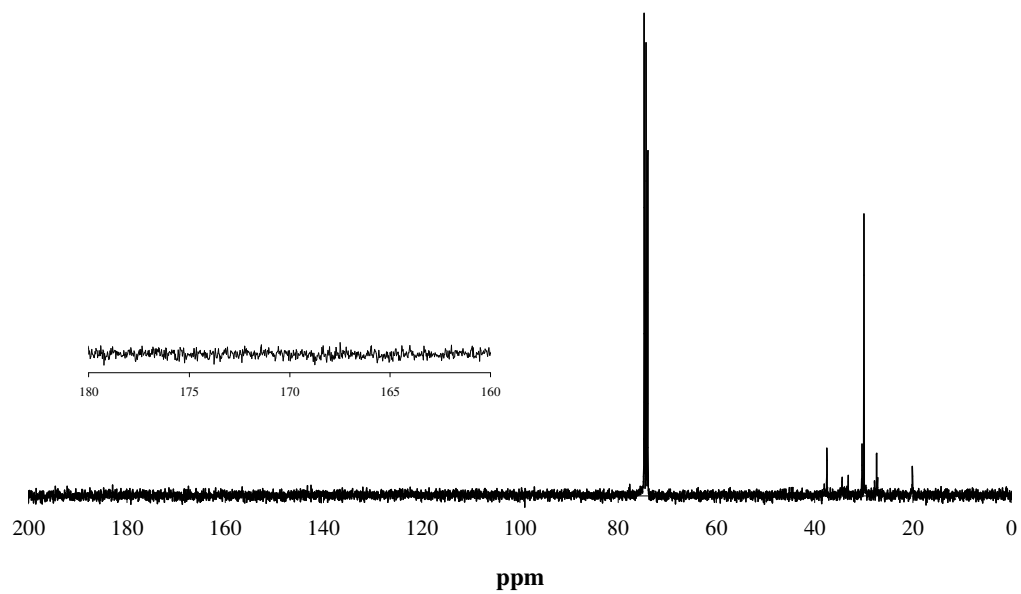
Figure A.10: Polymer produced by **5**/MAO (Table 2.6, entry 15) showing the absence of carbonyl peaks.

GC-MS Spectra.
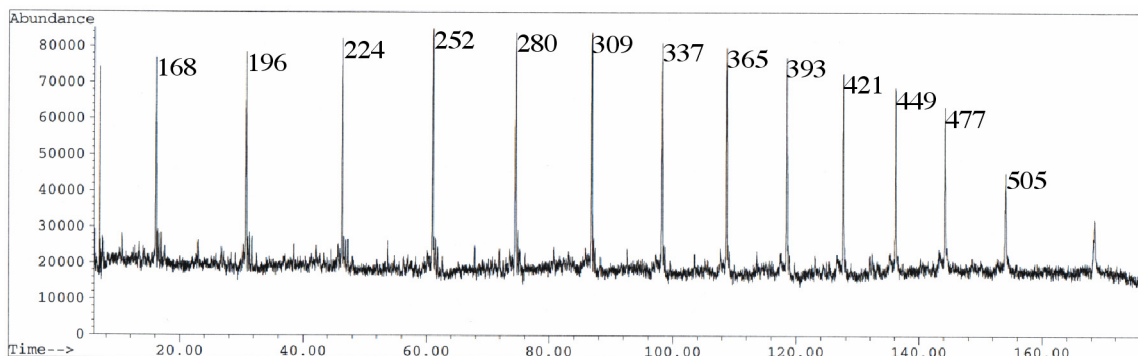
Figure A.11: GC traces of oligomers produced with **4**/MAO, (Table 2.6, entry 12), with the representative masses for each peak.
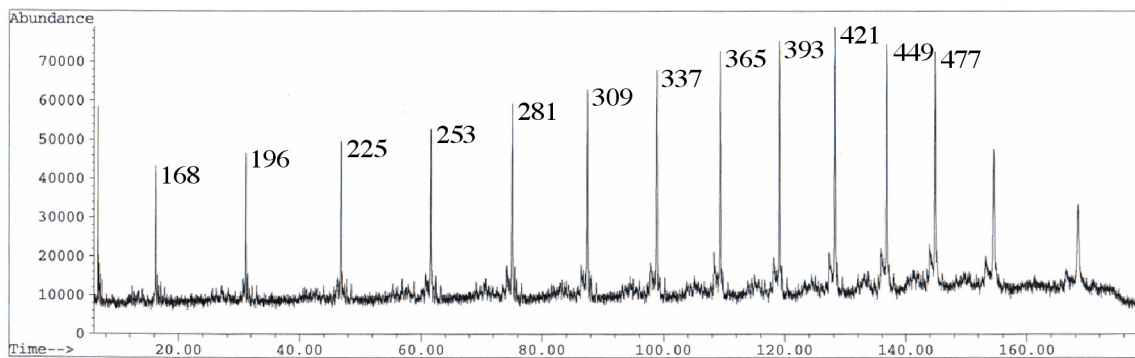
Figure A.12: GC traces of oligomers produced with **4**/MAO, (Table 2.6, entry 13), with the representative masses for each peak.
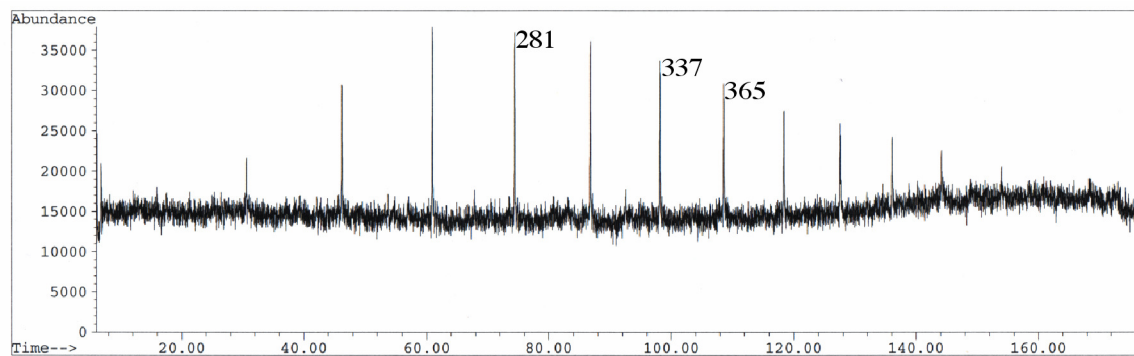
Figure A.13: GC traces of oligomers produced with **6**/MAO, (Table 2.6, entry 16), with the representative masses for each peak.

QUANTUM CHEMICAL CALCULATIONS

Computational methods. All calculations were performed using the Gaussian 03 suite of programs.[58] Geometry optimizations and frequency calculations were performed using Density Function Theory (DFT) employing Becke's 3-parameter hybrid functional (B3)[59] with the correlation functional of Lee, Yang and Parr (LYP).[60,61] Pople-style, double-ζ split polarized basis sets with pure d orbitals (6-31G(d') = 6-31G†) was used.[62,63] All energies include zero-point energies. The compounds are named in the following manner: Xchain$Y$ where X is the total number of monomer units in the chain and Y is the number of CO_2 units in the chain.

Geometry optomized structures and coordinates.

Table A.1: DFT Geometry Optimized Coordinates (B3LYP/6-31G(d')) for 2chain0.
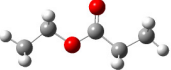
Atom	x	y	z	Atom	x	y	z
C	-0.7048	-1.8364	0.0000	H	-1.2565	0.0640	0.8788
C	-0.7048	-0.3036	0.0000	H	-1.2565	0.0640	-0.8788
C	0.7048	0.3036	0.0000	H	1.2565	-0.0640	-0.8788
C	0.7048	1.8364	0.0000	H	1.2565	-0.0640	0.8788
H	-1.7255	-2.2399	0.0000	H	1.7255	2.2399	0.0000
H	-0.1899	-2.2337	0.8854	H	0.1899	2.2337	0.8854
H	-0.1899	-2.2337	-0.8854	H	0.1899	2.2337	-0.8854

Table A.2: DFT Geometry Optimized Coordinates (B3LYP/6-31G(d')) for 3chain0.
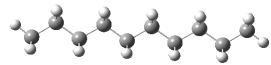
Atom	x	y	z	Atom	x	y	z
C	-1.3953	-2.9156	0.0000	H	-1.9608	-1.0195	-0.8785
C	-1.4059	-1.3827	0.0000	H	0.5556	-1.1316	-0.8789
C	0.0000	-0.7672	0.0000	H	0.5556	-1.1316	0.8789
C	0.0000	0.7672	0.0000	H	-0.5556	1.1316	0.8789
C	1.4059	1.3827	0.0000	H	-0.5556	1.1316	-0.8789
C	1.3953	2.9156	0.0000	H	1.9608	1.0195	-0.8785
H	-2.4136	-3.3253	0.0000	H	1.9608	1.0195	0.8785
H	-0.8779	-3.3094	0.8854	H	2.4136	3.3253	0.0000
H	-0.8779	-3.3094	-0.8854	H	0.8779	3.3094	0.8854
H	-1.9608	-1.0195	0.8785	H	0.8779	3.3094	-0.8854

Table A.3: DFT Geometry Optimized Coordinates (B3LYP/6-31G(d')) for 3chain1.
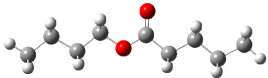
Atom	x	y	z	Atom	x	y	z
C	3.0159	-0.1625	0.0008	H	3.1498	0.4738	-0.8810
C	1.6362	-0.8196	-0.0007	H	1.5011	-1.4735	0.8722
C	0.5033	0.1912	-0.0003	H	1.5021	-1.4715	-0.8752
O	-0.6974	-0.4315	0.0001	H	-1.8158	1.0798	-0.8835
C	-1.8571	0.4317	0.0002	H	-1.8158	1.0797	0.8840
C	-3.0882	-0.4567	0.0002	H	-3.9945	0.1613	0.0003
O	0.6320	1.3935	-0.0004	H	-3.1084	-1.0987	0.8886
H	3.8039	-0.9248	0.0003	H	-3.1085	-1.0985	-0.8883
H	3.1489	0.4719	0.8840				

Table A.4: DFT Geometry Optimized Coordinates (B3LYP/6-31G(d')) for 4chain0.
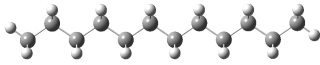
Atom	x	y	z	Atom	x	y	z
C	2.8131	-3.5239	0.0000	H	1.9625	-1.0196	-0.8787
C	1.4056	-2.9171	0.0000	H	1.9625	-1.0196	0.8787
C	1.4056	-1.3825	0.0000	H	-0.5563	-1.1310	0.8787
C	-0.0001	-0.7673	0.0000	H	-0.5563	-1.1310	-0.8787
C	0.0001	0.7673	0.0000	H	0.5563	1.1310	-0.8787
C	-1.4056	1.3825	0.0000	H	0.5563	1.1310	0.8787
C	-1.4056	2.9171	0.0000	H	-1.9625	1.0196	0.8787
C	-2.8131	3.5239	0.0000	H	-1.9625	1.0196	-0.8787
H	2.7780	-4.6209	0.0000	H	-0.8498	3.2795	-0.8784
H	3.3822	-3.2092	0.8854	H	-0.8498	3.2795	0.8784
H	3.3822	-3.2092	-0.8854	H	-2.7780	4.6209	0.0000
H	0.8498	-3.2795	0.8784	H	-3.3822	3.2092	0.8854
H	0.8498	-3.2795	-0.8784	H	-3.3822	3.2092	-0.8854

Table A.5: DFT Geometry Optimized Coordinates (B3LYP/6-31G(d')) for 5chain0.
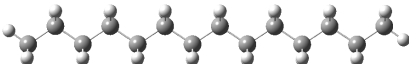
Atom	x	y	z	Atom	x	y	z
C	2.8008	5.0651	0.0000	H	0.8504	3.2807	0.8788
C	2.8118	3.5321	0.0000	H	1.9623	1.0181	0.8788
C	1.4061	2.9164	0.0000	H	1.9623	1.0181	-0.8788
C	1.4064	1.3817	0.0000	H	-0.5559	1.1310	-0.8788
C	0.0000	0.7673	0.0000	H	-0.5559	1.1310	0.8788
C	0.0002	-0.7675	0.0000	H	0.5561	-1.1312	0.8788
C	-1.4062	-1.3818	0.0000	H	0.5561	-1.1312	-0.8788
C	-1.4060	-2.9165	0.0000	H	-1.9621	-1.0182	-0.8788
C	-2.8118	-3.5320	0.0000	H	-1.9621	-1.0182	0.8788
C	-2.8011	-5.0649	0.0000	H	-0.8503	-3.2808	0.8788
H	3.8188	5.4753	0.0000	H	-0.8503	-3.2808	-0.8788
H	2.2831	5.4587	0.8854	H	-3.3668	-3.1689	-0.8785
H	2.2831	5.4587	-0.8854	H	-3.3668	-3.1689	0.8785
H	3.3669	3.1692	0.8785	H	-3.8193	-5.4748	0.0000
H	3.3669	3.1692	-0.8785	H	-2.2836	-5.4587	0.8854
H	0.8504	3.2807	-0.8788	H	-2.2836	-5.4587	-0.8854

Table A.6: DFT Geometry Optimized Coordinates (B3LYP/6-31G(d')) for 5chain1.

Atom	x	y	z	Atom	x	y	z
C	-3.0480	0.1723	0.0001	H	1.8517	1.1609	0.8840
C	-1.6988	-0.5500	-0.0003	H	1.8518	1.1609	-0.8837
C	-0.5135	0.3986	-0.0001	H	2.9794	-1.0945	-0.8805
O	0.6520	-0.2881	0.0001	H	2.9796	-1.0943	0.8810
C	1.8565	0.5104	0.0001	H	-4.1764	-1.4540	0.8780
C	3.0449	-0.4396	0.0001	H	-4.1767	-1.4531	-0.8792
O	-0.5761	1.6062	-0.0002	H	-6.4264	-0.7858	-0.0001
C	-4.2398	-0.7930	-0.0002	H	-5.7015	0.5689	-0.8845
C	-5.5926	-0.0723	0.0004	H	-5.7013	0.5677	0.8862
C	4.3865	0.3062	-0.0001	H	4.4383	0.9666	0.8786
C	5.5927	-0.6396	0.0001	H	4.4382	0.9662	-0.8791
H	-3.1026	0.8347	-0.8748	H	6.5371	-0.0812	-0.0002
H	-3.1025	0.8340	0.8754	H	5.5885	-1.2891	-0.8854
H	-1.6004	-1.2103	-0.8743	H	5.5887	-1.2886	0.8859
H	-1.6003	-1.2110	0.8732				

Table A.7: DFT Geometry Optimized Coordinates (B3LYP/6-31G(d')) for 6chain0.

Atom	x	y	z	Atom	x	y	z
C	-4.2201	5.6727	0.0000	H	-0.8500	3.2808	0.8788
C	-2.8123	5.0664	0.0000	H	-0.8500	3.2808	-0.8788
C	-2.8117	3.5318	0.0000	H	-1.9618	1.0186	-0.8788
C	-1.4059	2.9170	0.0000	H	-1.9618	1.0186	0.8788
C	-1.4059	1.3823	0.0000	H	0.5561	1.1310	0.8788
C	0.0002	0.7674	0.0000	H	0.5561	1.1310	-0.8788
C	-0.0002	-0.7674	0.0000	H	-0.5561	-1.1310	-0.8788
C	1.4059	-1.3823	0.0000	H	-0.5561	-1.1310	0.8788
C	1.4059	-2.9170	0.0000	H	1.9618	-1.0186	0.8788
C	2.8117	-3.5318	0.0000	H	1.9618	-1.0186	-0.8788
C	2.8123	-5.0664	0.0000	H	0.8500	-3.2808	-0.8788
C	4.2201	-5.6727	0.0000	H	0.8500	-3.2808	0.8788
H	-4.1853	6.7698	0.0000	H	3.3683	-3.1688	0.8788
H	-4.7891	5.3580	0.8854	H	3.3683	-3.1688	-0.8788
H	-4.7891	5.3580	-0.8854	H	2.2570	-5.4292	-0.8785
H	-2.2570	5.4292	0.8785	H	2.2570	-5.4292	0.8785
H	-2.2570	5.4292	-0.8785	H	4.1853	-6.7698	0.0000
H	-3.3683	3.1688	-0.8788	H	4.7891	-5.3580	0.8854
H	-3.3683	3.1688	0.8788	H	4.7891	-5.3580	-0.8854

Table A.8: DFT Geometry Optimized Coordinates (B3LYP/6-31G(d')) for 7chain0.
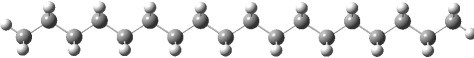
Atom	x	y	z	Atom	x	y	z
C	-8.3458	-0.3237	-0.0005	H	-4.4811	1.1407	-0.8791
C	-7.0580	0.5077	-0.0005	H	-3.2237	-1.0439	-0.8788
C	-5.7838	-0.3476	-0.0003	H	-3.2238	-1.0438	0.8787
C	-4.4893	0.4765	-0.0003	H	-1.9127	1.1090	0.8786
C	-3.2155	-0.3796	-0.0001	H	-1.9126	1.1088	-0.8789
C	-1.9209	0.4446	-0.0001	H	-0.6556	-1.0761	-0.8786
C	-0.6474	-0.4117	0.0000	H	-0.6557	-1.0760	0.8788
C	0.6474	0.4123	0.0000	H	0.6557	1.0766	0.8787
C	1.9208	-0.4442	0.0002	H	0.6558	1.0765	-0.8788
C	3.2156	0.3799	0.0001	H	1.9125	-1.1085	-0.8785
C	4.4892	-0.4764	0.0003	H	1.9125	-1.1083	0.8790
C	5.7839	0.3474	0.0003	H	3.2239	1.0443	0.8788
C	7.0579	-0.5082	0.0004	H	3.2240	1.0441	-0.8786
C	8.3459	0.3230	0.0004	H	4.4810	-1.1408	-0.8784
H	-9.2378	0.3159	-0.0006	H	4.4809	-1.1406	0.8791
H	-8.4008	-0.9715	0.8850	H	5.7931	1.0120	0.8790
H	-8.4007	-0.9717	-0.8858	H	5.7931	1.0118	-0.8786
H	-7.0494	1.1710	0.8780	H	7.0492	-1.1715	-0.8780
H	-7.0493	1.1709	-0.8790	H	7.0491	-1.1713	0.8789
H	-5.7928	-1.0121	-0.8790	H	9.2377	-0.3168	0.0005
H	-5.7929	-1.0120	0.8785	H	8.4010	0.9710	0.8857
H	-4.4812	1.1409	0.8784	H	8.4010	0.9708	-0.8851

Table A.9: DFT Geometry Optimized Coordinates (B3LYP/6-31G(d')) for 7chain1.
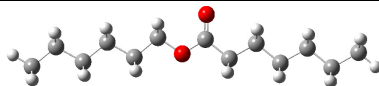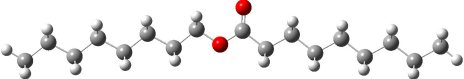
Atom	x	y	z	Atom	x	y	z
C	3.0550	0.3428	0.0000	H	-2.9600	-0.9832	0.8806
C	1.7134	-0.3939	-0.0002	H	-2.9601	-0.9831	-0.8808
C	0.5186	0.5427	-0.0001	H	4.2016	-1.2719	-0.8792
O	-0.6402	-0.1554	-0.0001	H	4.2015	-1.2724	0.8785
C	-1.8523	0.6316	0.0000	H	5.6632	0.7808	0.8790
C	-3.0321	-0.3292	-0.0001	H	5.6633	0.7813	-0.8783
O	0.5692	1.7509	0.0000	H	-4.4370	1.0670	-0.8791
C	4.2571	-0.6099	-0.0002	H	-4.4369	1.0670	0.8790
C	5.6073	0.1191	0.0001	H	-5.5290	-1.2038	0.8791
C	-4.3795	0.4061	0.0000	H	-5.5290	-1.2040	-0.8788
C	-5.5857	-0.5425	0.0001	H	6.7597	-1.4870	-0.8788
C	6.8158	-0.8264	0.0000	H	6.7596	-1.4875	0.8783
C	8.1604	-0.0903	0.0003	H	9.0031	-0.7934	0.0001
C	-6.9362	0.1859	0.0000	H	8.2624	0.5515	0.8859
C	-8.1368	-0.7670	0.0002	H	8.2625	0.5520	-0.8849
H	3.1015	1.0052	0.8752	H	-6.9919	0.8466	-0.8786
H	3.1016	1.0055	-0.8749	H	-6.9918	0.8468	0.8785
H	1.6218	-1.0557	0.8734	H	-9.0860	-0.2164	0.0001
H	1.6219	-1.0554	-0.8740	H	-8.1289	-1.4168	0.8858
H	-1.8536	1.2823	-0.8838	H	-8.1289	-1.4171	-0.8852
H	-1.8535	1.2822	0.8838				

Table A.10: DFT Geometry Optimized Coordinates (B3LYP/6-31G(d')) for 8chain0.
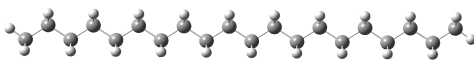
Atom	x	y	z	Atom	x	y	z
C	5.6318	-7.8173	0.0000	H	3.3692	-3.1665	-0.8788
C	4.2227	-7.2136	0.0000	H	3.3692	-3.1665	0.8788
C	4.2209	-5.6788	0.0000	H	0.8511	-3.2803	0.8788
C	2.8142	-5.0653	0.0000	H	0.8511	-3.2803	-0.8788
C	2.8136	-3.5304	0.0000	H	1.9624	-1.0178	-0.8788
C	1.4068	-2.9165	0.0000	H	1.9624	-1.0178	0.8788
C	1.4067	-1.3816	0.0000	H	-0.5557	-1.1312	0.8788
C	0.0000	-0.7675	0.0000	H	-0.5557	-1.1312	-0.8788
C	0.0000	0.7675	0.0000	H	0.5557	1.1312	-0.8788
C	-1.4067	1.3816	0.0000	H	0.5557	1.1312	0.8788
C	-1.4068	2.9165	0.0000	H	-1.9624	1.0178	0.8788
C	-2.8136	3.5304	0.0000	H	-1.9624	1.0178	-0.8788
C	-2.8142	5.0653	0.0000	H	-0.8511	3.2803	-0.8788
C	-4.2209	5.6788	0.0000	H	-0.8511	3.2803	0.8788
C	-4.2227	7.2136	0.0000	H	-3.3692	3.1665	0.8788
C	-5.6318	7.8173	0.0000	H	-3.3692	3.1665	-0.8788
H	5.5995	-8.9145	0.0000	H	-2.2586	5.4293	-0.8788
H	6.1998	-7.5009	0.8854	H	-2.2586	5.4293	0.8788
H	6.1998	-7.5009	-0.8854	H	-4.7771	5.3154	0.8788
H	3.6678	-7.5768	0.8785	H	-4.7771	5.3154	-0.8788
H	3.6678	-7.5768	-0.8785	H	-3.6678	7.5768	-0.8785
H	4.7771	-5.3154	-0.8788	H	-3.6678	7.5768	0.8785
H	4.7771	-5.3154	0.8788	H	-5.5995	8.9145	0.0000
H	2.2586	-5.4293	0.8788	H	-6.1998	7.5009	0.8854
H	2.2586	-5.4293	-0.8788	H	-6.1998	7.5009	-0.8854

Table A.11: DFT Geometry Optimized Coordinates (B3LYP/6-31G(d')) for 9chain0.
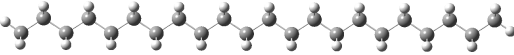
Atom	x	y	z	Atom	x	y	z
C	10.9125	-0.3458	-0.0001	H	5.7869	-1.0397	-0.8782
C	9.6289	0.4922	0.0002	H	4.4865	1.1196	-0.8779
C	8.3504	-0.3565	0.0003	H	4.4866	1.1194	0.8796
C	7.0601	0.4741	0.0006	H	3.2189	-1.0592	0.8794
C	5.7821	-0.3755	0.0006	H	3.2188	-1.0591	-0.8780
C	4.4916	0.4552	0.0008	H	1.9180	1.1000	-0.8778
C	3.2138	-0.3948	0.0008	H	1.9179	1.0997	0.8797
C	1.9231	0.4355	0.0009	H	0.6505	-1.0792	0.8793
C	0.6454	-0.4147	0.0007	H	0.6506	-1.0790	-0.8781
C	-0.6454	0.4155	0.0007	H	-0.6505	1.0799	-0.8780
C	-1.9230	-0.4349	0.0004	H	-0.6507	1.0796	0.8795
C	-3.2138	0.3954	0.0003	H	-1.9180	-1.0993	0.8790
C	-4.4915	-0.4548	-0.0002	H	-1.9177	-1.0991	-0.8784
C	-5.7821	0.3756	-0.0003	H	-3.2188	1.0598	-0.8784
C	-7.0600	-0.4743	-0.0008	H	-3.2191	1.0595	0.8791
C	-8.3505	0.3561	-0.0011	H	-4.4866	-1.1193	0.8785
C	-9.6288	-0.4929	-0.0016	H	-4.4862	-1.1190	-0.8790
C	-10.9126	0.3448	-0.0018	H	-5.7869	1.0401	-0.8789
H	11.8077	0.2892	-0.0001	H	-5.7874	1.0398	0.8785
H	10.9639	-0.9939	-0.8856	H	-7.0553	-1.1387	0.8778
H	10.9642	-0.9941	0.8853	H	-7.0548	-1.1384	-0.8797
H	9.6236	1.1556	-0.8782	H	-8.3561	1.0208	-0.8797
H	9.6239	1.1554	0.8788	H	-8.3566	1.0205	0.8778
H	8.3562	-1.0211	0.8790	H	-9.6237	-1.1564	0.8768
H	8.3560	-1.0209	-0.8785	H	-9.6232	-1.1560	-0.8802
H	7.0552	1.1386	-0.8781	H	-11.8076	-0.2905	-0.0022
H	7.0554	1.1384	0.8794	H	-10.9641	0.9931	-0.8871
H	5.7870	-1.0399	0.8793	H	-10.9646	0.9928	0.8837

Table A.12: DFT Geometry Optimized Coordinates (B3LYP/6-31G(d')) for 9chain1.

Atom	x	y	z	Atom	x	y	z
C	3.0587	0.4736	0.0001	H	4.2116	-1.1368	-0.8790
C	1.7197	-0.2677	-0.0002	H	4.2116	-1.1371	0.8787
C	0.5219	0.6651	-0.0002	H	5.6633	0.9228	0.8787
O	-0.6348	-0.0363	0.0000	H	5.6633	0.9229	-0.8785
C	-1.8490	0.7476	0.0001	H	-4.4336	1.1785	-0.8787
C	-3.0268	-0.2157	0.0001	H	-4.4337	1.1782	0.8793
O	0.5689	1.8735	-0.0003	H	-5.5222	-1.0940	0.8787
C	4.2644	-0.4746	-0.0001	H	-5.5223	-1.0935	-0.8792
C	5.6115	0.2607	0.0001	H	6.7719	-1.3416	-0.8788
C	-4.3753	0.5176	0.0002	H	6.7719	-1.3416	0.8789
C	-5.5805	-0.4327	-0.0001	H	8.2241	0.7189	0.8787
C	6.8243	-0.6794	0.0000	H	8.2241	0.7188	-0.8788
C	8.1708	0.0565	0.0000	H	-6.9875	0.9576	-0.8784
C	-6.9312	0.2955	0.0002	H	-6.9875	0.9570	0.8793
C	-8.1389	-0.6510	-0.0001	H	-8.0836	-1.3134	0.8785
C	9.3847	-0.8822	0.0001	H	-8.0837	-1.3127	-0.8792
C	10.7256	-0.1393	0.0001	H	9.3320	-1.5435	-0.8784
C	-9.4897	0.0774	0.0002	H	9.3320	-1.5434	0.8786
C	-10.6911	-0.8745	-0.0001	H	11.5721	-0.8379	0.0002
H	3.1028	1.1361	0.8752	H	10.8244	0.5033	0.8854
H	3.1029	1.1365	-0.8748	H	10.8245	0.5032	-0.8854
H	1.6301	-0.9299	0.8733	H	-9.5451	0.7387	-0.8780
H	1.6304	-0.9294	-0.8741	H	-9.5450	0.7379	0.8790
H	-1.8518	1.3983	-0.8837	H	-11.6403	-0.3236	0.0002
H	-1.8518	1.3982	0.8839	H	-10.6835	-1.5250	0.8850
H	-2.9535	-0.8695	0.8808	H	-10.6836	-1.5242	-0.8859
H	-2.9536	-0.8694	-0.8808				

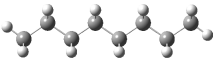**Table A.13:** DFT Geometry Optimized Coordinates (B3LYP/6-31G(d')) for 10chain0.
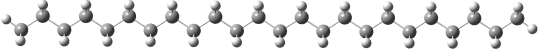
Atom	x	y	z	Atom	x	y	z
C	5.6279	-7.8280	0.0000	H	0.8501	-3.2808	-0.8785
C	4.2214	-7.2146	0.0000	H	1.9623	-1.0184	-0.8785
C	4.2198	-5.6799	0.0000	H	1.9623	-1.0184	0.8785
C	2.8133	-5.0661	0.0000	H	-0.5563	-1.1311	0.8785
C	2.8125	-3.5314	0.0000	H	-0.5563	-1.1311	-0.8785
C	1.4063	-2.9169	0.0000	H	0.5563	1.1311	-0.8785
C	1.4061	-1.3822	0.0000	H	0.5563	1.1311	0.8785
C	0.0000	-0.7673	0.0000	H	-1.9623	1.0184	0.8785
C	0.0000	0.7673	0.0000	H	-1.9623	1.0184	-0.8785
C	-1.4061	1.3822	0.0000	H	-0.8501	3.2808	-0.8785
C	-1.4063	2.9169	0.0000	H	-0.8501	3.2808	0.8785
C	-2.8125	3.5314	0.0000	H	-3.3686	3.1674	0.8785
C	-2.8133	5.0661	0.0000	H	-3.3686	3.1674	-0.8785
C	-4.2198	5.6799	0.0000	H	-2.2573	5.4302	-0.8785
C	-4.2214	7.2146	0.0000	H	-2.2573	5.4302	0.8785
C	-5.6279	7.8280	0.0000	H	-4.7757	5.3156	0.8785
C	5.6306	-9.3626	0.0000	H	-4.7757	5.3156	-0.8785
C	7.0395	-9.9663	0.0000	H	-3.6656	7.5790	-0.8786
C	-5.6305	9.3626	0.0000	H	-3.6656	7.5790	0.8786
C	-7.0395	9.9663	0.0000	H	-6.1843	7.4642	0.8786
H	6.1844	-7.4642	0.8786	H	-6.1843	7.4642	-0.8786
H	6.1844	-7.4642	-0.8786	H	5.0755	-9.7261	-0.8783
H	3.6656	-7.5790	0.8786	H	5.0755	-9.7261	0.8783
H	3.6656	-7.5790	-0.8786	H	7.0073	-11.0634	0.0000
H	4.7757	-5.3156	-0.8785	H	7.6076	-9.6498	0.8854
H	4.7757	-5.3156	0.8785	H	7.6076	-9.6498	-0.8854
H	2.2573	-5.4302	0.8785	H	-5.0755	9.7261	-0.8783
H	2.2573	-5.4302	-0.8785	H	-5.0755	9.7261	0.8783
H	3.3686	-3.1674	-0.8785	H	-7.0073	11.0634	0.0000
H	3.3686	-3.1674	0.8785	H	-7.6076	9.6498	0.8854
H	0.8501	-3.2808	0.8785	H	-7.6076	9.6498	-0.8854

Table A.14: DFT Geometry Optimized Coordinates (B3LYP/6-31G(d')) for 11chain0.
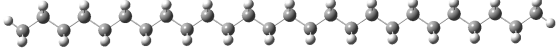
Atom	x	y	z	Atom	x	y	z
C	-13.4799	-0.3607	-0.0004	H	-7.0579	1.1220	-0.8785
C	-12.1987	0.4808	-0.0002	H	-5.7845	-1.0534	-0.8788
C	-10.9179	-0.3645	-0.0003	H	-5.7846	-1.0536	0.8787
C	-9.6298	0.4697	0.0000	H	-4.4892	1.1087	0.8790
C	-8.3495	-0.3765	-0.0001	H	-4.4892	1.1089	-0.8785
C	-7.0612	0.4575	0.0001	H	-3.2163	-1.0668	-0.8786
C	-5.7812	-0.3892	0.0001	H	-3.2164	-1.0669	0.8789
C	-4.4927	0.4445	0.0002	H	-1.9206	1.0951	0.8790
C	-3.2128	-0.4025	0.0002	H	-1.9205	1.0952	-0.8785
C	-1.9241	0.4309	0.0003	H	-0.6480	-1.0807	-0.8785
C	-0.6444	-0.4163	0.0002	H	-0.6480	-1.0807	0.8790
C	0.6444	0.4169	0.0002	H	0.6480	1.0813	0.8790
C	1.9241	-0.4303	0.0003	H	0.6480	1.0813	-0.8785
C	3.2129	0.4030	0.0002	H	1.9205	-1.0947	-0.8784
C	4.4926	-0.4441	0.0002	H	1.9205	-1.0946	0.8790
C	5.7813	0.3894	0.0001	H	3.2164	1.0674	0.8789
C	7.0612	-0.4574	0.0001	H	3.2164	1.0673	-0.8786
C	8.3496	0.3765	-0.0001	H	4.4891	-1.1085	-0.8784
C	9.6298	-0.4699	0.0000	H	4.4892	-1.1083	0.8790
C	10.9179	0.3640	-0.0003	H	5.7847	1.0539	0.8787
C	12.1986	-0.4815	-0.0002	H	5.7847	1.0537	-0.8787
C	13.4800	0.3598	-0.0005	H	7.0578	-1.1219	-0.8785
H	-14.3769	0.2718	-0.0004	H	7.0579	-1.1216	0.8790
H	-13.5298	-1.0092	0.8848	H	8.3529	1.0410	0.8786
H	-13.5297	-1.0089	-0.8860	H	8.3528	1.0407	-0.8789
H	-12.1954	1.1439	0.8784	H	9.6266	-1.1344	-0.8787
H	-12.1953	1.1443	-0.8786	H	9.6267	-1.1341	0.8789
H	-10.9217	-1.0288	-0.8792	H	10.9220	1.0287	0.8784
H	-10.9218	-1.0292	0.8784	H	10.9219	1.0284	-0.8792
H	-9.6269	1.1338	0.8789	H	12.1951	-1.1449	-0.8786
H	-9.6268	1.1341	-0.8787	H	12.1952	-1.1446	0.8784
H	-8.3526	-1.0407	-0.8789	H	14.3768	-0.2729	-0.0004
H	-8.3527	-1.0410	0.8785	H	13.5300	1.0083	0.8848
H	-7.0580	1.1217	0.8790	H	13.5299	1.0079	-0.8860

Table A.15: DFT Geometry Optimized Coordinates (B3LYP/6-31G(d')) for 11chain1.
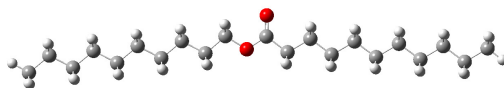
Atom	x	y	z	Atom	x	y	z
C	-3.0611	0.5872	0.0000	H	-5.6644	1.0418	-0.8782
C	-1.7231	-0.1558	-0.0006	H	-5.6642	1.0412	0.8789
C	-0.5243	0.7756	-0.0002	H	4.4306	1.2864	0.8786
O	0.6318	0.0731	-0.0013	H	4.4309	1.2865	-0.8794
C	1.8465	0.8562	-0.0009	H	5.5202	-0.9852	-0.8792
C	3.0239	-0.1076	-0.0007	H	5.5200	-0.9853	0.8786
O	-0.5701	1.9841	0.0011	H	-6.7784	-1.2204	0.8786
C	-4.2685	-0.3588	-0.0003	H	-6.7786	-1.2199	-0.8791
C	-5.6140	0.3792	0.0001	H	-8.2237	0.8450	-0.8783
C	4.3725	0.6256	-0.0004	H	-8.2235	0.8446	0.8791
C	5.5780	-0.3242	-0.0003	H	6.9838	1.0668	0.8788
C	-6.8291	-0.5579	-0.0001	H	6.9840	1.0669	-0.8788
C	-8.1735	0.1824	0.0002	H	8.0816	-1.2023	-0.8788
C	6.9282	0.4050	0.0000	H	8.0813	-1.2024	0.8788
C	8.1369	-0.5405	0.0001	H	-9.3403	-1.4153	0.8788
C	-9.3903	-0.7527	0.0001	H	-9.3404	-1.4149	-0.8788
C	-10.7343	-0.0120	0.0004	H	-10.7854	0.6507	-0.8783
C	9.4864	0.1903	0.0003	H	-10.7852	0.6504	0.8792
C	10.6968	-0.7527	0.0004	H	9.5410	0.8523	0.8791
C	-11.9516	-0.9463	0.0003	H	9.5412	0.8525	-0.8784
C	-13.2899	-0.1987	0.0005	H	10.6434	-1.4150	-0.8785
C	12.0458	-0.0212	0.0006	H	10.6431	-1.4151	0.8791
C	13.2497	-0.9700	0.0006	H	-11.9012	-1.6078	0.8787
H	-3.1044	1.2505	-0.8747	H	-11.9013	-1.6075	-0.8783
H	-3.1041	1.2497	0.8753	H	-14.1389	-0.8942	0.0005
H	-1.6346	-0.8173	-0.8747	H	-13.3865	0.4444	-0.8848
H	-1.6344	-0.8184	0.8727	H	-13.3863	0.4442	0.8860
H	1.8495	1.5068	0.8829	H	12.0995	0.6399	0.8791
H	1.8500	1.5068	-0.8847	H	12.0997	0.6400	-0.8778
H	2.9507	-0.7613	-0.8814	H	14.1977	-0.4169	0.0008
H	2.9504	-0.7613	0.8801	H	13.2438	-1.6201	-0.8848
H	-4.2168	-1.0217	0.8783	H	13.2436	-1.6203	0.8860
H	-4.2170	-1.0209	-0.8794				

Table A.16: DFT Geometry Optimized Coordinates (B3LYP/6-31G(d')) for 12chain0.
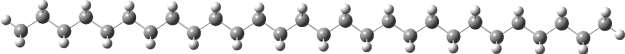
Atom	x	y	z	Atom	x	y	z
C	7.0329	-9.9780	0.0000	H	3.3679	-3.1681	0.8787
C	5.6264	-9.3644	0.0000	H	0.8497	-3.2807	0.8787
C	5.6254	-7.8296	0.0000	H	0.8497	-3.2807	-0.8787
C	4.2188	-7.2157	0.0000	H	1.9620	-1.0187	-0.8787
C	4.2183	-5.6810	0.0000	H	1.9620	-1.0187	0.8787
C	2.8119	-5.0666	0.0000	H	-0.5562	-1.1310	0.8787
C	2.8119	-3.5318	0.0000	H	-0.5562	-1.1310	-0.8787
C	1.4057	-2.9171	0.0000	H	0.5562	1.1310	-0.8787
C	1.4060	-1.3823	0.0000	H	0.5562	1.1310	0.8787
C	-0.0002	-0.7674	0.0000	H	-1.9620	1.0187	0.8787
C	0.0002	0.7674	0.0000	H	-1.9620	1.0187	-0.8787
C	-1.4060	1.3823	0.0000	H	-0.8497	3.2807	-0.8787
C	-1.4057	2.9171	0.0000	H	-0.8497	3.2807	0.8787
C	-2.8119	3.5318	0.0000	H	-3.3679	3.1681	0.8787
C	-2.8119	5.0666	0.0000	H	-3.3679	3.1681	-0.8787
C	-4.2183	5.6810	0.0000	H	-2.2561	5.4303	-0.8787
C	7.0349	-11.5126	0.0000	H	-2.2561	5.4303	0.8787
C	8.4439	-12.1166	0.0000	H	-4.7742	5.3171	0.8787
C	-4.2188	7.2157	0.0000	H	-4.7742	5.3171	-0.8787
C	-5.6254	7.8296	0.0000	H	6.4800	-11.8759	-0.8785
C	-5.6264	9.3644	0.0000	H	6.4800	-11.8759	0.8785
C	-7.0329	9.9780	0.0000	H	8.4114	-13.2137	0.0000
C	-7.0349	11.5126	0.0000	H	9.0120	-11.8004	0.8854
C	-8.4439	12.1166	0.0000	H	9.0120	-11.8004	-0.8854
H	7.5892	-9.6145	0.8788	H	-3.6630	7.5797	-0.8787
H	7.5892	-9.6145	-0.8788	H	-3.6630	7.5797	0.8787
H	5.0708	-9.7285	0.8788	H	-6.1811	7.4656	0.8787
H	5.0708	-9.7285	-0.8788	H	-6.1811	7.4656	-0.8787
H	6.1811	-7.4656	-0.8787	H	-5.0708	9.7285	-0.8788
H	6.1811	-7.4656	0.8787	H	-5.0708	9.7285	0.8788
H	3.6630	-7.5797	0.8787	H	-7.5892	9.6145	0.8788
H	3.6630	-7.5797	-0.8787	H	-7.5892	9.6145	-0.8788
H	4.7742	-5.3171	-0.8787	H	-6.4800	11.8759	-0.8785
H	4.7742	-5.3171	0.8787	H	-6.4800	11.8759	0.8785
H	2.2561	-5.4303	0.8787	H	-8.4114	13.2137	0.0000
H	2.2561	-5.4303	-0.8787	H	-9.0120	11.8004	0.8854
H	3.3679	-3.1681	-0.8787	H	-9.0120	11.8004	-0.8854

Table A.17: DFT Geometry Optimized Coordinates (B3LYP/6-31G(d')) for 13chain0.
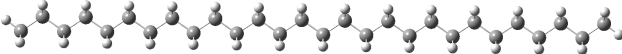
Atom	x	y	z	Atom	x	y	z
C	-16.0478	-0.3717	0.0001	H	-8.3514	-1.0516	0.8791
C	-14.7679	0.4721	-0.0003	H	-7.0594	1.1127	0.8785
C	-13.4857	-0.3711	0.0001	H	-7.0594	1.1123	-0.8790
C	-12.1991	0.4651	-0.0002	H	-5.7832	-1.0614	-0.8784
C	-10.9174	-0.3790	0.0001	H	-5.7833	-1.0610	0.8790
C	-9.6304	0.4572	-0.0002	H	-4.4906	1.1029	0.8786
C	-8.3491	-0.3875	0.0001	H	-4.4906	1.1026	-0.8789
C	-7.0618	0.4482	-0.0001	H	-3.2150	-1.0714	-0.8785
C	-5.7807	-0.3969	0.0001	H	-3.2150	-1.0712	0.8789
C	-4.4932	0.4384	0.0000	H	-1.9220	1.0925	0.8787
C	-3.2123	-0.4070	0.0001	H	-1.9220	1.0924	-0.8788
C	-1.9247	0.4281	0.0000	H	-0.6466	-1.0817	-0.8787
C	-0.6439	-0.4174	0.0000	H	-0.6466	-1.0817	0.8788
C	0.6438	0.4176	0.0001	H	0.6466	1.0819	0.8788
C	1.9246	-0.4279	0.0000	H	0.6465	1.0820	-0.8786
C	3.2123	0.4071	0.0001	H	1.9220	-1.0922	-0.8788
C	4.4932	-0.4382	-0.0001	H	1.9219	-1.0923	0.8787
C	5.7807	0.3970	0.0001	H	3.2150	1.0713	0.8789
C	7.0618	-0.4481	-0.0001	H	3.2149	1.0716	-0.8785
C	8.3491	0.3875	0.0001	H	4.4906	-1.1024	-0.8789
C	9.6304	-0.4572	-0.0002	H	4.4906	-1.1027	0.8786
C	10.9174	0.3789	0.0001	H	5.7833	1.0612	0.8790
C	12.1991	-0.4653	-0.0002	H	5.7832	1.0616	-0.8785
C	13.4857	0.3710	0.0001	H	7.0593	-1.1122	-0.8790
C	14.7679	-0.4723	-0.0002	H	7.0594	-1.1126	0.8785
C	16.0478	0.3713	0.0002	H	8.3514	1.0516	0.8790
H	-16.9458	0.2594	-0.0002	H	8.3514	1.0521	-0.8784
H	-16.0965	-1.0196	0.8858	H	9.6282	-1.1212	-0.8791
H	-16.0965	-1.0204	-0.8850	H	9.6282	-1.1218	0.8784
H	-14.7657	1.1357	0.8779	H	10.9195	1.0430	0.8790
H	-14.7657	1.1349	-0.8790	H	10.9195	1.0435	-0.8784
H	-13.4885	-1.0360	-0.8784	H	12.1971	-1.1293	-0.8792
H	-13.4886	-1.0353	0.8792	H	12.1971	-1.1299	0.8783
H	-12.1972	1.1298	0.8783	H	13.4886	1.0351	0.8792
H	-12.1971	1.1291	-0.8793	H	13.4886	1.0358	-0.8784
H	-10.9194	-1.0437	-0.8783	H	14.7657	-1.1352	-0.8790
H	-10.9195	-1.0430	0.8791	H	14.7657	-1.1359	0.8780
H	-9.6282	1.1218	0.8784	H	16.9458	-0.2598	-0.0001
H	-9.6282	1.1212	-0.8791	H	16.0966	1.0193	0.8858
H	-8.3514	-1.0521	-0.8784	H	16.0966	1.0201	-0.8850

Table A.18: DFT Geometry Optimized Coordinates (B3LYP/6-31G(d')) for 13chain1.
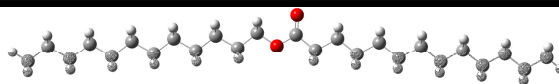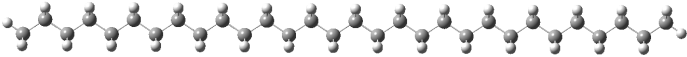
Atom	x	y	z	Atom	x	y	z
C	-3.0628	0.6915	0.0000	H	4.4283	1.3895	0.8791
C	-1.7252	-0.0524	-0.0005	H	4.4285	1.3895	-0.8789
C	-0.5260	0.8785	-0.0003	H	5.5192	-0.8816	-0.8787
O	0.6299	0.1757	-0.0004	H	5.5191	-0.8816	0.8791
C	1.8447	0.9587	-0.0002	H	-6.7825	-1.1122	0.8784
C	3.0221	-0.0050	0.0000	H	-6.7825	-1.1116	-0.8793
O	-0.5715	2.0870	0.0000	H	-8.2242	0.9558	-0.8785
C	-4.2710	-0.2536	-0.0004	H	-8.2241	0.9553	0.8789
C	-5.6157	0.4859	0.0000	H	6.9812	1.1717	0.8790
C	4.3705	0.7286	0.0001	H	6.9812	1.1718	-0.8785
C	5.5765	-0.2205	0.0002	H	8.0813	-1.0962	-0.8786
C	-6.8321	-0.4495	-0.0003	H	8.0813	-1.0962	0.8791
C	-8.1753	0.2930	0.0000	H	-9.3454	-1.3024	0.8785
C	6.9261	0.5099	0.0003	H	-9.3454	-1.3020	-0.8791
C	8.1359	-0.4343	0.0003	H	-10.7844	0.7674	-0.8785
C	-9.3940	-0.6397	-0.0002	H	-10.7843	0.7670	0.8789
C	-10.7362	0.1046	0.0001	H	9.5381	0.9607	0.8790
C	9.4843	0.2985	0.0003	H	9.5380	0.9607	-0.8784
C	10.6963	-0.6428	0.0002	H	10.6429	-1.3049	-0.8786
C	-11.9558	-0.8268	0.0000	H	10.6430	-1.3050	0.8789
C	-13.2977	-0.0824	0.0002	H	-11.9076	-1.4896	0.8786
C	12.0437	0.0919	0.0001	H	-11.9077	-1.4892	-0.8790
C	13.2569	-0.8475	0.0000	H	-13.3470	0.5805	-0.8784
C	-14.5176	-1.0133	0.0002	H	-13.3468	0.5801	0.8791
C	-15.8538	-0.2621	0.0004	H	12.0966	0.7542	0.8789
C	14.6039	-0.1122	0.0000	H	12.0965	0.7543	-0.8786
C	15.8105	-1.0575	-0.0002	H	13.2053	-1.5099	-0.8788
H	-3.1056	1.3548	-0.8747	H	13.2054	-1.5100	0.8788
H	-3.1055	1.3540	0.8753	H	-14.4689	-1.6751	0.8785
H	-1.6371	-0.7141	-0.8746	H	-14.4691	-1.6747	-0.8785
H	-1.6368	-0.7149	0.8729	H	-16.7048	-0.9553	0.0004
H	1.8478	1.6094	0.8835	H	-15.9487	0.3813	-0.8848
H	1.8481	1.6093	-0.8840	H	-15.9485	0.3810	0.8860
H	2.9491	-0.6588	-0.8807	H	14.6559	0.5491	0.8785
H	2.9489	-0.6587	0.8808	H	14.6558	0.5492	-0.8784
H	-4.2200	-0.9165	0.8782	H	16.7570	-0.5018	-0.0002
H	-4.2201	-0.9158	-0.8795	H	15.8063	-1.7077	-0.8856
H	-5.6652	1.1486	-0.8783	H	15.8064	-1.7078	0.8852
H	-5.6651	1.1480	0.8788				

Table A.19: DFT Geometry Optimized Coordinates (B3LYP/6-31G(d')) for 14chain0.

Atom	x	y	z	Atom	x	y	z
C	0.4245	-14.7683	0.0000	H	1.0841	-9.6314	0.8787
C	-0.4171	-13.4852	0.0000	H	-1.0854	-8.3480	0.8787
C	0.4217	-12.2000	0.0000	H	-1.0854	-8.3480	-0.8787
C	-0.4197	-10.9165	0.0000	H	1.0833	-7.0633	-0.8787
C	0.4197	-9.6317	0.0000	H	1.0833	-7.0633	0.8787
C	-0.4211	-8.3478	0.0000	H	-1.0857	-5.7791	0.8787
C	0.4189	-7.0634	0.0000	H	-1.0857	-5.7791	-0.8787
C	-0.4214	-5.7791	0.0000	H	1.0833	-4.4951	-0.8787
C	0.4190	-4.4950	0.0000	H	1.0833	-4.4951	0.8787
C	-0.4211	-3.2105	0.0000	H	-1.0854	-3.2104	0.8787
C	0.4195	-1.9265	0.0000	H	-1.0854	-3.2104	-0.8787
C	-0.4203	-0.6420	0.0000	H	1.0839	-1.9267	-0.8787
C	0.4203	0.6420	0.0000	H	1.0839	-1.9267	0.8787
C	-0.4195	1.9265	0.0000	H	-1.0847	-0.6418	0.8787
C	0.4211	3.2105	0.0000	H	-1.0847	-0.6418	-0.8787
C	-0.4190	4.4950	0.0000	H	1.0847	0.6418	-0.8787
C	-0.4132	-16.0541	0.0000	H	1.0847	0.6418	0.8787
C	0.4359	-17.3304	0.0000	H	-1.0839	1.9267	0.8787
C	0.4214	5.7791	0.0000	H	-1.0839	1.9267	-0.8787
C	-0.4189	7.0634	0.0000	H	1.0854	3.2104	-0.8787
C	0.4211	8.3478	0.0000	H	1.0854	3.2104	0.8787
C	-0.4197	9.6317	0.0000	H	-1.0833	4.4951	0.8787
C	0.4197	10.9165	0.0000	H	-1.0833	4.4951	-0.8787
C	-0.4217	12.2000	0.0000	H	-1.0765	-16.0546	-0.8785
C	0.4171	13.4852	0.0000	H	-1.0765	-16.0546	0.8785
C	-0.4245	14.7683	0.0000	H	-0.1913	-18.2311	0.0000
C	0.4132	16.0541	0.0000	H	1.0845	-17.3763	0.8854
C	-0.4359	17.3304	0.0000	H	1.0845	-17.3763	-0.8854
H	1.0891	-14.7684	0.8788	H	1.0857	5.7791	-0.8787
H	1.0891	-14.7684	-0.8788	H	1.0857	5.7791	0.8787
H	-1.0815	-13.4860	0.8788	H	-1.0833	7.0633	0.8787
H	-1.0815	-13.4860	-0.8788	H	-1.0833	7.0633	-0.8787
H	1.0860	-12.1993	-0.8787	H	1.0854	8.3480	-0.8787
H	1.0860	-12.1993	0.8787	H	1.0854	8.3480	0.8787
H	-1.0840	-10.9170	0.8787	H	-1.0841	9.6314	0.8787
H	-1.0840	-10.9170	-0.8787	H	-1.0841	9.6314	-0.8787
H	1.0841	-9.6314	-0.8787	H	1.0840	10.9170	-0.8787

Table A.19: Continued.

Atom	x	y	z		Atom	x	y	z
H	1.0840	10.9170	0.8787		H	-1.0891	14.7684	-0.8788
H	-1.0860	12.1993	0.8787		H	1.0765	16.0546	-0.8785
H	-1.0860	12.1993	-0.8787		H	1.0765	16.0546	0.8785
H	1.0815	13.4860	-0.8788		H	0.1913	18.2311	0.0000
H	1.0815	13.4860	0.8788		H	-1.0845	17.3763	0.8854
H	-1.0891	14.7684	0.8788		H	-1.0845	17.3763	-0.8854

Table A.20: DFT Geometry Optimized Coordinates (B3LYP/6-31G(d')) for 15chain0.

Atom	x	y	z	Atom	x	y	z
C	18.6158	-0.3819	-0.0005	H	17.3357	1.1268	-0.8790
C	17.3371	0.4636	-0.0005	H	17.3358	1.1269	0.8780
C	16.0537	-0.3778	-0.0003	H	16.0557	-1.0423	0.8785
C	14.7682	0.4602	-0.0003	H	16.0556	-1.0424	-0.8791
C	13.4854	-0.3822	-0.0001	H	14.7671	1.1245	-0.8791
C	12.1995	0.4556	-0.0001	H	14.7672	1.1246	0.8785
C	10.9171	-0.3874	0.0000	H	13.4866	-1.0465	0.8786
C	9.6309	0.4498	0.0000	H	13.4865	-1.0466	-0.8788
C	8.3488	-0.3937	0.0002	H	12.1981	1.1199	-0.8789
C	7.0622	0.4430	0.0002	H	12.1983	1.1200	0.8786
C	5.7804	-0.4010	0.0003	H	10.9187	-1.0517	0.8788
C	4.4936	0.4354	0.0003	H	10.9185	-1.0518	-0.8787
C	3.2120	-0.4089	0.0003	H	9.6292	1.1141	-0.8787
C	1.9250	0.4273	0.0003	H	9.6293	1.1142	0.8788
C	0.6435	-0.4172	0.0003	H	8.3506	-1.0580	0.8789
C	-0.6435	0.4188	0.0003	H	8.3505	-1.0581	-0.8785
C	-1.9250	-0.4257	0.0003	H	7.0603	1.1073	-0.8786
C	-3.2120	0.4104	0.0003	H	7.0604	1.1074	0.8789
C	-4.4935	-0.4341	0.0003	H	5.7824	-1.0652	0.8790
C	-5.7805	0.4021	0.0002	H	5.7823	-1.0653	-0.8784
C	-7.0621	-0.4421	0.0002	H	4.4915	1.0997	-0.8785
C	-8.3489	0.3944	0.0001	H	4.4916	1.0998	0.8790
C	-9.6307	-0.4495	0.0000	H	3.2141	-1.0732	0.8791
C	-10.9172	0.3874	0.0000	H	3.2141	-1.0732	-0.8784
C	-12.1994	-0.4560	-0.0001	H	1.9229	1.0916	-0.8784
C	-13.4855	0.3814	-0.0001	H	1.9229	1.0916	0.8790
C	-14.7681	-0.4614	-0.0003	H	0.6457	-1.0815	0.8791
C	-16.0539	0.3761	-0.0003	H	0.6457	-1.0815	-0.8784
C	-17.3369	-0.4658	-0.0005	H	-0.6457	1.0832	-0.8784
C	-18.6160	0.3792	-0.0005	H	-0.6457	1.0832	0.8791
H	19.5147	0.2480	-0.0006	H	-1.9228	-1.0900	0.8791
H	18.6636	-1.0303	-0.8859	H	-1.9228	-1.0900	-0.8784
H	18.6637	-1.0302	0.8849	H	-3.2141	1.0747	-0.8784

Table A.20: Continued.
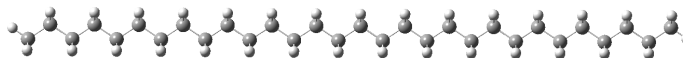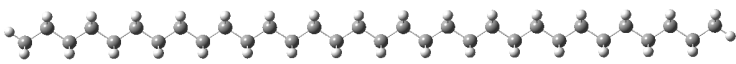
Atom	x	y	z	Atom	x	y	z
H	-3.2142	1.0747	0.8790	H	-12.1979	-1.1204	0.8786
H	-4.4914	-1.0984	0.8790	H	-12.1978	-1.1203	-0.8789
H	-4.4914	-1.0984	-0.8785	H	-13.4869	1.0458	-0.8788
H	-5.7825	1.0665	-0.8785	H	-13.4870	1.0457	0.8786
H	-5.7826	1.0665	0.8790	H	-14.7668	-1.1258	0.8784
H	-7.0602	-1.1064	0.8789	H	-14.7667	-1.1257	-0.8791
H	-7.0601	-1.1064	-0.8786	H	-16.0560	1.0407	-0.8790
H	-8.3507	1.0588	-0.8786	H	-16.0561	1.0406	0.8785
H	-8.3508	1.0587	0.8789	H	-17.3354	-1.1291	0.8780
H	-9.6290	-1.1138	0.8787	H	-17.3353	-1.1290	-0.8790
H	-9.6289	-1.1138	-0.8787	H	-19.5146	-0.2510	-0.0006
H	-10.9188	1.0518	-0.8787	H	-18.6640	1.0277	-0.8858
H	-10.9190	1.0517	0.8788	H	-18.6641	1.0275	0.8850

Table A.21: DFT Geometry Optimized Coordinates (B3LYP/6-31G(d')) for 15chain1.
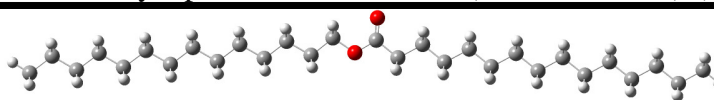
Atom	x	y	z	Atom	x	y	z
C	-3.0641	0.7901	0.0002	H	-4.2219	-0.8168	-0.8793
C	-1.7267	0.0460	-0.0001	H	-5.6660	1.2483	-0.8781
C	-0.5274	0.9769	-0.0001	H	-5.6660	1.2476	0.8790
O	0.6285	0.2741	0.0000	H	4.4266	1.4888	0.8790
C	1.8433	1.0572	-0.0001	H	4.4266	1.4887	-0.8790
C	3.0209	0.0937	0.0001	H	5.5185	-0.7818	-0.8788
O	-0.5728	2.1854	-0.0004	H	5.5185	-0.7817	0.8791
C	-4.2726	-0.1546	-0.0002	H	-6.7849	-1.0118	0.8784
C	-5.6169	0.5856	0.0002	H	-6.7850	-1.0110	-0.8793
C	4.3690	0.8278	0.0000	H	-8.2247	1.0577	-0.8782
C	5.5755	-0.1206	0.0001	H	-8.2246	1.0570	0.8791
C	-6.8340	-0.3490	-0.0002	H	6.9792	1.2726	0.8788
C	-8.1765	0.3947	0.0002	H	6.9792	1.2725	-0.8787
C	6.9246	0.6106	0.0001	H	8.0812	-0.9945	-0.8786
C	8.1352	-0.3325	0.0001	H	8.0812	-0.9944	0.8790
C	-9.3963	-0.5365	-0.0001	H	-9.3485	-1.1994	0.8784
C	-10.7374	0.2096	0.0002	H	-9.3486	-1.1987	-0.8792
C	9.4829	0.4017	0.0001	H	-10.7847	0.8726	-0.8782
C	10.6960	-0.5382	0.0001	H	-10.7846	0.8720	0.8791
C	-11.9586	-0.7198	-0.0001	H	9.5359	1.0640	0.8787
C	-13.2990	0.0276	0.0002	H	9.5359	1.0638	-0.8787
C	12.0423	0.1985	0.0000	H	10.6435	-1.2005	-0.8785
C	13.2570	-0.7393	0.0001	H	10.6436	-1.2003	0.8790
C	-14.5208	-0.9010	-0.0002	H	-11.9116	-1.3828	0.8784
C	-15.8611	-0.1538	0.0001	H	-11.9117	-1.3822	-0.8792
C	14.6025	-0.0009	-0.0001	H	-13.3458	0.6907	-0.8783
C	15.8182	-0.9371	0.0000	H	-13.3458	0.6900	0.8791
C	-17.0830	-1.0821	-0.0002	H	12.0942	0.8610	0.8786
C	-18.4176	-0.3280	0.0002	H	12.0941	0.8607	-0.8788
C	17.1633	-0.1985	-0.0002	H	13.2056	-1.4018	-0.8785
C	18.3723	-1.1408	-0.0001	H	13.2056	-1.4014	0.8790
H	-3.1067	1.4533	-0.8745	H	-14.4741	-1.5641	0.8783
H	-3.1067	1.4526	0.8754	H	-14.4742	-1.5634	-0.8792
H	-1.6386	-0.6159	-0.8740	H	-15.9089	0.5094	-0.8784
H	-1.6383	-0.6162	0.8735	H	-15.9089	0.5087	0.8792
H	1.8464	1.7080	0.8834	H	14.6536	0.6617	0.8785
H	1.8464	1.7076	-0.8840	H	14.6535	0.6613	-0.8790
H	2.9480	-0.5603	-0.8805	H	15.7683	-1.6000	-0.8786
H	2.9478	-0.5598	0.8810	H	15.7684	-1.5996	0.8790
H	-4.2219	-0.8175	0.8784	H	-17.0357	-1.7441	0.8780
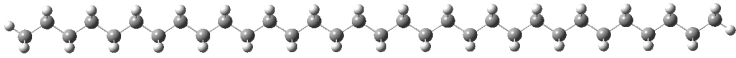
Table A.21: Continued.
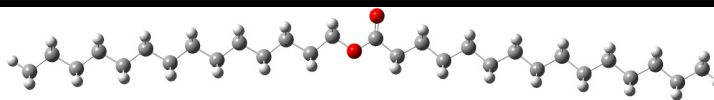
Atom	x	y	z	Atom	x	y	z
H	-17.0358	-1.7433	-0.8790	H	17.2136	0.4628	-0.8788
H	-19.2701	-1.0194	-0.0001	H	19.3174	-0.5828	-0.0002
H	-18.5111	0.3158	-0.8850	H	18.3696	-1.7912	-0.8853
H	-18.5110	0.3151	0.8859	H	18.3698	-1.7909	0.8854
H	17.2137	0.4631	0.8782				
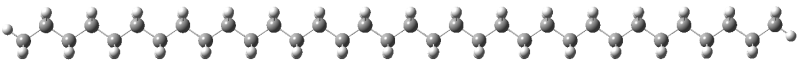
Table A.22: DFT Geometry Optimized Coordinates (B3LYP/6-31G(d')) for 16chain0.

Atom	x	y	z	Atom	x	y	z
C	0.4303	-17.3367	0.0000	H	-1.0823	-10.9170	0.8787
C	-0.4118	-16.0539	0.0000	H	-1.0823	-10.9170	-0.8787
C	0.4265	-14.7683	0.0000	H	1.0858	-9.6313	-0.8787
C	-0.4155	-13.4852	0.0000	H	1.0858	-9.6313	0.8787
C	0.4234	-12.2000	0.0000	H	-1.0838	-8.3481	0.8787
C	-0.4180	-10.9165	0.0000	H	-1.0838	-8.3481	-0.8787
C	0.4214	-9.6317	0.0000	H	1.0847	-7.0631	-0.8787
C	-0.4195	-8.3479	0.0000	H	1.0847	-7.0631	0.8787
C	0.4204	-7.0633	0.0000	H	-1.0845	-5.7793	0.8787
C	-0.4202	-5.7792	0.0000	H	-1.0845	-5.7793	-0.8787
C	0.4199	-4.4949	0.0000	H	1.0843	-4.4948	-0.8787
C	-0.4204	-3.2106	0.0000	H	1.0843	-4.4948	0.8787
C	0.4200	-1.9264	0.0000	H	-1.0847	-3.2106	0.8787
C	-0.4202	-0.6421	0.0000	H	-1.0847	-3.2106	-0.8787
C	0.4202	0.6421	0.0000	H	1.0843	-1.9265	-0.8787
C	-0.4200	1.9264	0.0000	H	1.0843	-1.9265	0.8787
C	-0.4070	-18.6228	0.0000	H	-1.0845	-0.6420	0.8787
C	0.4426	-19.8987	0.0000	H	-1.0845	-0.6420	-0.8787
C	0.4204	3.2106	0.0000	H	1.0845	0.6420	-0.8787
C	-0.4199	4.4949	0.0000	H	1.0845	0.6420	0.8787
C	0.4202	5.7792	0.0000	H	-1.0843	1.9265	0.8787
C	-0.4204	7.0633	0.0000	H	-1.0843	1.9265	-0.8787
C	0.4195	8.3479	0.0000	H	-1.0702	-18.6235	-0.8785
C	-0.4214	9.6317	0.0000	H	-1.0702	-18.6235	0.8785
C	0.4180	10.9165	0.0000	H	-0.1844	-20.7996	0.0000
C	-0.4234	12.2000	0.0000	H	1.0912	-19.9445	0.8854
C	0.4155	13.4852	0.0000	H	1.0912	-19.9445	-0.8854
C	-0.4265	14.7683	0.0000	H	1.0847	3.2106	-0.8787
C	0.4118	16.0539	0.0000	H	1.0847	3.2106	0.8787
C	-0.4303	17.3367	0.0000	H	-1.0843	4.4948	0.8787
C	0.4070	18.6228	0.0000	H	-1.0843	4.4948	-0.8787
C	-0.4426	19.8987	0.0000	H	1.0845	5.7793	-0.8787
H	1.0949	-17.3365	0.8788	H	1.0845	5.7793	0.8787
H	1.0949	-17.3365	-0.8788	H	-1.0847	7.0631	0.8787
H	-1.0761	-16.0550	0.8788	H	-1.0847	7.0631	-0.8787
H	-1.0761	-16.0550	-0.8788	H	1.0838	8.3481	-0.8787
H	1.0908	-14.7674	-0.8787	H	1.0838	8.3481	0.8787
H	1.0908	-14.7674	0.8787	H	-1.0858	9.6313	0.8787
H	-1.0798	-13.4860	0.8787	H	-1.0858	9.6313	-0.8787
H	-1.0798	-13.4860	-0.8787	H	1.0823	10.9170	-0.8787
H	1.0878	-12.1994	-0.8787	H	1.0823	10.9170	0.8787

Table A.22: Continued.

Atom	x	y	z	Atom	x	y	z
H	1.0878	-12.1994	0.8787	H	-1.0878	12.1994	0.8787
H	-1.0878	12.1994	-0.8787	H	-1.0949	17.3365	0.8788
H	1.0798	13.4860	-0.8787	H	-1.0949	17.3365	-0.8788
H	1.0798	13.4860	0.8787	H	1.0702	18.6235	-0.8785
H	-1.0908	14.7674	0.8787	H	1.0702	18.6235	0.8785
H	-1.0908	14.7674	-0.8787	H	0.1844	20.7996	0.0000
H	1.0761	16.0550	-0.8788	H	-1.0912	19.9445	0.8854
H	1.0761	16.0550	0.8788	H	-1.0912	19.9445	-0.8854

Table A.23: DFT Geometry Optimized Coordinates (B3LYP/6-31G(d')) for 17chain0.

Atom	x	y	z	Atom	x	y	z
C	21.1839	-0.3904	0.0000	H	18.6231	-1.0483	0.8788
C	19.9060	0.4564	0.0000	H	18.6231	-1.0483	-0.8788
C	18.6218	-0.3838	0.0000	H	17.3368	1.1199	-0.8788
C	17.3371	0.4555	0.0000	H	17.3367	1.1199	0.8788
C	16.0535	-0.3856	0.0000	H	16.0540	-1.0500	0.8787
C	14.7684	0.4535	0.0000	H	16.0540	-1.0499	-0.8788
C	13.4852	-0.3884	-0.0001	H	14.7677	1.1178	-0.8788
C	12.1998	0.4501	-0.0001	H	14.7677	1.1178	0.8787
C	10.9169	-0.3924	-0.0001	H	13.4861	-1.0527	0.8787
C	9.6311	0.4455	0.0000	H	13.4861	-1.0527	-0.8788
C	8.3486	-0.3974	0.0000	H	12.1987	1.1144	-0.8788
C	7.0624	0.4400	0.0000	H	12.1987	1.1144	0.8787
C	5.7802	-0.4034	0.0000	H	10.9181	-1.0567	0.8787
C	4.4938	0.4337	0.0000	H	10.9181	-1.0567	-0.8788
C	3.2118	-0.4100	0.0000	H	9.6298	1.1098	-0.8788
C	1.9252	0.4268	0.0000	H	9.6298	1.1098	0.8787
C	0.6433	-0.4170	0.0001	H	8.3500	-1.0618	0.8787
C	-0.6433	0.4196	0.0001	H	8.3500	-1.0618	-0.8788
C	-1.9252	-0.4242	0.0001	H	7.0609	1.1043	-0.8788
C	-3.2118	0.4124	0.0001	H	7.0609	1.1043	0.8787
C	-4.4937	-0.4314	0.0001	H	5.7818	-1.0677	0.8787
C	-5.7803	0.4054	0.0001	H	5.7818	-1.0677	-0.8787
C	-7.0623	-0.4382	0.0001	H	4.4921	1.0980	-0.8787
C	-8.3487	0.3988	0.0001	H	4.4921	1.0980	0.8787
C	-9.6309	-0.4445	0.0001	H	3.2135	-1.0743	0.8788
C	-10.9170	0.3929	0.0001	H	3.2135	-1.0743	-0.8787
C	-12.1996	-0.4500	0.0000	H	1.9234	1.0911	-0.8787
C	-13.4854	0.3879	0.0000	H	1.9234	1.0912	0.8788
C	-14.7683	-0.4545	0.0000	H	0.6452	-1.0813	0.8788
C	-16.0537	0.3840	0.0000	H	0.6452	-1.0814	-0.8787
C	-17.3369	-0.4578	-0.0001	H	-0.6452	1.0840	-0.8787
C	-18.6220	0.3809	-0.0001	H	-0.6452	1.0840	0.8788
C	-19.9058	-0.4599	-0.0001	H	-1.9233	-1.0886	0.8788
C	-21.1841	0.3861	-0.0001	H	-1.9233	-1.0886	-0.8787
H	22.0834	0.2385	0.0000	H	-3.2136	1.0768	-0.8787
H	21.2311	-1.0389	-0.8854	H	-3.2136	1.0768	0.8788
H	21.2310	-1.0389	0.8854	H	-4.4919	-1.0957	0.8788
H	19.9054	1.1197	-0.8785	H	-4.4919	-1.0957	-0.8786
H	19.9054	1.1196	0.8785	H	-5.7820	1.0697	-0.8786

Table A.23: Continued.
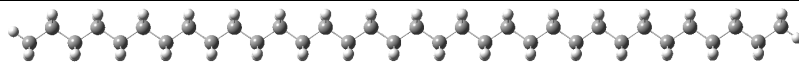
Atom	x	y	z	Atom	x	y	z
H	-5.7820	1.0697	0.8788	H	-14.7673	-1.1188	0.8787
H	-7.0606	-1.1026	0.8788	H	-14.7672	-1.1188	-0.8788
H	-7.0606	-1.1026	-0.8787	H	-16.0545	1.0483	-0.8787
H	-8.3503	1.0632	-0.8786	H	-16.0546	1.0483	0.8787
H	-8.3503	1.0631	0.8788	H	-17.3362	-1.1221	0.8787
H	-9.6294	-1.1088	0.8788	H	-17.3362	-1.1221	-0.8789
H	-9.6294	-1.1088	-0.8787	H	-18.6236	1.0454	-0.8788
H	-10.9185	1.0573	-0.8787	H	-18.6236	1.0454	0.8787
H	-10.9185	1.0572	0.8788	H	-19.9048	-1.1232	0.8784
H	-12.1983	-1.1143	0.8788	H	-19.9048	-1.1232	-0.8786
H	-12.1983	-1.1143	-0.8787	H	-22.0833	-0.2432	-0.0001
H	-13.4865	1.0523	-0.8787	H	-21.2316	1.0346	-0.8855
H	-13.4866	1.0522	0.8788	H	-21.2316	1.0346	0.8853

Table A.24: DFT Geometry Optimized Coordinates (B3LYP/6-31G(d')) for 17chain1.
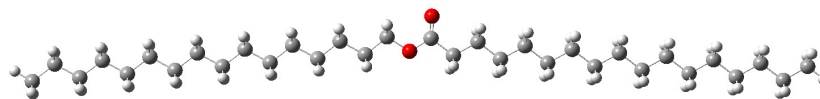
Atom	x	y	z	Atom	x	y	z
C	20.8597	-1.5468	0.1619	H	19.7922	0.3358	0.1985
C	19.6537	-0.6920	0.5674	H	19.6110	-0.6153	1.6647
C	18.3183	-1.2405	0.0468	H	18.1807	-2.2696	0.4152
C	17.1055	-0.3908	0.4488	H	18.3614	-1.3179	-1.0514
C	15.7697	-0.9406	-0.0694	H	17.2436	0.6377	0.0791
C	14.5576	-0.0899	0.3335	H	17.0647	-0.3123	1.5469
C	13.2205	-0.6415	-0.1794	H	15.6315	-1.9689	0.3009
C	12.0098	0.2103	0.2250	H	15.8101	-1.0196	-1.1674
C	10.6704	-0.3444	-0.2786	H	14.6944	0.9376	-0.0394
C	9.4617	0.5090	0.1288	H	14.5197	-0.0084	1.4314
C	8.1191	-0.0512	-0.3599	H	13.0836	-1.6687	0.1943
C	6.9131	0.8039	0.0521	H	13.2575	-0.7236	-1.2773
C	5.5668	0.2338	-0.4139	H	12.1442	1.2362	-0.1531
C	4.3647	1.0910	0.0051	H	11.9769	0.2968	1.3228
C	3.0172	0.4995	-0.4313	H	10.5359	-1.3698	0.1008
C	1.8428	1.3639	0.0032	H	10.7015	-0.4316	-1.3763
O	0.6271	0.7026	-0.4137	H	9.5919	1.5322	-0.2578
C	-0.5284	1.3051	-0.0507	H	9.4371	0.6034	1.2261
C	-1.7281	0.5089	-0.5322	H	7.9891	-1.0739	0.0284
C	-3.0620	1.0806	-0.0460	H	8.1408	-0.1465	-1.4571
C	-4.2696	0.2586	-0.5138	H	7.0358	1.8230	-0.3475
C	-5.6093	0.8172	-0.0156	H	6.9012	0.9103	1.1484
C	-6.8241	-0.0094	-0.4578	H	5.4439	-0.7842	-0.0119
C	-8.1606	0.5469	0.0518	H	5.5737	0.1265	-1.5099
C	-9.3775	-0.2851	-0.3749	H	4.4763	2.1034	-0.4136
C	-10.7114	0.2703	0.1425	H	4.3716	1.2143	1.0994
C	-11.9297	-0.5647	-0.2742	H	2.8935	-0.5063	-0.0050
C	-13.2617	-0.0095	0.2483	H	2.9917	0.3805	-1.5238
C	-14.4810	-0.8459	-0.1624	H	1.8781	2.3630	-0.4498
C	-15.8117	-0.2905	0.3629	H	1.8164	1.5002	1.0916
C	-17.0318	-1.1275	-0.0447	H	-1.5956	-0.5323	-0.2051
C	-18.3619	-0.5720	0.4815	H	-1.6876	0.4739	-1.6311
C	-19.5825	-1.4087	0.0754	H	-3.1565	2.1190	-0.3913
C	-20.9064	-0.8457	0.6046	H	-3.0504	1.1341	1.0514
O	-0.5734	2.3394	0.5744	H	-4.1598	-0.7824	-0.1698
H	21.7975	-1.1289	0.5499	H	-4.2803	0.2117	-1.6145
H	20.9516	-1.6123	-0.9308	H	-5.7248	1.8540	-0.3688
H	20.7681	-2.5719	0.5461	H	-5.5902	0.8751	1.0841

Table A.24: Continued.
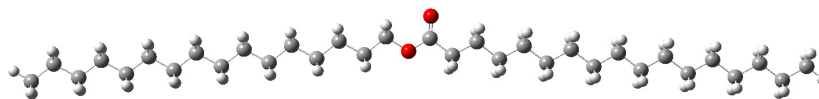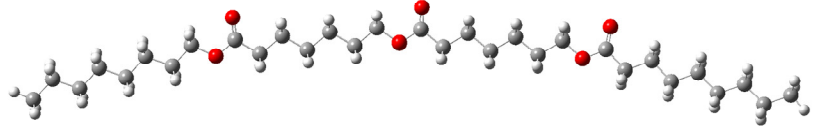
Atom	x	y	z	Atom	x	y	z
H	-6.7048	-1.0469	-0.1070	H	-14.5231	-0.9130	-1.2612
H	-6.8477	-0.0647	-1.5578	H	-15.9425	0.7423	0.0025
H	-8.2838	1.5817	-0.3050	H	-15.7685	-0.2220	1.4615
H	-8.1315	0.6098	1.1511	H	-16.9010	-2.1603	0.3157
H	-9.2525	-1.3204	-0.0198	H	-17.0755	-1.1959	-1.1433
H	-9.4102	-0.3463	-1.4743	H	-18.4940	0.4607	0.1209
H	-10.8388	1.3040	-0.2162	H	-18.3189	-0.5030	1.5803
H	-10.6751	0.3362	1.2416	H	-19.4518	-2.4401	0.4370
H	-11.8013	-1.5987	0.0835	H	-19.6261	-1.4774	-1.0224
H	-11.9683	-0.6295	-1.3732	H	-21.7586	-1.4656	0.2976
H	-13.3914	1.0236	-0.1115	H	-21.0834	0.1720	0.2308
H	-13.2209	0.0581	1.3471	H	-20.9080	-0.7978	1.7021
H	-14.3509	-1.8791	0.1969				

Table A.25: DFT Geometry Optimized Coordinates (B3LYP/6-31G(d')) for 17chain2.
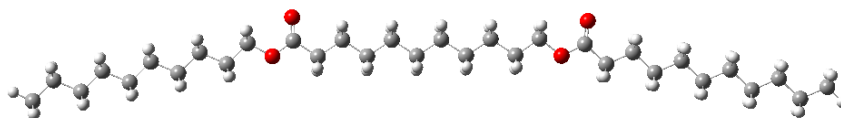
Atom	x	y	z	Atom	x	y	z
C	20.5442	2.1915	-0.1061	H	21.5454	1.7674	-0.2549
C	19.4544	1.1239	-0.2551	H	20.5208	2.6470	0.8933
C	18.0354	1.6733	-0.0557	H	20.4126	2.9992	-0.8389
C	16.9378	0.6114	-0.2048	H	19.6341	0.3131	0.4673
C	15.5193	1.1616	-0.0035	H	19.5276	0.6617	-1.2515
C	14.4216	0.0998	-0.1540	H	17.8567	2.4862	-0.7775
C	13.0043	0.6512	0.0512	H	17.9623	2.1357	0.9416
C	11.9063	-0.4100	-0.1029	H	17.1181	-0.2018	0.5160
C	10.4930	0.1498	0.1102	H	17.0110	0.1505	-1.2027
C	9.4187	-0.9150	-0.0543	H	15.3393	1.9754	-0.7237
O	8.1365	-0.2857	0.1687	H	15.4459	1.6217	0.9947
C	7.0527	-1.0837	0.0348	H	14.6023	-0.7154	0.5643
C	5.7754	-0.3074	0.3008	H	14.4928	-0.3582	-1.1533
C	4.5087	-1.1314	0.0588	H	12.8232	1.4673	-0.6659
C	3.2234	-0.3405	0.3332	H	12.9313	1.1068	1.0512
C	1.9469	-1.1504	0.0701	H	12.0886	-1.2285	0.6109
C	0.6557	-0.3637	0.3320	H	11.9755	-0.8616	-1.1049
C	-0.6194	-1.1717	0.0557	H	10.2995	0.9637	-0.6031
C	-1.9117	-0.3801	0.2961	H	10.4096	0.5891	1.1144
C	-3.1848	-1.1898	0.0147	H	9.5412	-1.7361	0.6635
C	-4.4729	-0.3820	0.2242	H	9.4284	-1.3554	-1.0593
C	-5.7221	-1.2053	-0.0532	H	5.7916	0.5960	-0.3254
O	-6.8679	-0.3433	0.1288	H	5.8181	0.0589	1.3374
C	-8.0772	-0.9120	-0.0818	H	4.5386	-2.0313	0.6879
C	-9.1906	0.1000	0.1200	H	4.5090	-1.4953	-0.9780
C	-10.5877	-0.4899	-0.0865	H	3.2115	0.5682	-0.2898
C	-11.7019	0.5491	0.0926	H	3.2235	0.0113	1.3774
C	-13.1095	-0.0290	-0.1069	H	1.9558	-2.0570	0.6954
C	-14.2269	1.0100	0.0571	H	1.9514	-1.5046	-0.9727
C	-15.6358	0.4337	-0.1379	H	0.6516	0.5453	-0.2904
C	-16.7520	1.4751	0.0191	H	0.6465	-0.0135	1.3763
C	-18.1617	0.8997	-0.1721	H	-0.6221	-2.0752	0.6856
C	-19.2777	1.9418	-0.0190	H	-0.6029	-1.5310	-0.9854
C	-20.6825	1.3578	-0.2073	H	-1.9086	0.5220	-0.3358
O	7.1186	-2.2559	-0.2553	H	-1.9323	-0.0195	1.3365
O	-8.2243	-2.0716	-0.3913	H	-3.1990	-2.0815	0.6608

Table A.25: Continued.
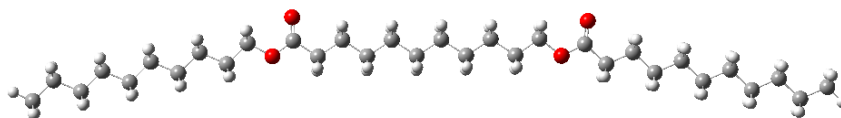
Atom	x	y	z	Atom	x	y	z
H	-3.1538	-1.5666	-1.0196	H	-14.0677	1.8312	-0.6598
H	-4.4748	0.4986	-0.4339	H	-14.1559	1.4662	1.0573
H	-4.5167	-0.0011	1.2546	H	-15.7969	-0.3842	0.5821
H	-5.8091	-2.0622	0.6267	H	-15.7056	-0.0266	-1.1362
H	-5.7337	-1.5988	-1.0777	H	-16.5917	2.2914	-0.7030
H	-9.0079	0.9385	-0.5680	H	-16.6804	1.9376	1.0164
H	-9.0817	0.5255	1.1282	H	-18.3241	0.0851	0.5517
H	-10.7346	-1.3229	0.6145	H	-18.2339	0.4349	-1.1683
H	-10.6463	-0.9335	-1.0897	H	-19.1179	2.7535	-0.7452
H	-11.5464	1.3787	-0.6156	H	-19.2047	2.4081	0.9755
H	-11.6312	0.9951	1.0975	H	-21.4564	2.1282	-0.0971
H	-13.2685	-0.8522	0.6072	H	-20.8885	0.5710	0.5311
H	-13.1774	-0.4822	-1.1083	H	-20.7971	0.9111	-1.2044

Table A.26: DFT Geometry Optimized Coordinates (B3LYP/6-31G(d')) for 17chain3.

Atom	x	y	z	Atom	x	y	z
C	-20.2668	2.5662	0.2347	H	-21.2931	2.1820	0.1740
C	-19.2366	1.4445	0.0615	H	-20.1528	3.3349	-0.5417
C	-17.7852	1.9361	0.1431	H	-20.1543	3.0626	1.2082
C	-16.7483	0.8181	-0.0283	H	-19.3965	0.9453	-0.9064
C	-15.2966	1.3084	0.0552	H	-19.4016	0.6733	0.8294
C	-14.2639	0.1852	-0.1100	H	-17.6253	2.4364	1.1116
C	-12.8130	0.6796	-0.0276	H	-17.6197	2.7085	-0.6250
C	-11.8115	-0.4556	-0.1799	H	-16.9084	0.3185	-0.9968
O	-10.4831	0.1090	-0.0940	H	-16.9157	0.0462	0.7396
C	-9.4604	-0.7713	-0.1770	H	-15.1358	1.8103	1.0222
C	-8.1232	-0.0574	-0.0872	H	-15.1256	2.0764	-0.7154
C	-6.9317	-1.0179	-0.0941	H	-14.4257	-0.3183	-1.0759
C	-5.5815	-0.2928	-0.0361	H	-14.4346	-0.5810	0.6624
C	-4.3850	-1.2539	-0.0349	H	-12.6402	1.1814	0.9351
C	-3.0303	-0.5336	0.0066	H	-12.6255	1.4299	-0.8089
C	-1.8633	-1.5098	0.0145	H	-11.9169	-0.9683	-1.1444
O	-0.6403	-0.7392	0.0382	H	-11.9268	-1.2121	0.6064
C	0.5074	-1.4543	0.0532	H	-8.1308	0.5667	0.8178
C	1.7171	-0.5366	0.0656	H	-8.0665	0.6512	-0.9269
C	3.0440	-1.2984	0.1026	H	-6.9821	-1.6459	-0.9937
C	4.2646	-0.3699	0.0852	H	-7.0218	-1.7097	0.7547
C	5.5970	-1.1309	0.1209	H	-5.5399	0.3408	0.8639
C	6.8217	-0.2068	0.0807	H	-5.4954	0.3943	-0.8928
C	8.1290	-0.9845	0.1207	H	-4.4334	-1.8938	-0.9295
O	9.2131	-0.0316	0.0482	H	-4.4672	-1.9336	0.8273
C	10.4614	-0.5527	0.0805	H	-2.9690	0.1045	0.8998
C	11.5071	0.5423	-0.0291	H	-2.9318	0.1338	-0.8614
C	12.9404	0.0193	0.0919	H	-1.8606	-2.1519	-0.8755
C	13.9928	1.1231	-0.0723	H	-1.8853	-2.1684	0.8918
C	15.4334	0.6079	0.0474	H	1.6196	0.1404	0.9266
C	16.4937	1.7027	-0.1316	H	1.6550	0.1117	-0.8207
C	17.9341	1.1871	-0.0124	H	3.0858	-1.9878	-0.7515
C	18.9958	2.2794	-0.1980	H	3.0694	-1.9348	0.9977
C	20.4315	1.7556	-0.0788	H	4.2170	0.3206	0.9420
O	0.5411	-2.6630	0.0534	H	4.2325	0.2639	-0.8151
O	10.6870	-1.7368	0.1764	H	5.6370	-1.8304	-0.7283
O	-9.6138	-1.9634	-0.3097	H	5.6344	-1.7542	1.0278

Table A.26: Continued.
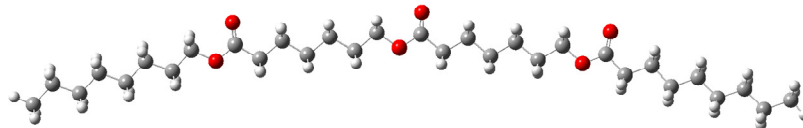
Atom	x	y	z	Atom	x	y	z
H	6.7954	0.4928	0.9283	H	15.5669	0.1276	1.0294
H	6.8001	0.4067	-0.8313	H	16.3284	2.4959	0.6149
H	8.2143	-1.6840	-0.7208	H	16.3593	2.1819	-1.1144
H	8.2302	-1.5701	1.0431	H	18.0988	0.3911	-0.7560
H	11.2890	1.2998	0.7372	H	18.0708	0.7113	0.9718
H	11.3529	1.0526	-0.9916	H	18.8327	3.0743	0.5459
H	13.0999	-0.7659	-0.6593	H	18.8590	2.7542	-1.1816
H	13.0638	-0.4739	1.0660	H	21.1655	2.5600	-0.2157
H	13.8236	1.9093	0.6807	H	20.6377	0.9848	-0.8338
H	13.8616	1.6117	-1.0511	H	20.6103	1.3061	0.9074
H	15.5981	-0.1844	-0.6996				

Table A.27: DFT Geometry Optimized Coordinates (B3LYP/6-31G(d')) for 17chain4.
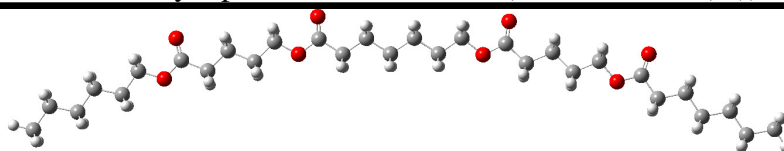
Atom	x	y	z	Atom	x	y	z
C	19.6759	3.5281	-0.0515	H	19.4977	4.1149	0.8598
C	18.8269	2.2520	-0.0649	H	19.4397	4.1720	-0.9094
C	17.3188	2.5293	-0.0057	H	19.1120	1.6124	0.7843
C	16.4603	1.2574	-0.0210	H	19.0535	1.6699	-0.9711
C	14.9541	1.5478	0.0377	H	17.0336	3.1707	-0.8545
C	14.1181	0.2768	0.0146	H	17.0913	3.1110	0.9015
O	12.7261	0.6655	0.0712	H	16.7445	0.6162	0.8280
C	11.8261	-0.3412	0.0292	H	16.6873	0.6764	-0.9285
C	10.4092	0.2006	0.1019	H	14.6602	2.1820	-0.8107
C	9.3455	-0.8917	-0.0305	H	14.7155	2.1152	0.9486
C	7.9208	-0.3291	0.0535	H	14.3389	-0.3763	0.8684
C	6.8662	-1.4180	-0.0807	H	14.2858	-0.3090	-0.8978
O	5.5710	-0.7823	-0.0002	H	10.2972	0.9655	-0.6795
C	4.4999	-1.6036	-0.0887	H	10.3054	0.7409	1.0543
C	3.2069	-0.8121	-0.0062	H	9.5039	-1.6447	0.7530
C	1.9581	-1.6968	-0.0241	H	9.4879	-1.4195	-0.9832
C	0.6587	-0.8840	0.0323	H	7.7609	0.4191	-0.7362
C	-0.6030	-1.7577	0.0169	H	7.7739	0.1923	1.0103
C	-1.8988	-0.9368	0.0699	H	6.9462	-2.1678	0.7162
C	-3.1422	-1.8135	0.0489	H	6.9444	-1.9483	-1.0381
O	-4.2937	-0.9408	0.1068	H	3.1990	-0.0994	-0.8441
C	-5.5014	-1.5463	0.0713	H	3.2457	-0.1918	0.9006
C	-6.6182	-0.5204	0.1493	H	1.9996	-2.3972	0.8214
C	-8.0119	-1.1424	0.0345	H	1.9724	-2.3214	-0.9273
C	-9.1247	-0.0907	0.1268	H	0.6256	-0.1847	-0.8180
C	-10.5112	-0.7063	0.0046	H	0.6547	-0.2571	0.9380
O	-11.4715	0.3693	0.0892	H	-0.5729	-2.4549	0.8684
C	-12.7732	0.0158	-0.0238	H	-0.5998	-2.3845	-0.8882
C	-13.6699	1.2371	0.0669	H	-1.9391	-0.2425	-0.7815
C	-15.1601	0.9048	-0.0403	H	-1.9148	-0.3176	0.9781
C	-16.0489	2.1533	0.0242	H	-3.1746	-2.5014	0.9033
C	-17.5476	1.8407	-0.0812	H	-3.2018	-2.4209	-0.8629
C	-18.4380	3.0892	-0.0267	H	-6.4481	0.2277	-0.6378
C	-19.9341	2.7721	-0.1314	H	-6.5051	0.0254	1.0975
O	12.1289	-1.5090	-0.0524	H	-8.1349	-1.8976	0.8222
O	4.5862	-2.8022	-0.2204	H	-8.0855	-1.6887	-0.9156
O	-5.6491	-2.7436	-0.0083	H	-9.0015	0.6624	-0.6648
O	-13.1435	-1.1245	-0.1787	H	-9.0585	0.4493	1.0823
H	20.7478	3.2970	-0.0941	H	-10.7119	-1.4295	0.8051

Table A.27: Continued.
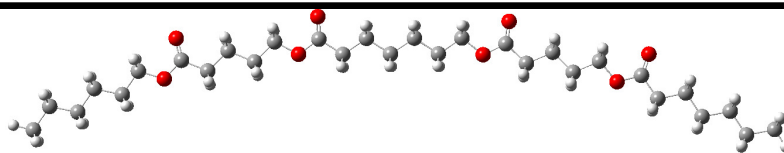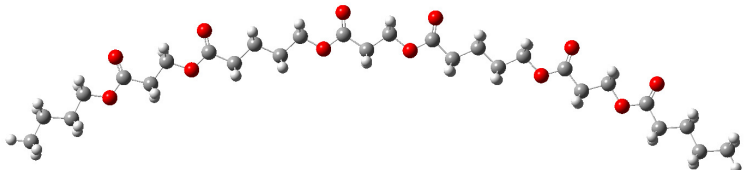
Atom	x	y	z	Atom	x	y	z
H	-10.6445	-1.2301	-0.9503	H	-17.8344	1.1532	0.7301
H	-13.3615	1.9366	-0.7239	H	-17.7409	1.2964	-1.0191
H	-13.4429	1.7522	1.0116	H	-18.1510	3.7749	-0.8385
H	-15.4333	0.2068	0.7629	H	-18.2433	3.6330	0.9104
H	-15.3416	0.3627	-0.9783	H	-20.5420	3.6848	-0.0873
H	-15.7652	2.8465	-0.7838	H	-20.2599	2.1153	0.6865
H	-15.8560	2.6938	0.9647	H	-20.1677	2.2620	-1.0758

Table A.28: DFT Geometry Optimized Coordinates (B3LYP/6-31G(d')) for 17chain5.
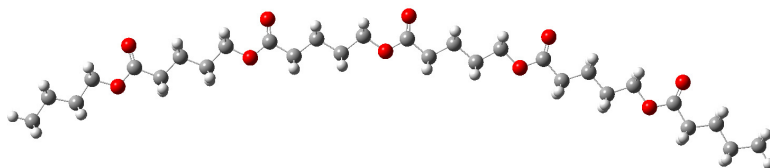
Atom	x	y	z	Atom	x	y	z
C	19.4830	3.5751	-0.0090	O	-15.4767	-0.2699	-0.2189
C	18.6859	2.2661	-0.0258	H	20.5628	3.3840	-0.0425
C	17.1682	2.4915	0.0211	H	19.2748	4.1561	0.8993
C	16.3920	1.1833	-0.0021	H	19.2289	4.2065	-0.8709
O	14.9821	1.5023	0.0458	H	18.9895	1.6411	0.8274
C	14.1369	0.4492	0.0056	H	18.9428	1.6924	-0.9290
C	12.6919	0.9125	0.0692	H	16.8537	3.1091	-0.8324
C	11.6944	-0.2422	-0.0494	H	16.8994	3.0519	0.9280
C	10.2373	0.2313	0.0284	H	16.6396	0.5441	0.8550
C	9.2590	-0.9281	-0.0913	H	16.5930	0.6030	-0.9114
O	7.9211	-0.3862	-0.0118	H	12.5382	1.6587	-0.7232
C	6.9147	-1.2856	-0.0839	H	12.5555	1.4591	1.0138
C	5.5651	-0.5948	0.0025	H	11.8978	-0.9745	0.7432
C	4.3931	-1.5784	-0.0329	H	11.8691	-0.7726	-0.9952
C	3.0331	-0.8720	0.0339	H	10.0295	0.9573	-0.7707
C	1.8781	-1.8622	-0.0007	H	10.0570	0.7536	0.9789
O	0.6477	-1.1052	0.0560	H	9.3939	-1.6628	0.7122
C	-0.4930	-1.8300	0.0272	H	9.3708	-1.4610	-1.0439
C	-1.7103	-0.9240	0.0849	H	5.5033	0.1270	-0.8250
C	-3.0289	-1.7006	0.0595	H	5.5515	0.0121	0.9190
C	-4.2527	-0.7767	0.1045	H	4.4928	-2.2868	0.8006
C	-5.5569	-1.5603	0.0717	H	4.4609	-2.1839	-0.9464
O	-6.6427	-0.6074	0.1194	H	2.9269	-0.1715	-0.8070
C	-7.8894	-1.1288	0.0774	H	2.9602	-0.2709	0.9516
C	-8.9360	-0.0307	0.1444	H	1.9082	-2.5569	0.8480
C	-10.3653	-0.5632	0.0185	H	1.8828	-2.4653	-0.9172
C	-11.4139	0.5529	0.1079	H	-1.6468	-0.2194	-0.7568
C	-12.8316	0.0153	-0.0243	H	-1.6291	-0.3043	0.9895
O	-13.7348	1.1397	0.0563	H	-3.0507	-2.3998	0.9062
C	-15.0520	0.8510	-0.0620	H	-3.0596	-2.3261	-0.8427
C	-15.8904	2.1132	0.0258	H	-4.2347	-0.0803	-0.7461
C	-17.3933	1.8470	-0.0864	H	-4.2305	-0.1590	1.0138
C	-18.2315	3.1298	-0.0201	H	-5.6455	-2.2444	0.9250
C	-19.7374	2.8665	-0.1310	H	-5.6504	-2.1618	-0.8409
O	14.5022	-0.7011	-0.0682	H	-8.7108	0.7031	-0.6424
O	7.0879	-2.4760	-0.2043	H	-8.7959	0.5081	1.0930
O	-0.5179	-3.0368	-0.0376	H	-10.5396	-1.3122	0.8024
O	-8.1171	-2.3136	0.0009	H	-10.4664	-1.1010	-0.9339

Table A.28: Continued.
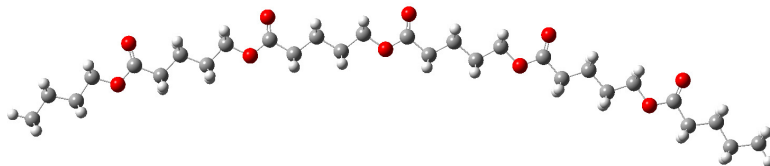
Atom	x	y	z	Atom	x	y	z
H	-11.2429	1.2996	-0.6809	H	-11.3221	1.0851	1.0656
H	-13.0759	-0.6975	0.7733	H	-17.9190	3.8131	-0.8248
H	-12.9866	-0.4992	-0.9809	H	-18.0203	3.6578	0.9226
H	-15.5478	2.7979	-0.7640	H	-20.3116	3.8002	-0.0792
H	-15.6434	2.6170	0.9716	H	-20.0875	2.2139	0.6800
H	-17.6987	1.1587	0.7137	H	-19.9859	2.3740	-1.0806
H	-17.5958	1.3157	-1.0265				

Table A.29: DFT Geometry Optimized Coordinates (B3LYP/6-31G(d')) for 17chain6.

Atom	x	y	z	Atom	x	y	z
C	-18.8367	4.3547	-0.1879	O	-2.0282	-3.3223	-0.1736
C	-18.2060	2.9584	-0.1492	O	3.0390	-3.1927	-0.1346
C	-16.6727	3.0006	-0.0861	O	10.5466	-1.7807	-0.2183
C	-16.0577	1.6100	-0.0498	O	15.2692	0.0516	-0.1280
O	-14.6193	1.7665	0.0076	H	-19.9312	4.2956	-0.2333
C	-13.9004	0.6270	0.0329	H	-18.4962	4.9206	-1.0653
C	-12.4148	0.9267	0.0935	H	-18.5704	4.9364	0.7046
C	-11.5847	-0.3483	0.0774	H	-18.5207	2.3894	-1.0369
O	-10.2021	0.0642	0.1378	H	-18.5933	2.4050	0.7194
C	-9.2869	-0.9321	0.0991	H	-16.3486	3.5580	0.8043
C	-7.8780	-0.3711	0.1753	H	-16.2762	3.5437	-0.9559
C	-6.8023	-1.4516	0.0421	H	-16.3134	1.0228	-0.9405
C	-5.3832	-0.8749	0.1289	H	-16.3856	1.0370	0.8266
C	-4.3215	-1.9560	-0.0092	H	-12.2085	1.5120	0.9992
O	-3.0281	-1.3117	0.0740	H	-12.1478	1.5748	-0.7512
C	-1.9567	-2.1241	-0.0268	H	-11.7540	-0.9347	-0.8314
C	-0.6663	-1.3324	0.0656	H	-11.8136	-0.9954	0.9302
C	0.5527	-2.2393	-0.0156	H	-7.7825	0.1678	1.1293
O	1.7093	-1.3788	0.0682	H	-7.7742	0.3965	-0.6044
C	2.9104	-1.9985	-0.0069	H	-6.9381	-1.9786	-0.9120
C	4.0426	-0.9918	0.0919	H	-6.9539	-2.2079	0.8236
C	5.4235	-1.6408	-0.0274	H	-5.2412	-0.3562	1.0878
C	6.5609	-0.6157	0.0673	H	-5.2295	-0.1231	-0.6584
C	7.9279	-1.2724	-0.0567	H	-4.3941	-2.4827	-0.9687
O	8.9253	-0.2278	0.0312	H	-4.3947	-2.7087	0.7854
C	10.2093	-0.6289	-0.0699	H	-0.6653	-0.7604	1.0025
C	11.1551	0.5527	0.0235	H	-0.6493	-0.5884	-0.7417
C	12.6097	0.1142	-0.0615	H	0.5799	-2.8028	-0.9537
O	13.4043	1.3163	0.0105	H	0.5755	-2.9670	0.8021
C	14.7473	1.1373	-0.0380	H	3.9352	-0.4562	1.0463
C	15.4716	2.4691	0.0316	H	3.8896	-0.2314	-0.6872
C	16.9951	2.3247	0.0226	H	5.4835	-2.1849	-0.9796
C	17.7217	3.6745	0.0717	H	5.5318	-2.4018	0.7569
C	19.2477	3.5313	0.0641	H	6.5096	-0.0766	1.0241
O	-14.3858	-0.4808	0.0108	H	6.4573	0.1412	-0.7234
O	-9.5755	-2.1021	0.0175	H	8.0463	-1.7961	-1.0133

Table A.29: Continued.
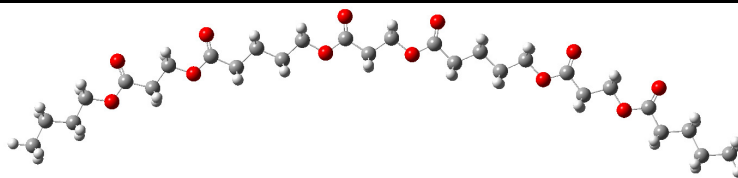
Atom	x	y	z	Atom	x	y	z
H	8.1071	-2.0029	0.7418	H	17.2986	1.7685	-0.8748
H	10.9636	1.0894	0.9618	H	17.3036	1.7028	0.8743
H	10.9167	1.2602	-0.7817	H	17.4095	4.2269	0.9715
H	12.8213	-0.4128	-0.9975	H	17.4071	4.2909	-0.7847
H	12.8820	-0.5581	0.7585	H	19.7419	4.5104	0.0971
H	15.1246	2.9963	0.9321	H	19.5932	3.0130	-0.8404
H	15.1254	3.0821	-0.8136	H	19.5967	2.9518	0.9293

Table A.30: DFT Geometry Optimized Coordinates (B3LYP/6-31G(d')) for 17chain7.
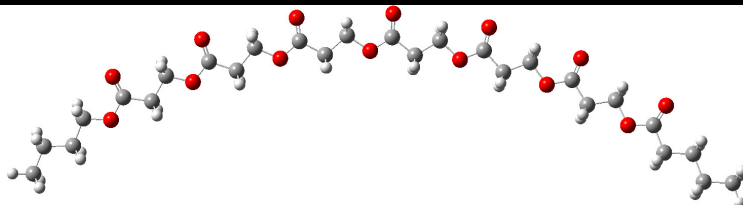
Atom	x	y	z	Atom	x	y	z
C	18.1362	5.0927	-0.3997	O	14.1175	-0.0745	0.1800
C	17.6220	3.6589	-0.2290	O	9.4918	-2.1472	0.2543
C	16.0893	3.5730	-0.2237	O	4.5726	-3.3989	0.1211
C	15.5955	2.1442	-0.0557	O	-0.4920	-3.7458	-0.1598
O	14.1472	2.1716	-0.0628	O	-5.5384	-3.1783	-0.3747
C	13.5344	0.9791	0.0650	O	-10.4104	-1.7348	-0.4159
C	12.0259	1.1399	0.0466	O	-14.9469	0.5499	-0.3163
C	11.3229	-0.2052	0.1495	H	19.2328	5.1244	-0.4002
O	9.9036	0.0711	0.1330	H	17.7838	5.7412	0.4134
C	9.0948	-1.0075	0.1933	H	17.7891	5.5295	-1.3455
C	7.6366	-0.5911	0.1770	H	18.0155	3.2374	0.7082
C	6.7133	-1.8005	0.1817	H	18.0211	3.0278	-1.0372
O	5.3634	-1.2832	0.1846	H	15.6869	3.9829	-1.1610
C	4.3793	-2.2067	0.1545	H	15.6810	4.1909	0.5887
C	3.0163	-1.5423	0.1719	H	15.9348	1.7002	0.8885
C	1.8954	-2.5655	0.0639	H	15.9393	1.4916	-0.8678
O	0.6580	-1.8200	0.1138	H	11.7341	1.6632	-0.8731
C	-0.4729	-2.5470	-0.0104	H	11.7295	1.7969	0.8749
C	-1.6971	-1.6554	0.0659	H	11.5825	-0.7324	1.0729
C	-2.9802	-2.4511	-0.1218	H	11.5768	-0.8651	-0.6860
O	-4.0658	-1.5030	-0.0138	H	7.4532	0.0363	-0.7047
C	-5.3081	-2.0115	-0.1618	H	7.4414	0.0476	1.0485
C	-6.3551	-0.9237	-0.0232	H	6.8677	-2.4284	1.0648
C	-7.7620	-1.4759	-0.1990	H	6.8619	-2.4326	-0.6994
O	-8.6607	-0.3559	-0.0404	H	2.9617	-0.8157	-0.6488
C	-9.9764	-0.6332	-0.1759	H	2.9196	-0.9601	1.0979
C	-10.8121	0.6169	0.0150	H	1.9218	-3.2884	0.8854
C	-12.2978	0.3323	-0.1509	H	1.9453	-3.1313	-0.8717
O	-12.9773	1.5865	0.0629	H	-1.6125	-0.8672	-0.6932
C	-14.3282	1.5529	-0.0520	H	-1.6996	-1.1411	1.0361
C	-14.9227	2.9269	0.1947	H	-3.0943	-3.2287	0.6400
C	-16.4492	2.9502	0.0875	H	-3.0183	-2.9427	-1.0991
C	-17.0412	4.3426	0.3393	H	-6.1514	-0.1375	-0.7618
C	-18.5701	4.3701	0.2336	H	-6.2451	-0.4490	0.9606

Table A.30: Continued.
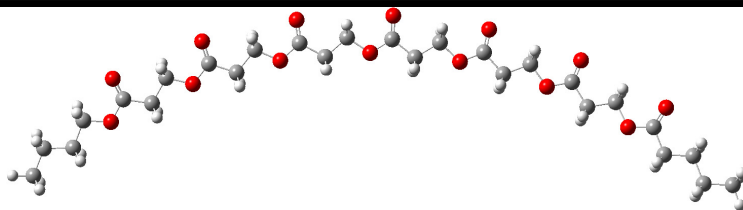
Atom	x	y	z	Atom	x	y	z
H	-7.9960	-2.2432	0.5459	H	-16.8718	2.2292	0.8006
H	-7.9049	-1.9252	-1.1869	H	-16.7465	2.5912	-0.9074
H	-10.4804	1.3791	-0.7021	H	-16.6112	5.0588	-0.3778
H	-10.6064	1.0312	1.0108	H	-16.7365	4.6951	1.3368
H	-12.6540	-0.4093	0.5717	H	-18.9660	5.3762	0.4208
H	-12.5312	-0.0493	-1.1503	H	-19.0308	3.6891	0.9616
H	-14.4623	3.6251	-0.5197	H	-18.9050	4.0600	-0.7652
H	-14.5874	3.2654	1.1859				

Table A.31: DFT Geometry Optimized Coordinates (B3LYP/6-31G(d')) for 18chain0.
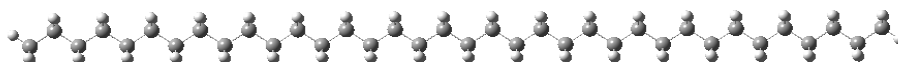
Atom	x	y	z	Atom	x	y	z
C	-0.4192	19.9056	0.0000	H	-1.0838	19.9055	0.8788
C	0.4227	18.6227	0.0000	H	-1.0838	19.9055	-0.8788
C	-0.4158	17.3372	0.0000	H	1.0870	18.6236	0.8788
C	0.4258	16.0539	0.0000	H	1.0870	18.6236	-0.8788
C	-0.4135	14.7689	0.0000	H	-1.0802	17.3365	-0.8787
C	0.4274	13.4851	0.0000	H	-1.0802	17.3365	0.8787
C	-0.4125	12.2006	0.0000	H	1.0901	16.0545	0.8787
C	0.4278	10.9163	0.0000	H	1.0901	16.0545	-0.8787
C	-0.4127	9.6322	0.0000	H	-1.0778	14.7685	-0.8787
C	0.4271	8.3476	0.0000	H	-1.0778	14.7685	0.8787
C	-0.4139	7.0638	0.0000	H	1.0917	13.4853	0.8787
C	0.4255	5.7789	0.0000	H	1.0917	13.4853	-0.8787
C	-0.4158	4.4953	0.0000	H	-1.0769	12.2005	-0.8787
C	0.4233	3.2103	0.0000	H	-1.0769	12.2005	0.8787
C	-0.4182	1.9268	0.0000	H	1.0921	10.9163	0.8787
C	0.4208	0.6417	0.0000	H	1.0921	10.9163	-0.8787
C	0.4182	21.1916	0.0000	H	-1.0771	9.6324	-0.8787
C	-0.4313	22.4677	0.0000	H	-1.0771	9.6324	0.8787
C	-0.4208	-0.6417	0.0000	H	1.0914	8.3473	0.8787
C	0.4182	-1.9268	0.0000	H	1.0914	8.3473	-0.8787
C	-0.4233	-3.2103	0.0000	H	-1.0782	7.0642	-0.8787
C	0.4158	-4.4953	0.0000	H	-1.0782	7.0642	0.8787
C	-0.4255	-5.7789	0.0000	H	1.0898	5.7784	0.8787
C	0.4139	-7.0638	0.0000	H	1.0898	5.7784	-0.8787
C	-0.4271	-8.3476	0.0000	H	-1.0802	4.4959	-0.8787
C	0.4127	-9.6322	0.0000	H	-1.0802	4.4959	0.8787
C	-0.4278	-10.9163	0.0000	H	1.0876	3.2097	0.8787
C	0.4125	-12.2006	0.0000	H	1.0876	3.2097	-0.8787
C	-0.4274	-13.4851	0.0000	H	-1.0825	1.9275	-0.8787
C	0.4135	-14.7689	0.0000	H	-1.0825	1.9275	0.8787
C	-0.4258	-16.0539	0.0000	H	1.0851	0.6410	0.8787
C	0.4158	-17.3372	0.0000	H	1.0851	0.6410	-0.8787
C	-0.4227	-18.6227	0.0000	H	1.0815	21.1923	-0.8785
C	0.4192	-19.9056	0.0000	H	1.0815	21.1923	0.8785
C	-0.4182	-21.1916	0.0000	H	0.1957	23.3686	0.0000
C	0.4313	-22.4677	0.0000	H	-1.0799	22.5134	0.8854

Table A.31: Continued.
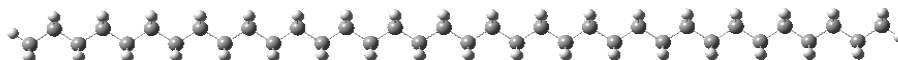
Atom	x	y	z	Atom	x	y	z
H	-1.0799	22.5134	-0.8854	H	1.0769	-12.2005	0.8787
H	-1.0851	-0.6410	-0.8787	H	1.0769	-12.2005	-0.8787
H	-1.0851	-0.6410	0.8787	H	-1.0917	-13.4853	-0.8787
H	1.0825	-1.9275	0.8787	H	-1.0917	-13.4853	0.8787
H	1.0825	-1.9275	-0.8787	H	1.0778	-14.7685	0.8787
H	-1.0876	-3.2097	-0.8787	H	1.0778	-14.7685	-0.8787
H	-1.0876	-3.2097	0.8787	H	-1.0901	-16.0545	-0.8787
H	1.0802	-4.4959	0.8787	H	-1.0901	-16.0545	0.8787
H	1.0802	-4.4959	-0.8787	H	1.0802	-17.3365	0.8787
H	-1.0898	-5.7784	-0.8787	H	1.0802	-17.3365	-0.8787
H	-1.0898	-5.7784	0.8787	H	-1.0870	-18.6236	-0.8788
H	1.0782	-7.0642	0.8787	H	-1.0870	-18.6236	0.8788
H	1.0782	-7.0642	-0.8787	H	1.0838	-19.9055	0.8788
H	-1.0914	-8.3473	-0.8787	H	1.0838	-19.9055	-0.8788
H	-1.0914	-8.3473	0.8787	H	-1.0815	-21.1923	-0.8785
H	1.0771	-9.6324	0.8787	H	-1.0815	-21.1923	0.8785
H	1.0771	-9.6324	-0.8787	H	-0.1957	-23.3686	0.0000
H	-1.0921	-10.9163	-0.8787	H	1.0799	-22.5134	0.8854
H	-1.0921	-10.9163	0.8787	H	1.0799	-22.5134	-0.8854

**Table A.32:** DFT Geometry Optimized Coordinates (B3LYP/6-31G(d')) for 19chain0.

Atom	x	y	z	Atom	x	y	z
C	23.7522	0.3947	-0.0001	H	12.1988	-1.1107	-0.8783
C	22.4748	-0.4526	-0.0001	H	10.9180	1.0603	-0.8783
C	21.1902	0.3870	0.0000	H	10.9181	1.0603	0.8791
C	19.9059	-0.4529	0.0000	H	9.6299	-1.1063	0.8793
C	18.6218	0.3876	0.0001	H	9.6299	-1.1063	-0.8782
C	17.3372	-0.4520	0.0001	H	8.3499	1.0651	-0.8783
C	16.0536	0.3892	0.0002	H	8.3499	1.0652	0.8792
C	14.7685	-0.4498	0.0003	H	7.0611	-1.1010	0.8793
C	13.4853	0.3921	0.0003	H	7.0611	-1.1011	-0.8782
C	12.1998	-0.4464	0.0004	H	5.7816	1.0707	-0.8783
C	10.9169	0.3960	0.0004	H	5.7816	1.0708	0.8792
C	9.6311	-0.4420	0.0005	H	4.4923	-1.0952	0.8793
C	8.3485	0.4008	0.0005	H	4.4924	-1.0953	-0.8781
C	7.0625	-0.4367	0.0005	H	3.2133	1.0767	-0.8783
C	5.7801	0.4064	0.0005	H	3.2133	1.0769	0.8792
C	4.4939	-0.4309	0.0005	H	1.9237	-1.0889	0.8793
C	3.2117	0.4125	0.0005	H	1.9237	-1.0891	-0.8782
C	1.9253	-0.4246	0.0005	H	0.6449	1.0831	-0.8784
C	0.6432	0.4188	0.0004	H	0.6448	1.0832	0.8791
C	-0.6432	-0.4183	0.0004	H	-0.6449	-1.0825	0.8792
C	-1.9253	0.4252	0.0003	H	-0.6448	-1.0827	-0.8783
C	-3.2117	-0.4119	0.0002	H	-1.9237	1.0895	-0.8785
C	-4.4939	0.4314	0.0001	H	-1.9238	1.0896	0.8790
C	-5.7801	-0.4059	0.0001	H	-3.2133	-1.0762	0.8790
C	-7.0625	0.4371	0.0000	H	-3.2132	-1.0763	-0.8785
C	-8.3485	-0.4005	-0.0001	H	-4.4923	1.0957	-0.8787
C	-9.6312	0.4422	-0.0002	H	-4.4924	1.0957	0.8788
C	-10.9169	-0.3958	-0.0003	H	-5.7816	-1.0703	0.8788
C	-12.1998	0.4465	-0.0003	H	-5.7815	-1.0703	-0.8786
C	-13.4852	-0.3920	-0.0004	H	-7.0611	1.1014	-0.8788
C	-14.7685	0.4497	-0.0004	H	-7.0612	1.1015	0.8787
C	-16.0535	-0.3894	-0.0005	H	-8.3499	-1.0648	0.8786
C	-17.3372	0.4517	-0.0006	H	-8.3498	-1.0649	-0.8788
C	-18.6218	-0.3880	-0.0007	H	-9.6299	1.1065	-0.8789
C	-19.9059	0.4524	-0.0007	H	-9.6300	1.1066	0.8785
C	-21.1901	-0.3876	-0.0008	H	-10.9180	-1.0601	0.8785
C	-22.4748	0.4519	-0.0008	H	-10.9179	-1.0601	-0.8790
C	-23.7522	-0.3956	-0.0009	H	-12.1988	1.1108	-0.8790
H	24.6520	-0.2338	-0.0001	H	-12.1989	1.1108	0.8784

Table A.32: Continued.
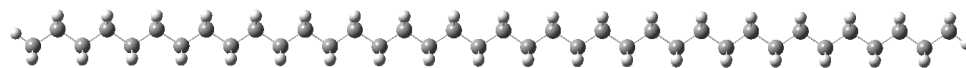
Atom	x	y	z	Atom	x	y	z
H	23.7992	1.0432	0.8854	H	-13.4861	-1.0564	0.8783
H	23.7991	1.0433	-0.8854	H	-13.4860	-1.0564	-0.8791
H	22.4745	-1.1159	0.8784	H	-14.7678	1.1140	-0.8791
H	22.4744	-1.1158	-0.8786	H	-14.7679	1.1140	0.8783
H	21.1911	1.0515	-0.8787	H	-16.0541	-1.0538	0.8782
H	21.1912	1.0514	0.8788	H	-16.0540	-1.0537	-0.8793
H	19.9058	-1.1173	0.8788	H	-17.3368	1.1161	-0.8793
H	19.9058	-1.1172	-0.8788	H	-17.3369	1.1160	0.8782
H	18.6221	1.0520	-0.8786	H	-18.6221	-1.0524	0.8780
H	18.6221	1.0519	0.8789	H	-18.6220	-1.0523	-0.8794
H	17.3368	-1.1164	0.8789	H	-19.9059	1.1168	-0.8794
H	17.3367	-1.1163	-0.8786	H	-19.9059	1.1167	0.8781
H	16.0541	1.0536	-0.8785	H	-21.1911	-1.0521	0.8780
H	16.0542	1.0535	0.8790	H	-21.1910	-1.0521	-0.8796
H	14.7678	-1.1141	0.8790	H	-22.4745	1.1152	-0.8793
H	14.7677	-1.1141	-0.8785	H	-22.4746	1.1151	0.8777
H	13.4861	1.0564	-0.8784	H	-24.6521	0.2329	-0.0009
H	13.4862	1.0564	0.8791	H	-23.7991	-1.0441	0.8845
H	12.1988	-1.1107	0.8791	H	-23.7990	-1.0440	-0.8864

Table A.33: DFT Geometry Optimized Coordinates (B3LYP/6-31G(d')) for 19chain1.
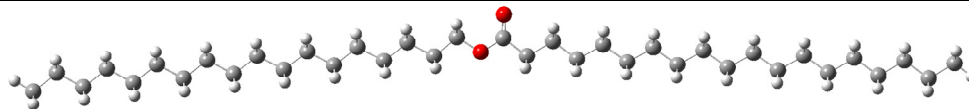
Atom	x	y	z	Atom	x	y	z
C	-18.3814	-0.9169	-0.0003	H	-18.3332	-1.5792	0.8787
C	-17.1619	0.0148	-0.0005	H	-18.3331	-1.5797	-0.8788
C	-15.8194	-0.7288	-0.0001	H	-17.2105	0.6778	0.8780
C	-14.6010	0.2042	-0.0003	H	-17.2104	0.6772	-0.8794
C	-13.2575	-0.5377	0.0001	H	-15.7705	-1.3916	-0.8787
C	-12.0406	0.3973	0.0000	H	-15.7707	-1.3911	0.8788
C	-10.6958	-0.3422	0.0004	H	-14.6504	0.8670	0.8782
C	-9.4810	0.5956	0.0004	H	-14.6502	0.8665	-0.8792
C	-8.1344	-0.1407	0.0007	H	-13.2075	-1.2004	-0.8785
C	-6.9226	0.8009	0.0006	H	-13.2078	-1.1999	0.8791
C	-5.5743	0.0681	0.0009	H	-12.0911	1.0600	0.8785
C	-4.3668	1.0154	0.0007	H	-12.0909	1.0595	-0.8789
C	-3.0194	0.2802	0.0009	H	-10.6444	-1.0047	-0.8783
C	-1.8411	1.2429	0.0007	H	-10.6447	-1.0043	0.8793
O	-0.6267	0.4592	0.0008	H	-9.5330	1.2581	0.8789
C	0.5294	1.1616	-0.0002	H	-9.5328	1.2577	-0.8785
C	1.7285	0.2305	-0.0002	H	-8.0812	-0.8029	-0.8781
C	3.0660	0.9746	-0.0002	H	-8.0814	-0.8026	0.8796
C	4.2746	0.0301	-0.0001	H	-6.9764	1.4630	0.8793
C	5.6187	0.7709	-0.0001	H	-6.9763	1.4628	-0.8782
C	6.8364	-0.1629	-0.0001	H	-5.5179	-0.5933	-0.8779
C	8.1782	0.5821	-0.0002	H	-5.5180	-0.5929	0.8800
C	9.3991	-0.3476	-0.0002	H	-4.4239	1.6766	0.8796
C	10.7391	0.4006	-0.0003	H	-4.4239	1.6762	-0.8784
C	11.9620	-0.5265	-0.0003	H	-2.9468	-0.3738	-0.8797
C	13.3008	0.2239	-0.0004	H	-2.9468	-0.3734	0.8819
C	14.5250	-0.7016	-0.0003	H	-1.8438	1.8937	0.8843
C	15.8630	0.0502	-0.0004	H	-1.8439	1.8934	-0.8831
C	17.0880	-0.8742	-0.0002	H	1.6402	-0.4315	-0.8740
C	18.4256	-0.1218	-0.0002	H	1.6402	-0.4316	0.8735
O	0.5752	2.3701	-0.0011	H	3.1084	1.6376	0.8747
C	-19.7233	-0.1721	-0.0006	H	3.1085	1.6375	-0.8752
C	-20.9434	-1.1027	-0.0002	H	4.2242	-0.6325	-0.8789
C	19.6508	-1.0459	0.0000	H	4.2241	-0.6323	0.8788
C	20.9884	-0.2939	0.0001	H	5.6674	1.4334	0.8784
C	-22.2852	-0.3580	-0.0005	H	5.6674	1.4333	-0.8786
C	-23.4984	-1.2948	-0.0001	H	6.7878	-0.8253	-0.8789
C	22.2135	-1.2180	0.0004	H	6.7878	-0.8252	0.8788
C	23.5455	-0.4593	0.0004	H	8.2257	1.2449	0.8784

Table A.33: Continued.
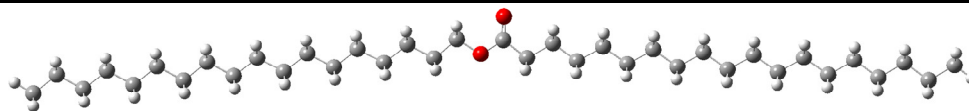
Atom	x	y	z	Atom	x	y	z
H	8.2256	1.2448	-0.8789	H	-19.7713	0.4908	0.8780
H	9.3522	-1.0103	-0.8789	H	-20.8965	-1.7653	0.8788
H	9.3523	-1.0102	0.8787	H	-20.8965	-1.7659	-0.8788
H	10.7852	1.0635	0.8783	H	19.6065	-1.7090	-0.8786
H	10.7852	1.0633	-0.8791	H	19.6063	-1.7087	0.8789
H	11.9164	-1.1894	-0.8790	H	21.0338	0.3692	0.8787
H	11.9165	-1.1892	0.8785	H	21.0340	0.3689	-0.8788
H	13.3460	0.8868	0.8782	H	-22.3325	0.3034	-0.8792
H	13.3459	0.8866	-0.8792	H	-22.3325	0.3040	0.8778
H	14.4803	-1.3645	-0.8790	H	-24.4410	-0.7326	-0.0003
H	14.4803	-1.3643	0.8785	H	-23.4987	-1.9448	0.8855
H	15.9076	0.7133	0.8782	H	-23.4987	-1.9454	-0.8853
H	15.9076	0.7130	-0.8792	H	22.1687	-1.8799	-0.8780
H	17.0437	-1.5372	-0.8789	H	22.1685	-1.8797	0.8789
H	17.0436	-1.5370	0.8786	H	24.4004	-1.1476	0.0006
H	18.4698	0.5412	0.8784	H	23.6366	0.1846	0.8858
H	18.4700	0.5410	-0.8791	H	23.6368	0.1844	-0.8851
H	-19.7713	0.4902	-0.8795				

APPENDIX B

ELECTRONIC DIFFERENCES IN A SERIES OF STERICALLY-EXPANDED CYCLOPENTADIENYL-BASED LIGANDS

Generation of Figure 3.2 and determination of K_{eq} for Figure 3.3. Inside the box, OctH (0.027 g, 7.57 μmol) and FluH (0.012 g, 7.57 μmol) were charged to a J. Young tube and dissolved in THF-d_8. The NMR spectrum was recorded, using 64 transients (entry 1). The tube was taken into the box and 1 μL of a *tert*-butyl lithium solution (1.5 M in pentane) was added. Again, the NMR spectrum was recorded (entry 2). This process was repeated until, in entry 5, peaks were observed for all four species. The reaction was allowed to stand at room temperature for 150 minutes to ensure equilibrium had been reached. Another spectrum (entry 6) showed nearly identical intensities to those observed in entry 5. Several more additions of ^{t}BuLi were made to ensure that the remaining FluH completely reacted.

Table B.1: Characteristic Chemical Shifts Used in the Generation of Figure 3.2 and Table 3.1.

Species	Atom Used	Chemical Shift [a] (ppm)
FluH	H_2C-Ar$_2$	3.84
OctH	H_2C-Ar$_2$	3.75
FluLi	HC-Ar$_2$	5.90
OctLi	HC-Ar$_2$	5.44

[a] Referenced to residual 2-proteo THF at 3.58 ppm.

Table B.2: Percent of Each Species Present in the Competitive Deprotonation of OctH and FluH.

Entry	Total Volume of Base Added (µL)	FluH	OctH	FluLi	OctLi
1	0	49.85	50.15	0.00	0.00
2	1	45.91	51.63	2.46	0.00
3	2	43.35	52.60	4.04	0.00
4	3	10.69	64.81	24.50	0.00
5	4	0.23	66.19	32.35	1.22
6	4	0.23	66.79	31.77	1.21
7	5	0.00	53.86	35.15	10.99
8	6	0.00	48.41	36.98	14.61
9	7	0.00	41.91	38.57	19.52

^{1}H NMR spectra for Table B.2, entries 1-9.
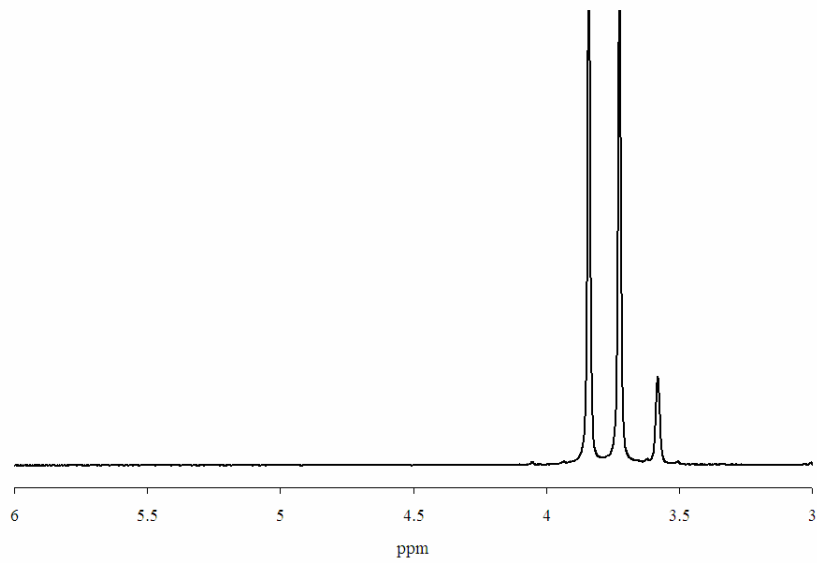
Figure B.1: ^{1}H NMR spectrum for Table B.2, Entry 1.
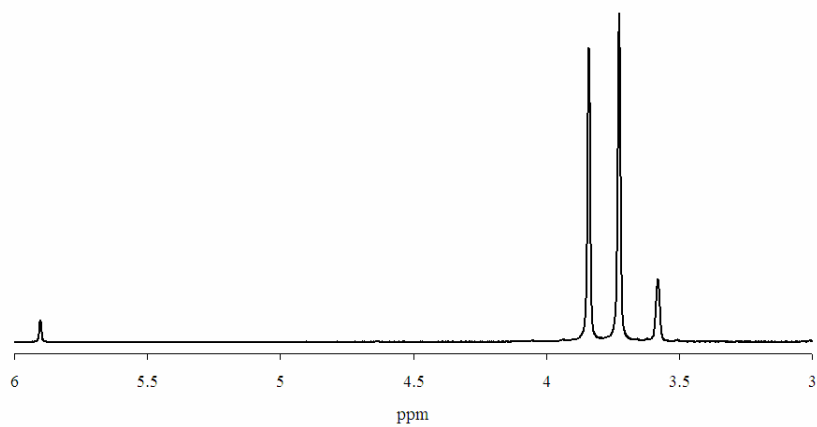
Figure B.2: ^{1}H NMR spectrum for Table B.2, Entry 2.
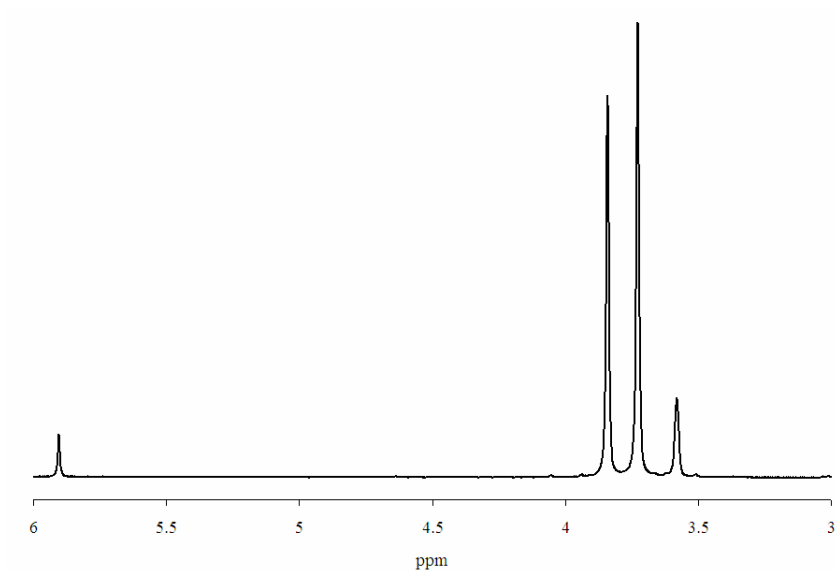
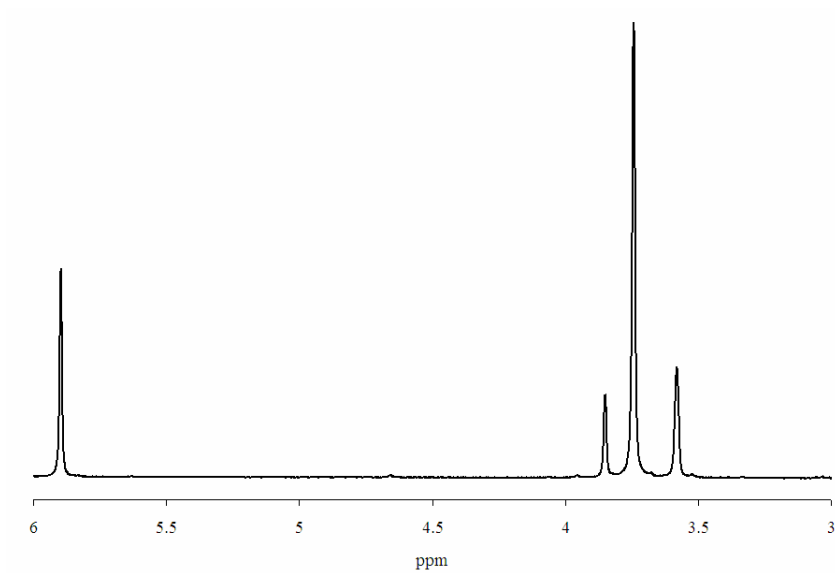**Figure B.3:** ^{1}H NMR spectrum for Table B.2, Entry 3.

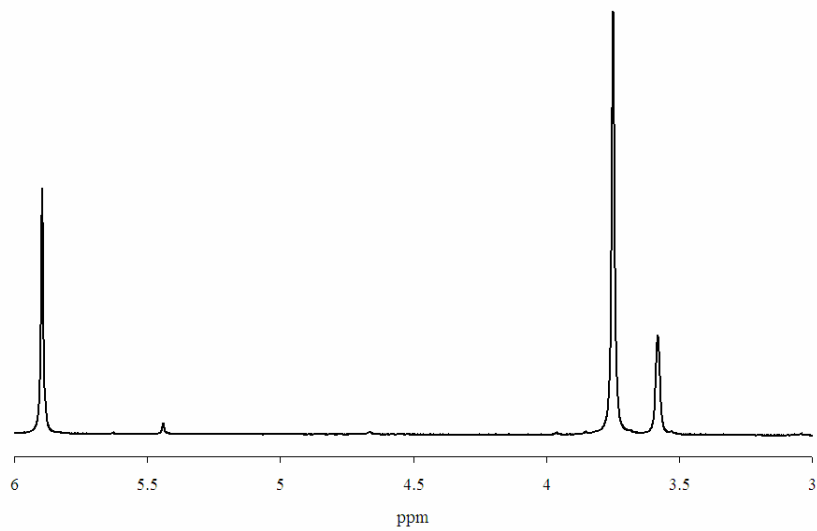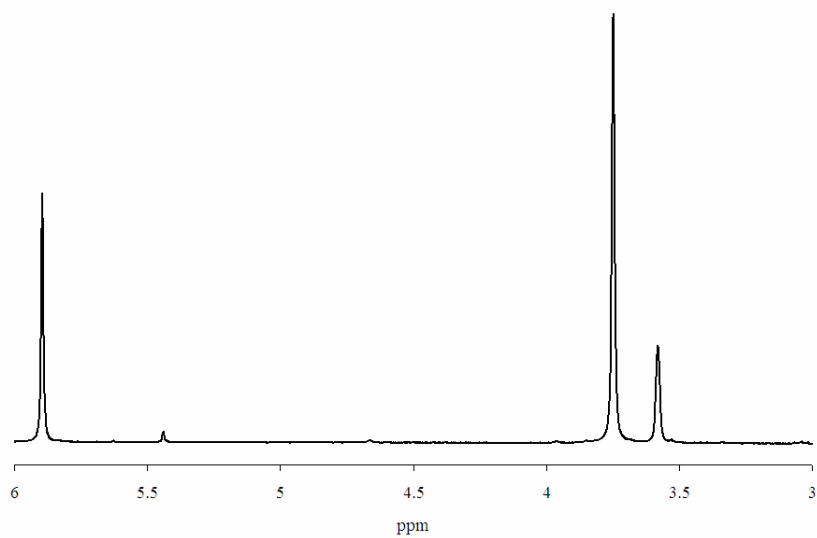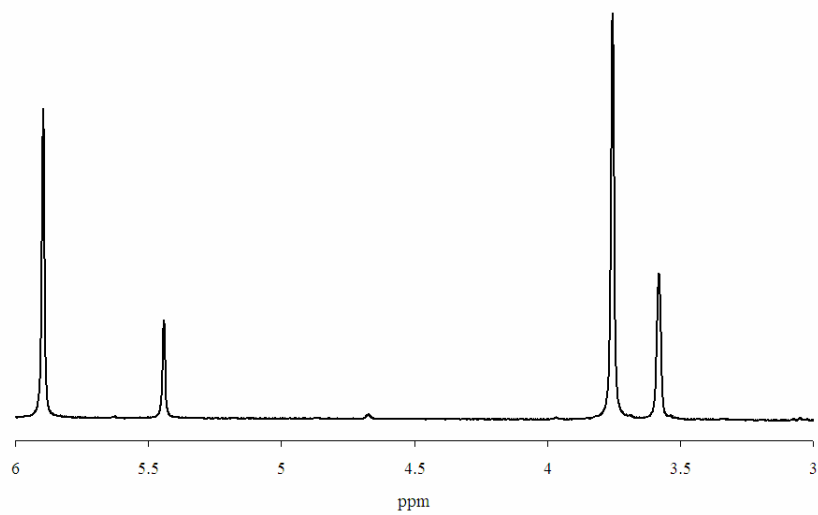**Figure B.4:** ^{1}H NMR spectrum for Table B.2, Entry 4.

Figure B.5: [superscript]1[/superscript]H NMR spectrum for Table B.2, Entry 5.

Figure B.6: [superscript]1[/superscript]H NMR spectrum for Table B.2, Entry 6.

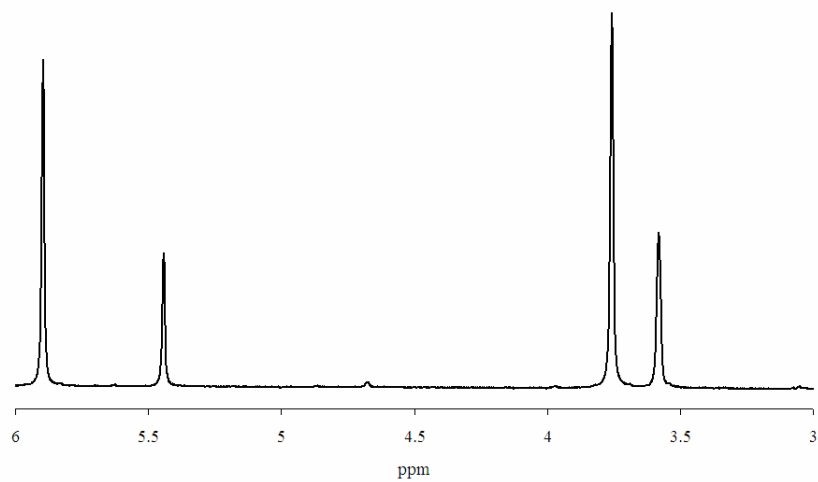**Figure B.7:** ^{1}H NMR spectrum for Table B.2, Entry 7.

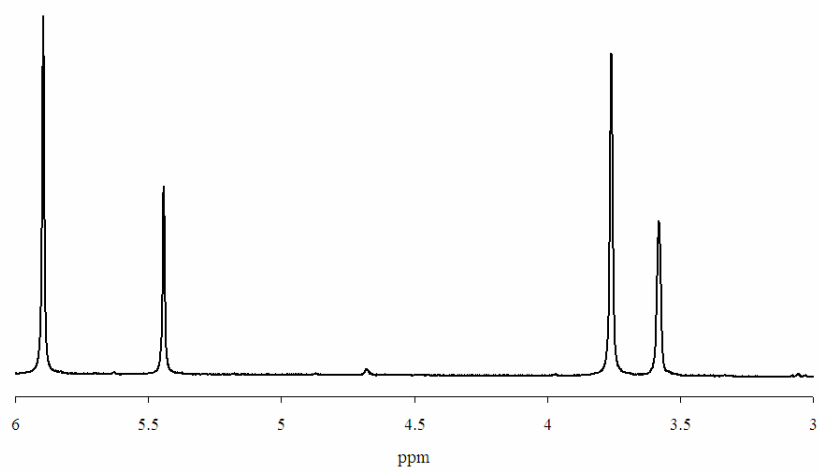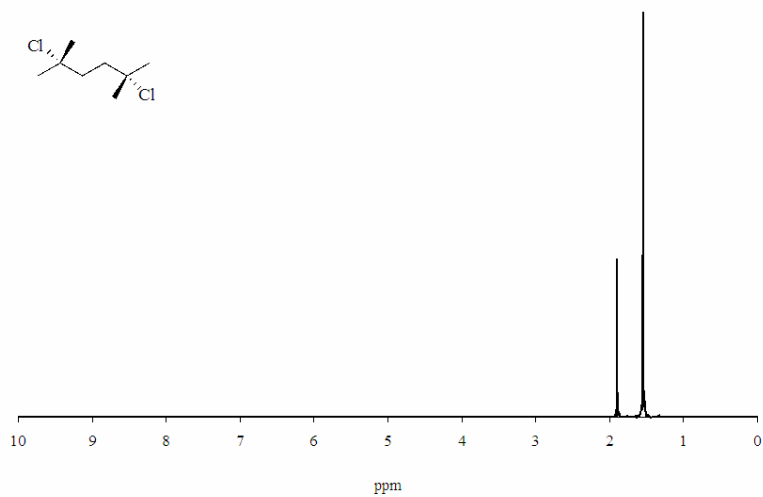**Figure B.8:** ^{1}H NMR spectrum for Table B.2, Entry 8.
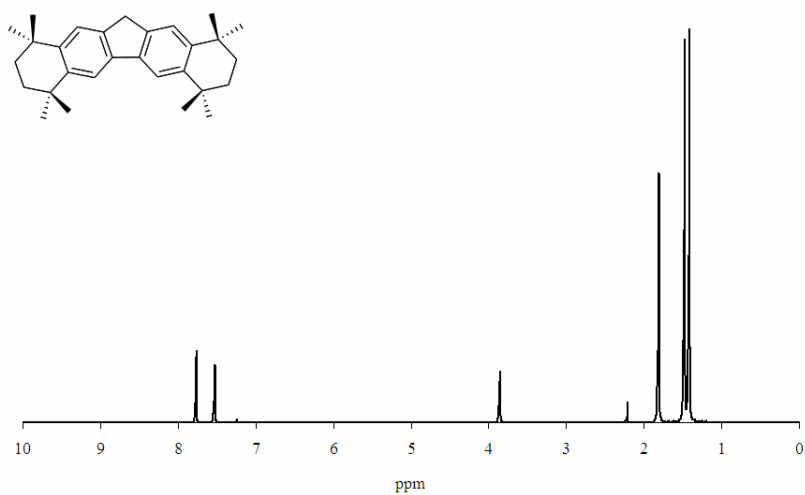
Figure B.9: ^{1}H NMR spectrum for Table B.2, Entry 9.

¹H NMR spectra.

Figure B.10: ¹H NMR spectrum for 2,5-dichloro-2,5-dimethylhexane.

Figure B.11: ¹H NMR spectrum for 2,2,5,5,8,8,11,11-octamethyl-2,3,4,5,8,9,10,11-octahydrodibenzo[*b,e*]fluorene (OctH).

Figure B.12: ^{1}H NMR spectrum for Mn(η^5-Flu)(CO)$_3$ (**7**).

Figure B.13: ^{1}H NMR spectrum for Mn(η^5-Oct)(CO)$_3$ (**8**).

¹³C NMR spectra.

Figure B.14: ¹³C NMR spectrum for 2,5-dichloro-2,5-dimethylhexane
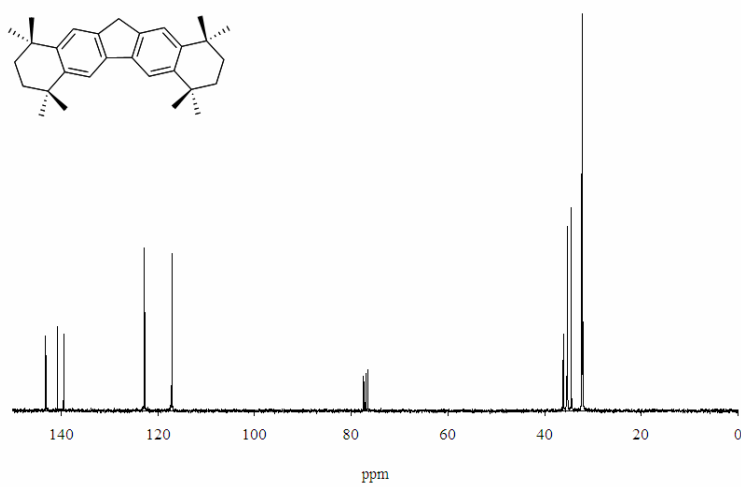
Figure B.15: ¹³C NMR spectrum for 2,2,5,5,8,8,11,11-octamethyl-2,3,4,5,8,9,10,11-octahydrodibenzo[*b,e*]fluorene (OctH).
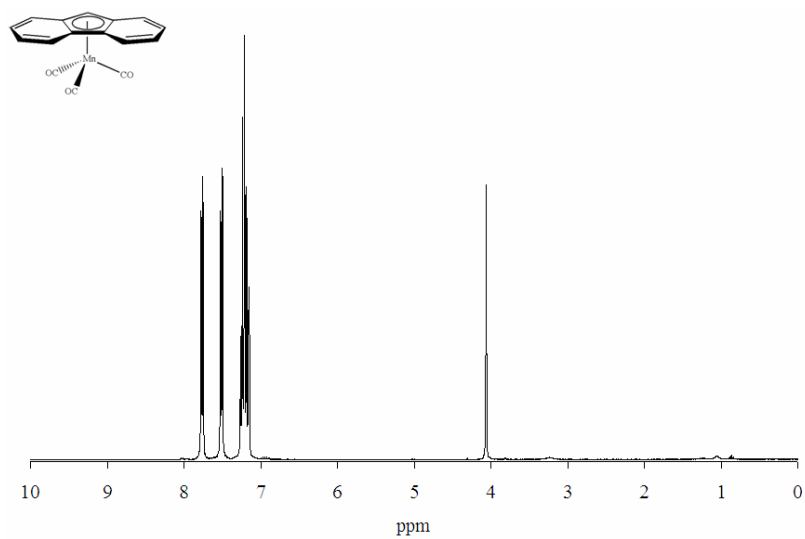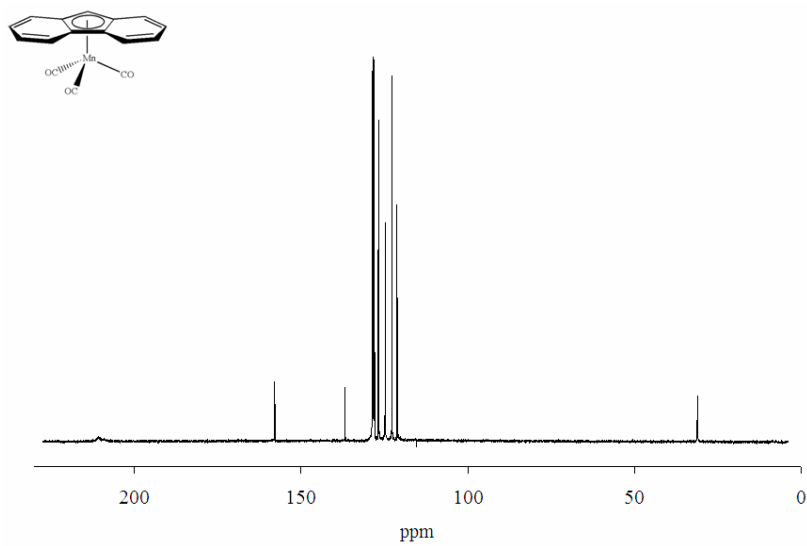
Figure B.16: ^{13}C NMR spectrum for Mn(η^5-Flu)(CO)$_3$ (**7**).

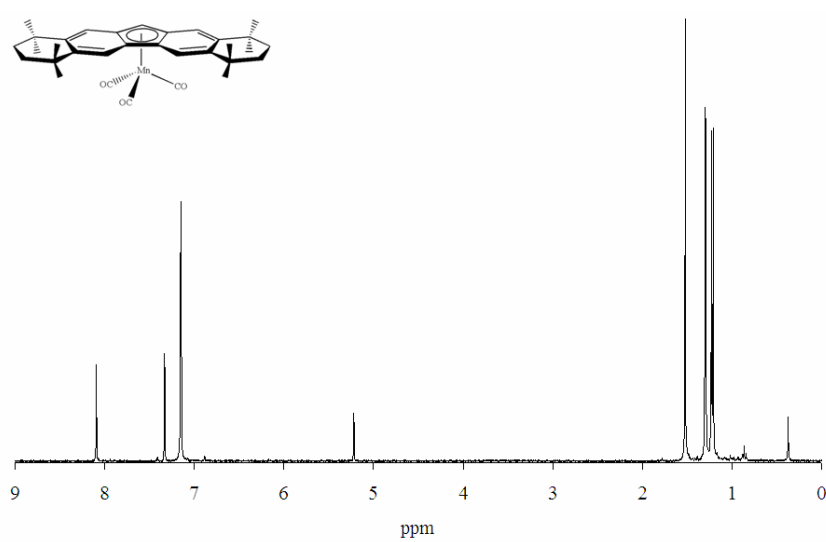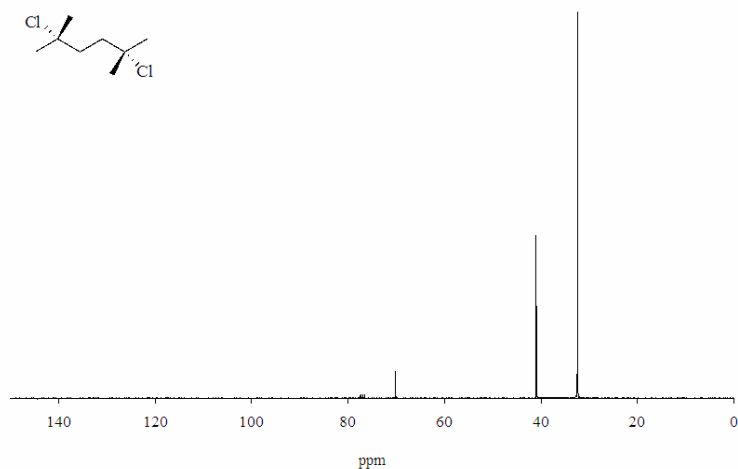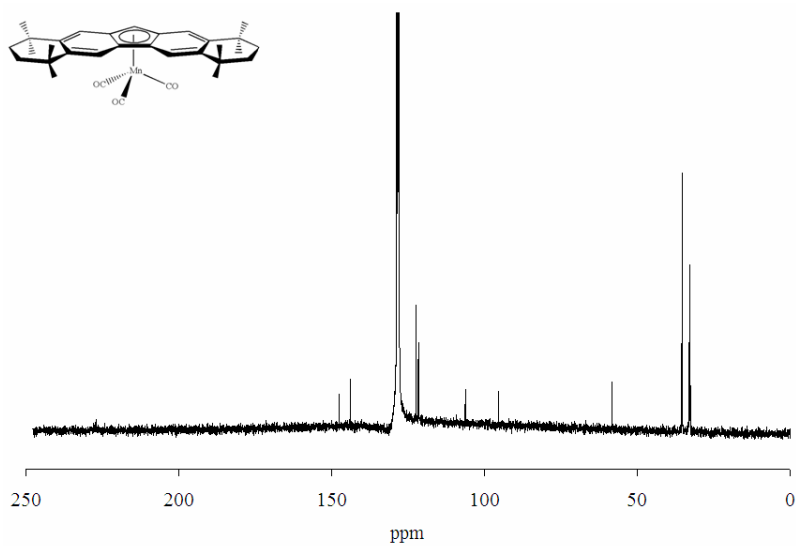**Figure B.17:** ^{13}C NMR spectrum for Mn(η^5-Oct)(CO)$_3$ (**8**).

IR spectra.
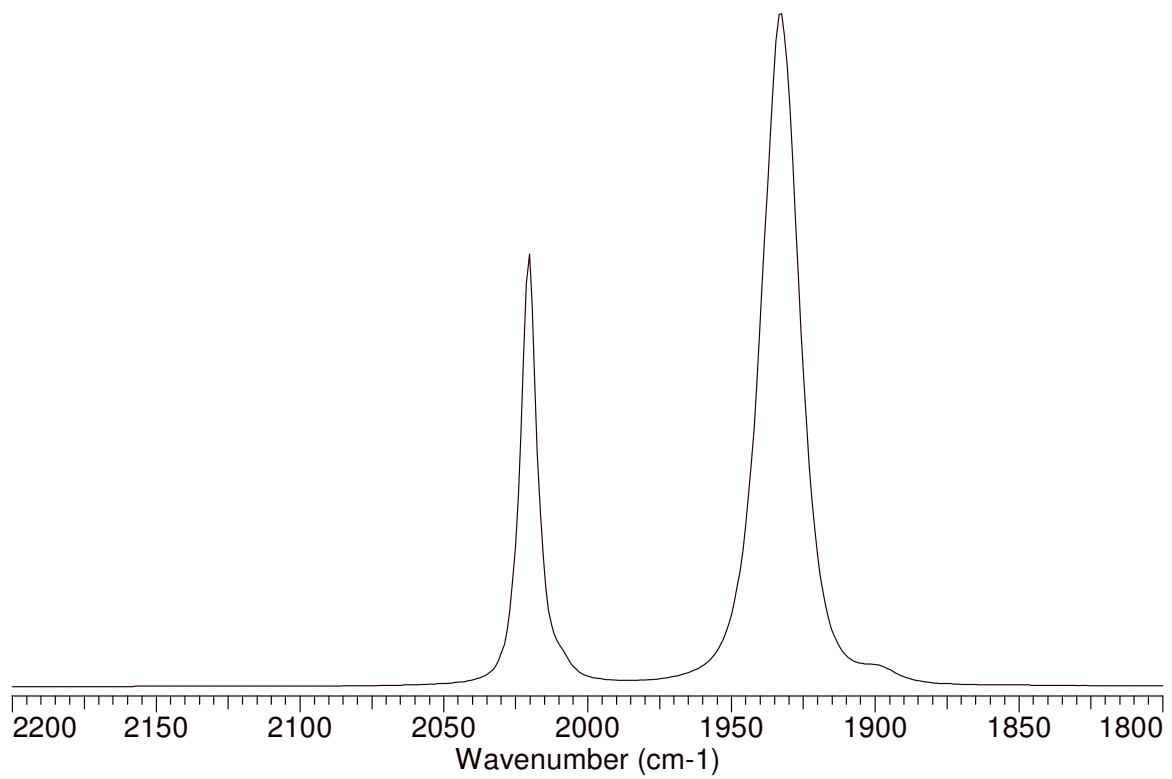
Figure B.18: The IR spectrum of **5**.
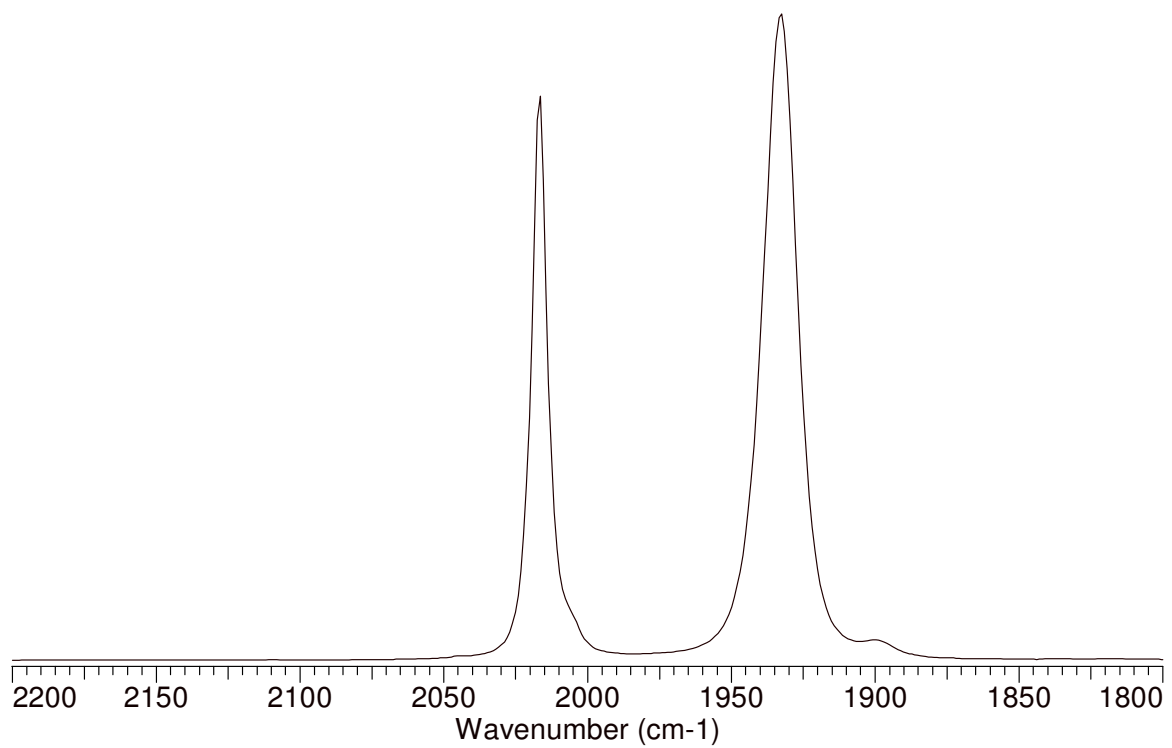
Figure B.19: The IR spectrum of **7**.
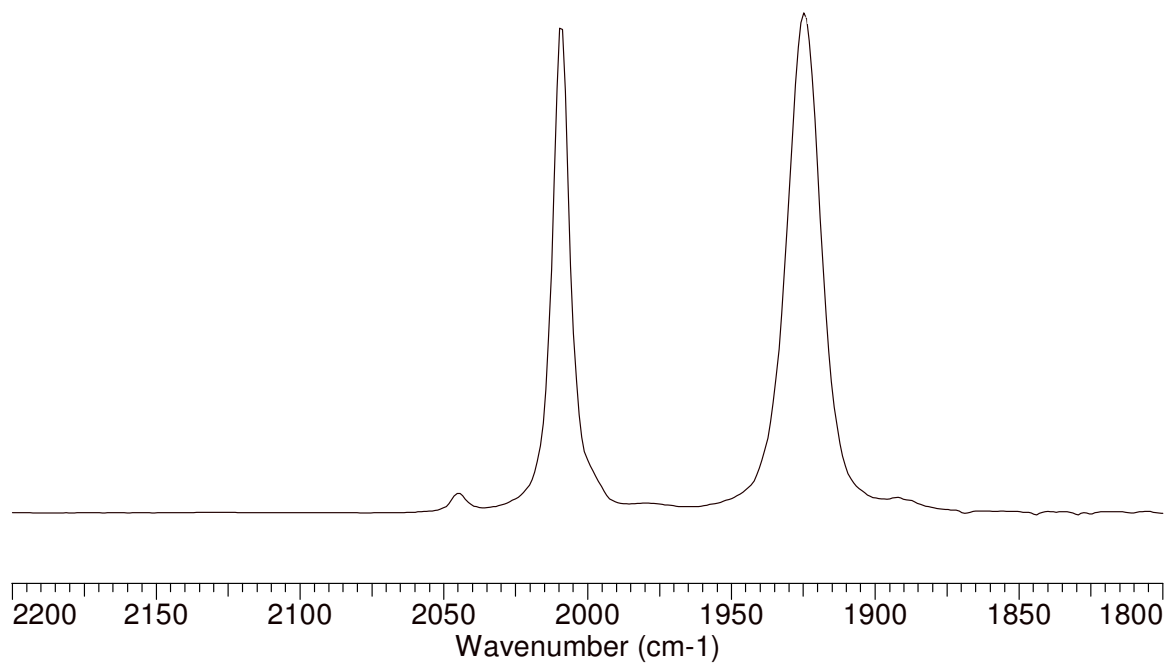
Figure B.19: The IR spectrum of **8**.

Computational methods. DFT calculations were carried out with the Gaussian 03 suite of programs[58] using the gradient-corrected Becke exchange functional[59] and the correlation functional of Lee, Yang and Parr[60,61] (B3LYP). Full geometry optimization calculations were carried out on OctH, FluH, OctLi and FluLi using a 6-31G† basis set,[63] followed by single point frequency calculations using a 6-311+G(2d,p) basis set.[96,97] The reaction enthalpy (ΔH) was derived from the energy of each molecule (from the single-point calculation) corrected to enthalpy by the "thermal correction to enthalpy term" obtained from the frequency calculation. Single-point calculations were carried out on **7** and **9** using the geometries obtained from the crystal structures using a LanL2DZ basis set[94,95] for the Zr atom and 6-31+G(2d,p) for all other atoms.[96,97]

DFT structures and coordinates. Geometry optimized structures and coordinates used for single point calculations are as follows.

Table B.3: Coordinates Used for **1** (B3LYP 6-31G**/LanL2DZ).
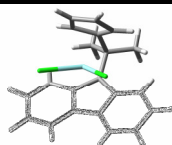
Atom	x	y	z	Atom	x	y	z
C	1.7456	-2.6209	-0.7259	H	-1.1608	-3.7245	-0.7731
C	0.7580	-1.6613	-0.9980	H	-3.5240	-3.6196	-0.9301
C	-0.6664	-1.7736	-1.1027	H	-4.5092	-1.2549	-1.3828
C	-1.5285	-2.8685	-0.9545	H	-2.9711	0.4820	-1.6931
C	-2.8906	-2.7354	-1.0670	H	1.8228	2.4531	-1.4249
C	-3.4301	-1.4429	-1.3423	H	0.9195	3.7245	-1.7836
C	-0.0903	0.4796	-1.4307	H	1.1590	2.5785	-2.8737
C	-2.5886	-0.3661	-1.5043	H	-2.2180	2.1050	-1.9542
C	-1.1817	-0.4628	-1.4002	H	-1.2357	2.3772	-3.1882
C	1.1161	-0.2932	-1.2179	H	-1.4806	3.5189	-2.0945
C	-0.2110	2.0180	-1.4121	H	1.5905	2.4336	0.8740
C	1.0356	2.7605	-1.9205	H	0.5445	1.9918	3.1882
C	-1.3939	2.5527	-2.2372	H	-1.9747	1.7709	2.9073
C	-0.4053	2.2287	0.0855	H	-2.5397	2.0536	0.3929
C	0.6378	2.1804	1.0409	H	2.7483	0.9371	-1.2975
C	0.0563	1.9654	2.3156	H	4.5092	-0.5935	-0.9324
C	-1.3109	1.8532	2.1655	H	3.8067	-3.0562	-0.4370
C	-1.6207	1.9812	0.7813	H	-0.2901	1.1234	-0.4591
C	2.4857	0.0336	-1.1647	Cl	-2.0839	-1.2721	1.9484
C	3.4621	-0.9165	-0.9276	Cl	1.5692	-0.9180	2.2134
C	3.0782	-2.2723	-0.6756	Zr	-0.2720	-0.0681	0.8925
H	1.4917	-3.5236	-0.5748				

Table B.4: Coordinates Used for **3** (B3LYP 6-31G**/LanL2DZ).
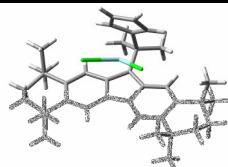
Atom	x	y	z	Atom	x	y	z
C	-1.6446	1.7077	-0.2106	H	-4.9875	-0.2953	-2.8895
C	-0.7124	0.7179	-0.5590	H	-6.1891	-1.0930	-2.1948
C	0.7198	0.7369	-0.5913	H	-4.7119	-1.7084	-2.1902
C	1.6461	1.7397	-0.2742	H	-5.1546	-0.6389	1.2051
C	2.9998	1.5213	-0.3471	H	-4.8129	-1.9194	0.3070
C	3.9578	2.6580	0.0322	H	-6.2897	-1.3041	0.2937
C	5.3533	2.1266	0.2867	H	-4.1458	3.8810	1.7763
C	5.8112	1.1639	-0.7295	H	-2.6212	3.5363	1.4348
C	4.9459	-0.1279	-0.7851	H	-3.5329	2.4647	2.1979
C	3.4630	0.2352	-0.7580	H	-4.5562	4.3846	-0.6235
C	0.0085	-1.4119	-1.2183	H	-4.2336	3.2896	-1.7453
C	2.5592	-0.7494	-1.0857	H	-3.0374	4.0234	-0.9735
C	1.1587	-0.5628	-1.0274	H	4.2275	3.9410	1.6426
C	-5.2344	-0.8809	-2.1432	H	3.6841	2.5023	2.0835
C	-5.3353	-1.0913	0.3549	H	2.6906	3.5590	1.4087
C	-3.5262	3.1698	1.5159	H	4.0609	3.4593	-1.8542
C	-3.9458	3.6653	-0.8858	H	4.4516	4.5076	-0.7099
C	3.6087	3.2145	1.4160	H	2.9179	4.1272	-0.9553
C	3.8363	3.7863	-0.9582	H	5.1964	-0.0148	-2.8301
C	5.3546	-0.6883	-2.1361	H	4.8247	-1.4888	-2.3301
C	5.2104	-1.1918	0.2661	H	6.3060	-0.9237	-2.1183
C	-1.1515	-0.5837	-0.9604	H	4.6337	-1.9672	0.0986
C	0.0232	-2.9460	-1.3851	H	5.0178	-0.8283	1.1555
C	-1.2445	-3.5282	-2.0313	H	6.1494	-1.4682	0.2229
C	1.2061	-3.4630	-2.2214	H	-2.0323	-3.2257	-1.5337
C	0.1290	-3.3491	0.0817	H	-1.2011	-4.5076	-2.0101
C	-0.9542	-3.3397	0.9928	H	-1.3083	-3.2242	-2.9589
C	-0.4227	-3.3230	2.3067	H	2.0439	-3.1145	-1.8521
C	0.9547	-3.2945	2.2271	H	1.1071	-3.1632	-3.1490
C	1.3227	-3.2773	0.8514	H	1.2197	-4.4431	-2.1958
C	-2.5411	-0.8130	-1.0036	H	-1.9125	-3.5002	0.7575
C	-3.4611	0.1709	-0.6906	H	-0.9539	-3.4183	3.1490
C	-4.9404	-0.1658	-0.8120	H	1.5853	-3.3511	2.9997
C	-5.7864	1.1151	-0.7933	H	2.2525	-3.3698	0.4945
C	-5.3880	2.0374	0.3407	H	-2.8578	-1.6721	-1.2576
C	-3.9602	2.5803	0.1693	H	-5.6773	1.5912	-1.6546

Table B.4: Continued.
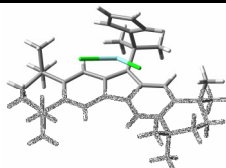
Atom	x	y	z	Atom	x	y	z
C	-2.9987	1.4546	-0.2578	H	-6.7410	0.8733	-0.6974
H	-1.3377	2.5646	0.0611	H	-5.4486	1.5459	1.1968
H	1.3289	2.5923	-0.0035	H	-6.0223	2.7972	0.3807
H	5.3264	1.6194	1.1015	H	0.1161	-2.1808	-0.3265
H	5.9685	2.8525	0.4039	Cl	1.9482	-0.2311	2.4294
H	6.7410	0.9440	-0.6312	Cl	-1.7291	-0.3450	2.5006
H	5.6933	1.6197	-1.5657	Zr	0.1127	-1.1627	1.1603
H	2.8919	-1.5944	-1.3622				

Table B.5: Geometry Optimized Coordinates (B3LYP 6-31G**) for OctH.
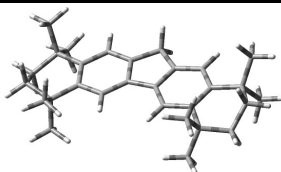
Atom	x	y	z	Atom	x	y	z
C	0.0000	0.0000	0.0000	H	-1.2016	3.1843	-0.0115
C	0.0000	1.4080	0.0000	H	5.5055	4.6754	1.4447
C	1.3931	1.8760	0.0000	H	5.7635	5.8299	0.1471
C	2.2431	0.7534	-0.0067	H	7.2345	3.8787	-0.2016
C	1.4242	-0.5244	-0.0057	H	6.0338	3.9301	-1.4828
C	1.9410	3.1545	0.0124	H	-4.9372	0.2372	1.4856
C	3.3348	3.3516	0.0156	H	-5.8657	-0.5225	0.2023
C	4.1890	2.2213	-0.0268	H	-5.8713	1.9228	-0.1346
C	3.6160	0.9320	-0.0214	H	-4.9710	1.1644	-1.4375
C	-1.2023	-0.6865	0.0134	H	-4.6170	-2.4808	1.1796
C	-2.4374	-0.0046	0.0242	H	-3.4059	-1.5616	2.0974
C	-2.4388	1.4125	-0.0115	H	-2.8977	-2.7289	0.8631
C	-1.2086	2.0966	-0.0071	H	-4.8402	-2.1241	-1.3428
C	3.8600	4.7999	0.0362	H	-3.0853	-2.1354	-1.6097
C	5.3692	4.8268	0.3642	H	-4.0430	-0.7480	-2.1356
C	6.1589	3.7708	-0.4020	H	-4.6360	3.8740	-1.1649
C	5.7251	2.3306	-0.0513	H	-3.4379	2.9432	-2.0883
C	-3.7281	-0.8448	0.0468	H	-2.9119	4.1239	-0.8749
C	-4.9426	0.0398	0.4038	H	-4.8260	3.5414	1.3670
C	-4.9518	1.3621	-0.3560	H	-3.0672	3.5580	1.6081
C	-3.7318	2.2502	-0.0259	H	-4.0146	2.1743	2.1612
C	-3.6481	-1.9680	1.1073	H	3.6023	6.6348	1.1846
C	-3.9370	-1.4977	-1.3425	H	3.2105	5.1650	2.1014
C	-3.6665	3.3611	-1.0997	H	2.0766	5.7946	0.8928
C	-3.9218	2.9167	1.3596	H	3.9509	6.4966	-1.3486
C	3.1389	5.6410	1.1153	H	2.5381	5.4495	-1.5925
C	3.6070	5.4527	-1.3457	H	4.1278	4.9207	-2.1507
C	6.3376	1.3920	-1.1175	H	7.4196	1.5683	-1.1906
C	6.2881	1.9294	1.3351	H	5.8977	1.5748	-2.1060
H	1.6318	-1.1496	-0.8874	H	6.1989	0.3312	-0.8783
H	1.6375	-1.1523	0.8727	H	7.3862	1.9751	1.3338
H	1.2789	4.0174	0.0219	H	5.9943	0.9056	1.5979
H	4.2666	0.0599	-0.0323	H	5.9214	2.5873	2.1320
H	-1.1945	-1.7745	0.0190				

Table B.6: Geometry Optimized Coordinates (B3LYP 6-31G†) for OctLi.
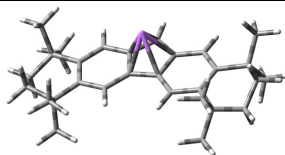
Atom	x	y	z	Atom	x	y	z
C	0.0000	0.0000	0.0000	H	-5.1591	-5.6340	-0.3103
C	0.0000	2.4532	0.0000	H	-4.0791	-5.0721	-1.5762
C	1.3909	2.4706	0.0000	H	3.6878	3.5531	1.4197
C	2.1206	1.2284	-0.0170	H	4.1079	4.6384	0.1045
C	1.4089	0.0318	0.0012	H	5.3414	2.5232	-0.1773
C	-1.7550	-4.8377	-0.0549	H	4.1746	2.6813	-1.4801
C	-3.0689	-5.5863	0.2596	H	2.0572	5.7542	1.0205
C	-4.2665	-5.0185	-0.4941	H	1.4768	4.3957	2.0053
C	-4.5795	-3.5561	-0.1082	H	0.4422	5.0948	0.7455
C	2.0970	3.8424	-0.0271	H	2.4436	5.4418	-1.4875
C	3.5916	3.6949	0.3333	H	0.8987	4.5922	-1.7056
C	-0.9724	-1.0774	-0.0078	H	2.4026	3.8203	-2.2133
C	4.2633	2.5352	-0.3941	H	5.2806	0.1862	-1.1044
C	3.6611	1.1636	-0.0179	H	3.7833	0.3409	-2.0488
C	1.4746	4.8229	0.9940	H	3.9220	-0.8962	-0.7872
C	1.9547	4.4581	-1.4421	H	5.2563	0.6685	1.4079
C	4.1842	0.1359	-1.0483	H	3.7530	-0.2407	1.6652
C	4.1593	0.7399	1.3871	H	3.8523	1.4526	2.1624
C	-5.5824	-3.0118	-1.1520	H	-6.4410	-3.6926	-1.2344
C	-5.2556	-3.5132	1.2855	H	-5.1172	-2.9311	-2.1423
C	-0.7126	-5.2801	0.9981	H	-5.9773	-2.0246	-0.8857
C	-1.2368	-5.2522	-1.4554	H	-6.1878	-4.0960	1.2833
C	-2.2853	-0.4705	-0.0277	H	-5.5035	-2.4823	1.5673
C	-2.1430	0.9562	0.0294	H	-4.6053	-3.9197	2.0697
C	-0.7381	1.2441	-0.0121	H	-0.6418	-6.3765	1.0186
C	-0.8602	-2.4823	-0.0016	H	-0.9974	-4.9420	2.0030
C	-1.9778	-3.3124	-0.0257	H	0.2922	-4.8961	0.7862
C	-3.2872	-2.7132	-0.0718	H	-1.0605	-6.3366	-1.5012
C	-3.4124	-1.3280	-0.0512	H	-0.2917	-4.7459	-1.6875
Li	-1.2701	0.1570	1.7599	H	-1.9472	-4.9894	-2.2482
H	-0.5490	3.3926	-0.0128	H	-2.9472	1.6825	-0.0293
H	1.9497	-0.9129	-0.0016	H	0.1349	-2.9239	0.0019
H	-3.2600	-5.5413	1.3417	H	-4.4024	-0.8775	-0.0763
H	-2.9387	-6.6516	0.0200				

Table B.7: Geometry Optimized Coordinates (B3LYP 6-31G†) for FluH.
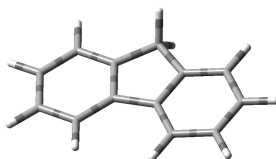
Atom	x	y	z	Atom	x	y	z
C	0.0000	0.0000	0.0000	C	-1.0549	-0.9169	0.0000
C	0.0000	1.4700	0.0000	H	2.9442	0.7350	0.8801
C	1.3374	1.9202	0.0000	H	2.9443	0.7350	-0.8800
C	2.2834	0.7350	0.0000	H	-2.0890	2.0470	0.0000
C	1.3374	-0.4502	0.0000	H	-1.5742	4.4780	0.0000
C	-1.0549	2.3869	0.0000	H	0.7763	5.2664	0.0000
C	-0.7623	3.7533	0.0000	H	2.6538	3.6341	0.0000
C	0.5651	4.1990	0.0000	H	2.6537	-2.1641	0.0000
C	1.6233	3.2816	0.0000	H	0.7762	-3.7964	0.0000
C	1.6233	-1.8116	0.0000	H	-1.5742	-3.0079	0.0000
C	0.5650	-2.7289	0.0000	H	-2.0891	-0.5769	0.0000
C	-0.7624	-2.2833	0.0000				

Table B.8: Geometry Optimized Coordinates (B3LYP 6-31G†) for FluLi.
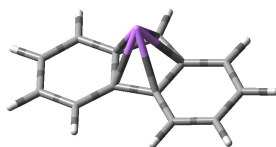
Atom	x	y	z	Atom	x	y	z
C	0.0000	0.0000	0.0000	C	-1.0411	-0.9598	-0.0014
C	0.0000	1.4487	0.0000	Li	1.0234	0.7243	1.7771
C	1.3880	1.8805	0.0000	H	3.3166	0.7243	0.0161
C	2.2319	0.7243	0.0526	H	-2.0814	2.0849	-0.0154
C	1.3880	-0.4319	0.0000	H	-1.5234	4.4984	-0.0210
C	-1.0411	2.4084	-0.0014	H	0.8461	5.2493	-0.0216
C	-0.7283	3.7561	-0.0083	H	2.7026	3.6206	-0.0099
C	0.6271	4.1829	-0.0081	H	2.7026	-2.1720	-0.0099
C	1.6695	3.2757	0.0018	H	0.8461	-3.8006	-0.0216
C	1.6695	-1.8270	0.0018	H	-1.5234	-3.0497	-0.0210
C	0.6271	-2.7342	-0.0081	H	-2.0814	-0.6363	-0.0154
C	-0.7283	-2.3074	-0.0083				

VITA

Craig Justin Price

Texas A&M University
Department of Chemistry
PO Box 30012
College Station, TX 77842-3012

craigjprice@gmail.com

B.S.; Chemistry, North Carolina State University, Raleigh, NC, 2001

Ph.D.; Chemistry, Texas A&M University, College Station, TX, 2007